

Sustainable Geotextiles for Transportation Applications from Recycled Textiles

FINAL REPORT
August 2019

Submitted by:

Christopher L. Meehan¹
Associate Professor

Abigail R. Clarke-Sather²
Assistant Professor

Tyler M. Poggiogalle³
Staff Engineer

¹ Associate Professor, University of Delaware, Department of Civil and Environmental Engineering, 301 DuPont Hall, Newark, DE 19716, U.S.A. E-mail: cmeehan@udel.edu.

² Assistant Professor, University of Minnesota Duluth, Swenson College of Science and Engineering, 1303 Ordean Court, 217 ENGR, Duluth, MN 55812, U.S.A. E-mail: abbie@d.umn.edu.

³ Staff Engineer, Haley & Aldrich of New York, 1441 Broadway #6031, New York, NY 10018, U.S.A. E-mail: tpoggiogalle@haleyaldrich.com.

External Project Manager
Colleen Morrone

In cooperation with

Rutgers, The State University of New Jersey
And
U.S. Department of Transportation

Disclaimer Statement

The contents of this report reflect the views of the authors, who are responsible for the facts and the accuracy of the information presented herein. This document is disseminated under the sponsorship of the Department of Transportation, University Transportation Centers Program, in the interest of information exchange. The U.S. Government assumes no liability for the contents or use thereof.

The Center for Advanced Infrastructure and Transportation (CAIT) is a National UTC Consortium led by Rutgers, The State University of New Jersey. Members of the consortium are the University of Delaware, Utah State University, Columbia University, New Jersey Institute of Technology, Princeton University, University of Texas at El Paso, Virginia Polytechnic Institute, and University of South Florida. The Center is funded by the U.S. Department of Transportation.

| | | | | | |
|---|--|---|----------------------------|--|-----------|
| 1. Report No. CAIT-UTC-NC43 | | 2. Government Accession No. | | 3. Recipient's Catalog No. | |
| 4. Title and Subtitle Sustainable Geotextiles for Transportation Applications from Recycled Textiles | | | | 5. Report Date August 2019 | |
| | | | | 6. Performing Organization Code CAIT/University of Delaware | |
| 7. Author(s) Christopher L. Meehan¹, Abigail R. Clarke-Sather², Tyler M. Poggiogalle³ | | | | 8. Performing Organization Report No. CAIT-UTC-NC43 | |
| | | | | 10. Work Unit No. | |
| 9. Performing Organization Name and Address ¹ Associate Professor, University of Delaware, Department of Civil and Environmental Engineering, 301 DuPont Hall, Newark, DE 19716, U.S.A. E-mail: cmeehan@udel.edu ² Assistant Professor, University of Minnesota Duluth, Swenson College of Science and Engineering, 1303 Ordean Court, 217 ENGR, Duluth, MN 55812, U.S.A. E-mail: abbie@d.umn.edu ³ Staff Engineer, Haley & Aldrich of New York, 1441 Broadway #6031, New York, NY 10018, U.S.A. E-mail: tpoggiogalle@haleyaldrich.com | | | | 11. Contract or Grant No. DTRT13-G-UTC28 | |
| | | | | 13. Type of Report and Period Covered Final Report 9/1/16 – 8/31/18 | |
| 12. Sponsoring Agency Name and Address Center for Advanced Infrastructure and Transportation Rutgers, The State University of New Jersey 100 Brett Road | | | | 14. Sponsoring Agency Code | |
| | | | | 15. Supplementary Notes U.S. Department of Transportation/OST-R 1200 New Jersey Avenue, SE Washington, DC 20590-0001 | |
| 16. Abstract Geosynthetic fabrics and fibers are used in a wide variety of transportation applications. Geosynthetics in transportation applications perform at least one of the following functions: separation, filtration, reinforcement, drainage, protection, or fluid barrier. Traditional geosynthetic fabrics and fibers are engineered with specific performance applications in mind but with a relatively high material cost. Apparel and home textiles are routinely landfilled, representing a large waste stream that is increasing in volume; this waste stream is a potential feedstock that could improve the sustainability and reduce the cost of geotextiles/geosynthetics for a wide variety of transportation applications. This report describes the results of tests conducted to measure the engineering properties of common apparel fabrics, to explore their potential for beneficial re-use within the transportation infrastructure construction community. | | | | | |
| 17. Key Words Geosynthetics; Sustainability; Beneficial Re-use; Transportation Infrastructure; Strength; Permittivity | | | 18. Distribution Statement | | |
| 19. Security Classification (of this report) Unclassified | | 20. Security Classification (of this page) Unclassified | | 21. No. of Pages 97 | 22. Price |

Acknowledgments

The findings presented in this report are based upon work supported by The Center for Advanced Infrastructure and Transportation (CAIT), a national UTC Consortium led by Rutgers, The State University of New Jersey. The authors would like to acknowledge the student colleagues who have provided support for this project in various ways: Raphael Affinito, Travis Plystak, Andrew Yurish, Miao Wang, Ben Zbornik, Isabella Asward, and Eric Johnson. The authors would like to thank Goodwill of Delaware and Goodwill of Duluth for their cooperation in supplying the recycled textiles used in this project.

TABLE OF CONTENTS

| | |
|-----------------------|------|
| LIST OF TABLES..... | iii |
| LIST OF FIGURES | v |
| ABSTRACT..... | viii |

CHAPTERS

| | |
|---|----|
| 1 DESCRIPTION OF THE PROBLEM..... | 1 |
| 1.1 Introduction | 1 |
| 1.2 Function and Applications..... | 2 |
| 1.2.1 Separation | 2 |
| 1.2.2 Filtration..... | 4 |
| 1.2.3 Reinforcement..... | 6 |
| 1.2.4 Drainage..... | 8 |
| 1.2.5 Protection | 9 |
| 1.2.6 Fluid Barrier..... | 10 |
| 1.3 Geotextile Property Requirements | 11 |
| References | 15 |
| 2 APPROACH | 18 |
| 2.1 Materials..... | 18 |
| 2.2 Preparation of Specimens for Tensile Testing..... | 20 |
| 2.2.1 Screen Printing Method..... | 21 |
| 2.3 Preparation of Specimens for Permittivity Testing | 24 |
| References | 26 |
| 3 METHODOLOGY | 27 |
| 3.1 Tensile Testing Program | 27 |
| 3.2 Permittivity Testing Program | 29 |
| 4 FINDINGS..... | 34 |
| 4.1 Strain Rate Effect on Tensile Strength | 34 |
| 4.1.1 100% Cotton Denim | 34 |

| | |
|---|----|
| 4.1.2 100% Polyester | 39 |
| 4.2 Tensile Testing of 100% Cotton Denim..... | 43 |
| 4.2.1 Tensile Testing of 100% Cotton Denim – Machine Direction Results | 44 |
| 4.2.2 Tensile Testing of 100% Cotton Denim - Cross Direction Results | 51 |
| 4.2.3 Tensile Testing of 100% Cotton Denim - Machine vs. Cross Direction Comparison | 58 |
| 4.3 Permittivity Testing of 100% Cotton Denim..... | 60 |
| 4.4 Tensile Testing of 100% Polyester..... | 61 |
| 4.4.1 Tensile Testing of 100% Polyester - Machine Direction Results | 64 |
| 4.4.2 Tensile Testing of 100% Polyester - Cross Direction Results..... | 69 |
| 4.4.3 Tensile Testing of 100% Polyester - Machine vs. Cross Direction Comparison..... | 76 |
| 4.5 Permittivity Testing of 100% Polyester | 78 |
| | |
| 5 CONCLUSIONS..... | 79 |
| | |
| 6 RECOMMENDATIONS..... | 82 |

LIST OF TABLES

| | |
|---|----|
| Geotextile Applications - Primary Separation Function (Adapted from Holtz et al. 2008) | 1 |
| Table 1.2: Geotextile Applications - Primary Filtration Function (Adapted from Holtz et al. 2008) | 5 |
| Table 1.3: Geotextile Applications - Primary Reinforcement Function (Adapted from Holtz et al. 2008) | 7 |
| Table 1.4: Geotextile Applications - Primary Drainage Function (Adapted from Holtz et al. 2008) | 9 |
| Table 1.5: Geotextile Applications - Primary Protection Function (Adapted from Holtz et al. 2008) | 10 |
| Table 1.6: Geotextile Applications - Primary Fluid Barrier Function (Adapted from Holtz et al. 2008) | 11 |
| Table 1.7: Geotextile Strength Property Requirements (Adapted from AASHTO M288, 2015) . | 12 |
| Table 1.8: Subsurface Drainage Geotextile Requirements (Adapted from AASHTO 2015)..... | 12 |
| Table 1.9: Separation Geotextile Property Requirements (Adapted from AASHTO 2015) | 12 |
| Table 1.10: Required Degree of Survivability as a Function of Subgrade Conditions, Construction Equipment, and Lift Thickness ^{a,b} (Adapted from AASHTO 2015)..... | 13 |
| Table 1.11: Stabilization Geotextile Property Requirements (Adapted from AASHTO 2015) | 13 |
| Table 1.12: Permanent Erosion Control Geotextile Requirements (Adapted from AASHTO 2015) | 14 |
| Table 1.13: Temporary Silt Fence Property Requirements (Adapted from AASHTO 2015) | 14 |
| Table 1.14: Paving Fabric Property Requirements ^a (Adapted from AASHTO 2015)..... | 14 |
| Table 2.1: Bale Material Composition Distribution | 19 |
| Table 4.1: 100% Cotton Denim - 400%/min Strain Rate Results..... | 34 |
| Table 4.2: 100% Cotton Denim - 100%/min Strain Rate Results..... | 35 |
| Table 4.3: 100% Cotton Denim - 10%/min Strain Rate Results..... | 35 |
| Table 4.4: 100% Cotton Denim - 5%/min Strain Rate Results..... | 36 |
| Table 4.5: 100% Cotton Denim - 1%/min Strain Rate Results..... | 36 |
| Table 4.6: 100% Cotton Denim - Average Strain Rate Results..... | 37 |
| Table 4.7: 100% Polyester - 400%/min Strain Rate Results | 39 |
| Table 4.8: 100% Polyester - 100%/min Strain Rate Results | 39 |
| Table 4.9: 100% Polyester - 10%/min Strain Rate Results | 40 |
| Table 4.10: 100% Polyester - 5%/min Strain Rate Results | 40 |
| Table 4.11: 100% Polyester - 1%/min Strain Rate Results | 41 |

| | |
|--|----|
| Table 4.12: 100% Polyester - Average Strain Rate Results..... | 42 |
| Table 4.13: 100% Cotton Denim Machine Direction Testing Results Summary..... | 50 |
| Table 4.14: 100% Cotton Denim Cross Direction Testing Results Summary..... | 57 |
| Table 4.15: 100% Cotton Denim Break Force Comparison - Machine vs. Cross Direction..... | 58 |
| Table 4.16: 100% Cotton Denim Machine Break Strain Comparison - Machine vs. Cross Direction | 59 |
| Table 4.17: 100% Cotton Denim Global I.A. Break Strain Comparison - Machine vs. Cross Direction | 59 |
| Table 4.18: 100% Cotton Denim Local I.A. Break Strain Comparison - Machine vs. Cross Direction | 60 |
| Table 4.19: 100% Polyester Machine Direction Testing Results Summary..... | 68 |
| Table 4.20: 100% Polyester Cross Direction Testing Results Summary..... | 75 |
| Table 4.21: 100% Polyester Break Force Comparison - Machine vs. Cross Direction..... | 76 |
| Table 4.22: 100% Polyester Machine Break Strain Comparison - Machine vs. Cross Direction . | 77 |
| Table 4.23: 100% Polyester Global I.A. Break Strain Comparison - Machine vs. Cross Direction | 77 |
| Table 4.24: 100% Polyester Local I.A. Break Strain Comparison - Machine vs. Cross Direction | 78 |
| Table 6.1: Quality Condition Rating System..... | 83 |

LIST OF FIGURES

| | |
|---|----|
| Figure 2.1 University of Delaware students sorting one bale..... | 18 |
| Figure 2.2 Selecting materials for testing. | 20 |
| Figure 2.3 (a) A 175 mm x 100 mm cut specimen, and (b) a cut specimen with painted targets.. | 21 |
| Figure 2.4 Materials required to create custom screen-printing stencil..... | 22 |
| Figure 2.5 (a) Emulsion application to screen, (b) emulsion drying in dark atmosphere, and (c) screen after the emulsion has dried. | 22 |
| Figure 2.6 (a) Placement of transparency paper, and (b/c) application of light to screen. | 23 |
| Figure 2.7 Screen washing after light exposure..... | 23 |
| Figure 2.8 Preparation of textile specimens for permittivity testing: (a) Denim specimen and associated preparation tools, (b) cutting of specimen, and (c) final specimen for permittivity testing..... | 24 |
| Figure 3.1 General setup for tensile testing. | 27 |
| Figure 3.2. Strain calculation approach for tested specimens: a) Idealized initial position of marking points, with data point groups that were assessed identified, and b) final position of marking points, with data point groups that were assessed identified..... | 28 |
| Figure 3.3 Permittivity testing setup. | 29 |
| Figure 3.4 Calibration curves for the testing apparatus and for the standard No. 200 sieve. | 31 |
| Figure 3.5. Steps to permittivity testing: (a) Measuring head with calipers, and (b) measuring flow volume..... | 32 |
| Figure 3.6 Steps to permittivity testing: (a) Keeping time on a stopwatch to determine flow rate, and (b) checking dissolved oxygen levels with AMTAST Portable Dissolved Oxygen and Temperature Meter..... | 33 |
| Figure 4.1. 100% cotton denim - 400%/min strain rate results. | 35 |
| Figure 4.2. 100% cotton denim - 100%/min strain rate results. | 35 |
| Figure 4.3. 100% cotton denim - 10%/min strain rate results. | 36 |
| Figure 4.4. 100% cotton denim - 5%/min strain rate results. | 36 |
| Figure 4.5. 100% cotton denim - 1%/min strain rate results. | 37 |
| Figure 4.6. 100% cotton denim - average strain rate results..... | 38 |
| Figure 4.7. Strain rate effect on break force in 100% cotton denim..... | 38 |
| Figure 4.8. 100% polyester - 400%/min strain rate results..... | 39 |
| Figure 4.9. 100% polyester - 100%/min strain rate results..... | 40 |
| Figure 4.10. 100% polyester - 10%/min strain rate results..... | 40 |
| Figure 4.11. 100% polyester - 5%/min strain rate results..... | 41 |

| | |
|--|----|
| Figure 4.12. 100% polyester - 1%/min strain rate results..... | 41 |
| Figure 4.13. 100% polyester - average strain rate results..... | 42 |
| Figure 4.14. Strain rate effect on break force in 100% polyester..... | 43 |
| Figure 4.15 100% cotton denim machine direction - machine break strain vs. break force..... | 44 |
| Figure 4.16 100% cotton denim machine direction - global image analysis break strain vs. break force..... | 45 |
| Figure 4.17 100% cotton denim machine direction - local image analysis break strain vs. break force..... | 45 |
| Figure 4.18 100% cotton denim machine direction - combined break strains vs. break force..... | 46 |
| Figure 4.19 100% cotton denim machine direction - break force histogram and box plot..... | 47 |
| Figure 4.20 100% cotton denim machine direction - machine break strain histogram and box plot..... | 48 |
| Figure 4.21 100% cotton denim machine direction - global image analysis break strain histogram and box plot..... | 49 |
| Figure 4.22 100% cotton denim machine direction - local image analysis break strain histogram and box plot..... | 50 |
| Figure 4.23 100% cotton denim cross direction - machine break strain vs. break force..... | 51 |
| Figure 4.24 100% cotton denim cross direction - global image analysis break strain vs. break force..... | 52 |
| Figure 4.25 100% cotton denim cross direction - local image analysis break strain vs. break force..... | 52 |
| Figure 4.26 100% cotton denim cross direction - combined break strains vs. break force..... | 53 |
| Figure 4.27 100% cotton denim cross direction - break force histogram and box plot..... | 54 |
| Figure 4.28 100% cotton denim cross direction - machine break strain histogram and box plot..... | 55 |
| Figure 4.29 100% cotton denim cross direction - global image analysis break strain histogram and box plot..... | 56 |
| Figure 4.30 100% cotton denim cross direction - local image analysis break strain histogram and box plot..... | 57 |
| Figure 4.31 100% cotton denim permittivity test results..... | 61 |
| Figure 4.32 100% polyester machine direction - machine break strain vs. break force..... | 62 |
| Figure 4.33 100% polyester machine direction - global image analysis break strain vs. break force..... | 62 |
| Figure 4.34 100% polyester machine direction - local image analysis break strain vs. break force..... | 63 |
| Figure 4.35 100% polyester machine direction - combined break strains vs. break force..... | 63 |
| Figure 4.36 100% polyester machine direction - break force histogram and box plot..... | 65 |

| | |
|--|----|
| Figure 4.37 100% polyester machine direction - machine break strain histogram and box plot... | 66 |
| Figure 4.38 100% polyester machine direction - global image analysis break strain histogram and box plot. | 67 |
| Figure 4.39 100% polyester machine direction - local image analysis break strain histogram and box plot. | 68 |
| Figure 4.40 100% polyester cross direction - machine break strain vs. break force. | 69 |
| Figure 4.41 100% polyester cross direction - global image analysis break strain vs. break force. | 70 |
| Figure 4.42 100% polyester cross direction - local image analysis break strain vs. break force. | 70 |
| Figure 4.43 100% polyester cross direction - combined break strains vs. break force..... | 71 |
| Figure 4.44 100% polyester cross direction - break force histogram and box plot. | 72 |
| Figure 4.45 100% polyester cross direction - machine break strain histogram and box plot. | 73 |
| Figure 4.46 100% polyester cross direction - global image analysis break strain histogram and box plot. | 74 |
| Figure 4.47 100% polyester cross direction - local image analysis break strain histogram and box plot. | 75 |
| Figure 4.48 100% polyester permittivity results..... | 78 |
| Figure 6.1 Fiberizer shredded 100% polyester (a) woven, (b) knit, and (c) 55%/45% cotton/polyester blended knit..... | 84 |
| Figure 6.2 100% Cotton (a) Fiberizer shredded woven, (b) Fiberizer shredded knit, and (c) researcher's equipment shredded woven. | 84 |
| Figure 6.3 (a) Carding wire wound cylinder drums for shredding recycled textiles and (b) 100% cotton denim shredded from the drums. | 85 |
| Figure 6.4 Researchers' fiber shredder design..... | 85 |
| Figure 6.5 Charred shredded cotton and polyester recycled textiles after attempted thermal bonding. | 85 |

CHAPTER 1 – DESCRIPTION OF THE PROBLEM

1.1 Introduction

In the United States alone, 16.03 million tons of textile waste were produced in 2016 (Environmental Protection Agency (EPA) 2018). Of that 16.03 million tons of textile waste, most of it ended up in landfills, 10.53 million tons; of the remaining textile waste, 2.45 million tons were recycled, and 3.05 million tons were combusted for energy recovery (EPA 2018a). According to the EPA (2018b), there has been an increase of 276% of generated textile waste by weight between 1990 and 2015. Given that apparel and home textiles are routinely landfilled, and that this large waste stream is increasing drastically in volume on a year to year basis (EPA 2018b), alternative methods for reducing, reusing, and/or recycling these materials are needed. The current study suggests that recycled textiles may have a place for use in some engineering applications where new geotextiles or geosynthetics are traditionally used. Potentially, this waste stream could be a feedstock that could improve the sustainability and reduce the cost of geotextiles/geosynthetics for a wide variety of transportation infrastructure applications.

Utilizing recycled materials to make geotextiles is not a completely new idea. Nonwoven geotextiles have been produced with recycled materials such as soda bottles (Gorchakova et al. 2013). Researchers have also used recycled fibers to make nonwoven geotextiles for specific applications such as erosion control (Lin et al. 2013), water retention (Li et al. 2016), clay soil reinforcement (Chen et al. 2015), and other more generic applications (Leon et al. 2016, Trajkovic et al. 2015, Lin et al. 2011). Researchers have considered a wide variety of material types to produce geotextiles from recycled materials including the following: recycled polyethylene terephthalate (PET) (Lin et al. 2013), recycled polyester (Trajkovic et al. 2015), preconsumer polyester waste fabric (Leon et al. 2016), recycled Kevlar (Lin et al. 2013), Kevlar selvages (Li et al. 2016), polypropylene selvages (Lin et al. 2011), postconsumer used polypropylene textile bags (Chen et al. 2015), and postconsumer polyacrylonitrile (PAN) knitted clothes (Leon et al. 2016).

It should be noted that only one type of used clothing, PAN knits, has been evaluated and tested as an input for geotextiles. A variety of textile materials show promise for different geotextile applications and for creating a circular textile industry or economy (Leon et al. 2016). Circular use, also called cradle to cradle design or use, refers to designing and utilizing materials in such a way that they can be reutilized so that the materials can have multiple lives (McDonough and Braungart, 2002).

The American Society for Testing and Materials (ASTM) defines a geosynthetic as “a planar product manufactured from polymeric material used with soil, rock, earth, or other geotechnical engineering related material as an integral part of a man-made project, structure, or system” (ASTM D4439 2017). The two basic goals of soil improvement using geosynthetics are to improve the behavior of the system as a whole and to be more economical than other improvement techniques (Koerner 2005). The use of planar materials to improve structures and systems dates back to 3000 B.C., when timbers were lashed together to make a planar surface to improve roads over peat bogs in Britain (Dewar 1962). In modern usage, numerous geosynthetic products are available, with at least eight different categorical product types being commonly used, including:

geotextiles, geogrids, geonets, geomembranes, geosynthetic clay liners, geopipes, geofoam, and geocomposites (Koerner 2005).

Looking more closely at geotextiles, it can be observed that they are similar to common textiles but instead of cotton, wool, or silk fibers, the fibers are synthetic (Koerner 2005). In some cases, geotextiles with natural fibers such as cotton, jute, coir, and sisal have been used for temporary applications or where biodegradability of the geotextile is a favorable characteristic (e.g., Sarsby 2007). Modern use of geotextiles is typically dated back to the 1950s, where geotextiles were used behind seawalls as filters to facilitate drainage behind the walls while keeping the soil from escaping from the joints (Agerschou 1961, Barrett 1966). Barret (1966) also discussed geotextiles being used for scour protection in coastal environments as well as for use with water collector pipes. For this application, collector pipes could be wrapped in geotextile to prevent soil infiltration while still allowing water to freely flow and in some cases, it was possible for the geotextile to replace the collector pipe all together and act as a drain. Today, geotextiles are used in a wide variety of applications with their main functions consisting of separation, filtration, reinforcement, drainage, and protection (Zornbreg 2017, Shukla and Yin 2006, Koerner 2005, Santvoort 1995). Geotextiles being used as a fluid barrier is discussed as a sixth common geotextile function by the Federal Highway Administration (FHWA) (Holtz et al. 2008).

1.2 Functions and Applications

1.2.1 Separation

Koerner (2005) defines geotextile separation as the placement of a flexible porous textile between dissimilar materials so that the integrity and functioning of both materials can remain intact and be improved. Geotextiles are used as a form of separation by placing a layer of the textile between two different materials (typically soil or aggregate materials) to maintain the properties of both those materials separately. Geotextiles always serve a separation function because if they do not, any other function they are performing in that application cannot be served (Koerner 2005). Key properties of geotextiles for separation include soil retention and permeability (Santvoort 1995). Soil retention is directly related to the opening size of the geotextile and the grain size of the soils that are to be separated (Koerner 2005). Table 1.1 displays several applications where separation is the primary function; in this table, “X” indicates the primary function while “O” indicates a secondary function.

Table 1.1: Geotextile Applications - Primary Separation Function (Adapted from Holtz et al. 2008)

| Application | Separation | Filtration | Reinforcement | Drainage | Protection | Fluid Barrier |
|---------------------------------------|------------|------------|---------------|----------|------------|---------------|
| Unpaved Roads (temporary & permanent) | X | O | O | O | | |
| Paved Roads (temporary & permanent) | X | O | | O | | |
| Railroads (new construction) | X | O | O | O | | |
| Railroads (rehabilitation) | X | O | O | O | | |
| Paved & Unpaved Parking Facilities | X | O | O | O | | |
| Construction Access Roads | X | O | O | O | | |
| Working Platforms | X | O | O | O | | |
| Landfill Covers | X | | O | O | O | |
| Preloading (stabilization) | X | | O | O | | |
| General Fill Areas | X | O | O | O | | |
| Marine Causeways | X | O | O | O | | |
| Coastal & River Protection | X | O | O | O | | |
| Cattle Corrals | X | O | O | O | | |
| Sports Fields | X | O | | O | O | |

As shown in Table 1.1, the most common geotextile application is to prevent the mixing of a larger particle sized aggregate base layer with a fine-grained soil subgrade layer (Koerner 2005). Zornberg (2017) states that even a small amount of fine grain soil entering the granular layer can decrease its shear strength, decrease the hydraulic conductivity, and increase frost susceptibility; the aggregate base could eventually behave more like a fine-grained soil if enough infiltration occurs. For this purpose, geotextiles are used between the subgrade and aggregate base layers in paved and unpaved roads, between subgrade and ballast in railroads, beneath sidewalk slabs, beneath parking lots, and between different soil layers in embankments (e.g., Zornberg 2017, Li et al. 2016).

During construction, geotextiles can be used for construction access roads as well as working platforms. Construction access roads are temporary roads used for construction vehicles to access the site; geotextiles would be used similarly to unpaved roads for construction access roads. Working platforms are used if the underlying soil is too weak to support the construction equipment needed on site; this platform is created by using geosynthetics in combination with gravel to form a stronger base (Holtz et al. 2008).

A temporary cover is required over an active landfill after each day, with a much more durable cover system being used to cap the landfill when it is set to be permanently closed. For this application, a geotextile can potentially be used for daily coverage to minimize leachate generation, control odors, protect against littering, and eliminate scavenging (Koerner 2005). However, it should be noted that geotextiles cannot be used for permanent coverage as they do not

serve the function of a fluid barrier, which is necessary to prevent rainfall infiltration. Geotextiles are also used for stabilization of preloading embankments on soft or problematic foundation soils; similar to this application, geotextiles are also used for general fill areas (Holtz et al. 2008).

When using geotextiles in marine environments, several functions come in to play in addition to the primary function of separation: filtration, drainage, and reinforcement. Geotextiles are used in marine environments in the following ways: erosion control; filtration for stream bank protection; cut and fill slope protection; protection of various small drainage structures and ditches; wave protection for marine causeways and shoreline roadway embankments; and scour protection for structures that in direct contact with moving water (Holtz et al. 2008).

Holtz et al. (2008) also notes some miscellaneous applications for geotextiles where the primary function is separation. This includes sports field where a geotextile layer is used to separate the in-situ soils from the playing surface whether that be some artificial surface or a planted sod. The geotextile is also used for drainage, filtration, and protection purposes. Geotextiles are also used in livestock operations to help eliminate the extremely wet soil conditions that occur (Ruhl et al. 1999). Ruhl et al. (1999) states that using geotextiles with gravel can help provided a proper surface so livestock operations can continue in a safe manner.

1.2.2 Filtration

Filtration is perhaps the oldest function of geotextiles and is an important function for geotextiles that are used for transportation infrastructure applications. Geotextiles are used for filtration by holding back soil while enabling water or other liquids to flow freely through the fabric; important properties for a geotextile being used for filtration purposes are cross-plane permeability and soil retention (Koerner 2005). It should be stated that the geotextile will only retain soil with particles larger than the textile pore opening size (Shukla and Yin 2006). Table 1.2 displays several applications where filtration is the primary function; in this table, “X” indicates the primary function while “O” indicates a secondary function.

Table 1.2: Geotextile Applications - Primary Filtration Function (Adapted from Holtz et al. 2008)

| Application | Separation | Filtration | Reinforcement | Drainage | Protection | Fluid Barrier |
|--|------------|------------|---------------|----------|------------|---------------|
| Trench Drains | O | X | | O | | |
| Pipe Wrapping | O | X | | O | O | |
| Base Course Drains | O | X | | O | | |
| Structural Drains | O | X | | O | | |
| Toe Drains in Dams | O | X | | O | | |
| Culvert Outlets | O | X | | | | |
| High Embankments | | X | | O | | |
| Frost Protection | O | X | O | O | | |
| Filter Below Fabric-Form | O | X | | O | | |
| Silt Fences | O | X | | O | | |
| Silt Screens | O | X | | | | |
| Reverse Filters for Erosion Control | O | X | | | | |
| Seeding and Mulching | O | X | | | | |
| Beneath Gabions | O | X | | | | |
| Ditch Armoring | O | X | | | | |
| Embankment Protection (Coastal) | O | X | | | | |
| Embankment Protection (Rivers & Streams) | O | X | | | | |
| Embankment Protection (Lakes) | O | X | | | | |
| Vertical Drains (Wicks) | O | X | | | | |

Geotextiles can be placed around crushed stone surrounding drains to prevent soil from intruding into the crushed stone while allowing water to flow through the geotextile, then through the crushed stone into the drain; similarly, the geotextile can be placed around crushed stone without the underdrain for the same purpose as the crushed stone acts as a drain in this case. Wrapping a geotextile around a perforated undrain pipe prevents soil from intruding into the perforations, thus clogging the pipe and preventing drainage. If the geotextile does not prevent soil particles from entering the drainage system, the entire system can fail. These failures can be catastrophic when they occur in structures like dams, retaining walls, and bridge abutments. Geotextiles can also be placed at culvert outlets to filter out sediment and debris before allowing water to travel through (Guyer et al. 2013).

Geotextiles can be used to replace sand filters as a surface runoff treatment system (Franks et al. 2012). Using geotextiles in this application has advantages over sand filters in that it is easier to install and remove and the geotextiles are much lighter in weight and can be rolled or folded for transportation (Franks et al. 2012).

To reduce frost heave geotextiles have been used as they can act as capillary breaks to reduce the flow of water to the freezing point (Henry 1990).

A very common and popular use of geotextiles is in silt fencing applications since some type of sediment and erosion control is required in all construction processes (Koerner 2005). To perform as a silt fence, the geotextile is typically attached to posts in the ground with the bottom of the textile anchored in a small trench so no sediment can escape underneath it; this allows water to flow freely while retaining any sediments to the construction site (Koerner 2005). Similar to silt fencing applications, geotextiles can also be used as silt screens, which are typically used for marine applications. Typically, these silt screens are seen in areas where pollutants are trying to be filtered out or contained. For example, the geotextile silt screen can be placed across the width of a stream to collect debris while allowing the stream to continue to flow. A geotextile silt screen can also be used as a protective barrier to hinder particles from spreading from the dredging area of a lake (Bremle et al. 1998).

Geotextiles can be used as revegetation mats and blankets in that the geotextile holds the soil and seeding in place while allowing water to enter the system and allowing the vegetation to grow through the textile; biodegradable geotextiles see high usage in this application as once vegetation has rooted into the slope, it becomes stabilized and there is no need for the geotextile anymore (Caltrans 2003, Lekha 2004).

1.2.3 Reinforcement

Geotextiles are also used for their reinforcement capabilities in several different applications. One reason geotextiles are effective for reinforcement is due to the fact that soil is good in compression but poor in tension while geotextiles are good in tension but poor in compression; the combination of these materials thus forms a composite reinforced soil mass with high compressive and tensile strengths (Shukla and Yin 2006, Koerner 2005, Santvoort 1995). This is done by improving the properties of the soil via the soil's own inclusion; these properties include one or more of the following: strength, stiffness, and permeability (Shukla and Yin 2006, Santvoort 1995). Tensile strength and material stiffness are the main properties that one is concerned about when using geotextiles for a reinforcement application. Adding reinforcement can also allow for an overall increase in permeability in the soil mass, which can be advantageous to the soil's strength by encouraging more drainage for a reinforced soil relative to the same soil if the reinforcement were not included. Table 1.3 displays several applications where reinforcement is the primary function; in this table, "X" indicates the primary function while "O" indicates a secondary function.

Table 1.3: Geotextile Applications - Primary Reinforcement Function (Adapted from Holtz et al. 2008)

| Application | Separation | Filtration | Reinforcement | Drainage | Protection | Fluid Barrier |
|--|------------|------------|---------------|----------|------------|---------------|
| Pavement Overlays | | | X | | | |
| Membrane Support | | | X | O | | |
| Subbase Reinforcement in Roadways & Retaining Structures | | O | X | | | |
| Geosynthetic Reinforced Soil Walls/Abutments | | | X | O | | |
| Embankment Reinforcement | O | O | X | O | O | |
| Fill Reinforcement | | | X | O | | |
| Foundation Support | | | X | O | | |
| Soil Encapsulation | | | X | O | | |
| Net Against Rockfalls | O | O | X | O | | |
| Fabric Retention Systems | | | X | O | | |
| Sandbags | | | X | O | | |
| Reinforcement of Membranes | | | X | | | |
| Load Redistribution | | | X | | O | |
| Bridging Nonuniformity Soft Soil Areas | O | | X | | | |
| Encapsulated Hydraulic Fills | O | | X | | | |
| Bridge Piles for Fill Placement | O | | X | | | |

Geotextiles can be used in two ways to reinforce embankments. Both are to prevent embankment-edge failure but the first is caused by the collapse of the subsoil in less steep embankments (Santvoort 1995). To prevent this, a layer of geotextile can be placed beneath the constructed embankment to deliver a reaction force to contribute to the resistance against the sliding of the embankment (Santvoort 1995). The second prevents embankment-edge failure in steeper embankments by incorporating layers of geotextile within the embankment itself (Santvoort 1995). In both cases, the geotextile must be long enough to extend past the slip surface by a calculated distance. The geotextile provides tensile reinforcement, which thus reduces the stresses and strain with the embankment allowing the embankment to resist large differential settlements, lateral spreading, or slope movements (FEMA 2008). Geotextiles are used similarly to construct geosynthetic reinforced soil (GRS) retaining walls where the main purpose is to restrict the lateral movement of the soil behind the wall. GRS uses closely spaced layers of geosynthetic reinforcement with compacted granular fill to create a soil mass used behind a wall face (Wu and Ooi 2015).

The geosynthetic reinforced soil integrated bridge system (GRS-IBS) is a composite bridge structure with prefabricated bridge superstructure elements atop geosynthetic reinforced soil (GRS) abutments (Adams et al. 2011). The GRS abutment is constructed by alternating layers of compacted soil with geosynthetic reinforcements (Talebi 2016). The geosynthetic is frictionally

connected to the facing elements, most commonly concrete masonry unit (CMU) blocks, of the GRS abutment; there are no connection elements as seen in mechanically stabilized earth (MSE) structures (Adams et al. 2011). The close spacing of the reinforcement allows for stress arching between the soil reinforcement layers to play a more significant role thus preventing the facing elements from holding back as much soil as typically seen in MSE facing elements (Talebi 2016).

Geotextiles can also be used between old and new layers of asphalt to mitigate reflective cracking in the new asphalt layer (Zornberg 2017). When a new layer of asphalt is placed, the crack from the old layer grows up to the surface; this mechanism is said to be traffic or thermally induced (Shukla and Yin 2006). The geotextile develops tensile forces near the crack and reduces the stress and strain in the new asphalt and thus preventing the continuation of the existing crack into the new material (Zornberg 2017). A geotextile layer can also be placed between the subbase and the subgrade of the roadway; by placing the geotextile here, it will ultimately increase the bearing capacity of the subgrade soils. (Zornberg 2017). If wheel load stresses are large enough to cause plastic deformation, thus causing wheel ruts in the subgrade, a geotextile with a high tensile modulus placed beneath the subgrade will help support the large wheel load stress; this membrane support application is typically for temporary roads (Holtz et al. 2008).

If foundation soils do not have adequate strengths for a given application, geotextiles can be used in some cases to provide reinforcement; this will increase the stability of the foundation soils and prevent failure (Holtz et al. 2008). Soil encapsulation is another application used to reinforce foundation soils. One example of this is seen in geotextile-encapsulated granular columns; the geotextile can provide the required confining pressure, allowing for increases in the bearing capacity and stiffness of the column (Khabbazian et al. 2010).

Other applications where geotextiles are primarily used for their reinforcement component are as follows: as a net to protect against rockfalls, in fabric retention systems, sand bags, reinforcement on membranes, load redistribution, bridging nonuniformity in soft soil areas, encapsulated hydraulic fills, and bridge piles for fill placement (Holtz et al. 2008).

1.2.4 Drainage

Geotextiles used to transmit liquids along the plane of placement are said to be used for their drainage function (Koerner 2005). Important properties for geotextiles to be used for drainage include permeability in both the in-plane and cross-plane, as well as soil retention or pore opening size (Koerner 2005). Without proper drainage in a soil system, high pore-water pressure can develop or the water in the system can be subject to freezing and thawing cycles; these instances can ultimately cause a structure or system to fail in some form. Table 1.4 displays several applications where drainage is the primary function; in this table, “X” indicates the primary function while “O” indicates a secondary function.

Table 1.4: Geotextile Applications - Primary Drainage Function (Adapted from Holtz et al. 2008)

| Application | Separation | Filtration | Reinforcement | Drainage | Protection | Fluid Barrier |
|---|------------|------------|---------------|----------|------------|---------------|
| Retaining Walls | O | O | | X | | |
| Earth Dams | | O | | X | | |
| Vertical Drains | O | O | | X | | |
| Horizontal Drains | | | O | X | | |
| Below Membranes (Drainage of Gas and Water) | | | O | X | O | |
| Below Concrete (Decking & Slabs) | | | | X | O | |

The applications shown in Table 1.4 all use geotextile in a similar manner to drain water from a structure or system. Geotextiles are used in retaining walls and earth dams to prevent pore-water pressure from building up and thus ultimately failing the structure; this approach is also used beneath membranes and concrete decks/slabs. Depending upon its configuration in the field, the geotextile itself acts as a vertical or horizontal “drain” to remove water.

1.2.5 Protection

Geotextiles used to prevent material from moving, washing away, or any other form of erosion are said to be used mainly for the function of protection. The protection function also describes applications where the geotextile is preventing damage to a structure or soil mass. Table 1.5 displays several applications where protection is the primary function; in this table, “X” indicates the primary function while “O” indicates a secondary function.

Table 1.5: Geotextile Applications - Primary Protection Function (Adapted from Holtz et al. 2008)

| Application | Separation | Filtration | Reinforcement | Drainage | Protection | Fluid Barrier |
|---------------------------|------------|------------|---------------|----------|------------|---------------|
| Geomembrane Cushion | | | | O | X | |
| Asphalt Overlay | | | | | X | O |
| Temporary Erosion Control | | | | | X | O |
| Permanent Erosion Control | | | O | | X | O |

If the geotextile is asphalt-saturated and properly installed, it will protect the pavement beneath it from any further damage due to infiltration of surface water; for this reason, the geotextile will provide the protection function as a stress relief interlay and will provide the fluid barrier function as a water proofing membrane (Holtz et al. 2008). If this layer of geotextile is sufficiently thick, it can be used as a cushion layer and will absorb movement from the old pavement without transferring that movement and stress to the new pavement (Holtz et al. 2008).

To prevent erosion on slopes, geotextiles are placed over the soil surface and will protect the slope from water and wind erosion; this is typically used for slope stabilization in steep slopes and slopes where the potential for erosion is high (Caltrans 2003, Theisen 1992).

1.2.6 Fluid Barrier

Fluid barriers are used to impede the flow of liquid or gas (Holtz et al. 2008). For this reason, geotextiles can rarely serve this function as they are fundamentally porous (Koerner 2005). However, Table 1.6 displays several applications where fluid barrier is the primary function of geotextiles; in this table, “X” indicates the primary function while “O” indicates a secondary function.

Table 1.6: Geotextile Applications - Primary Fluid Barrier Function (Adapted from Holtz et al. 2008)

| Application | Separation | Filtration | Reinforcement | Drainage | Protection | Fluid Barrier |
|---|------------|------------|---------------|----------|------------|---------------|
| Asphalt Pavement Overlays | | | | | O | X |
| Liners for Canals and Reservoirs | | | | | | X |
| Liners for Landfills and Waste Repositories | | | | | | X |
| Covers for Landfill and Waster Repositories | | | | | | X |
| Cutoff Walls for Seepage Control | | | | | | X |
| Waterproofing Tunnels | | | | | | X |
| Facing for Dams | | | | | | X |
| Membrane Encapsulated Soil Layers | | | | | | X |
| Expansive Soils | | | | | | X |
| Flexible Formwork | | | | | | X |

Geotextiles used as asphalt pavement overlays, liners for canals and reservoirs, liners for landfills and waste repositories, covers for landfill and waste repositories, cutoff walls for seepage control, waterproofing tunnels, facing for dams, membrane encapsulated soil layers, expansive soils, and flexible framework all require the primary function of fluid barrier. As discussed, this is generally not possible for most geotextiles as they are characteristically porous in nature.

1.3 Geotextile Property Requirements

Geotextile properties for several different functions and applications were gathered from the American Association of State Highway and Transportation Officials (AASHTO) and the Federal Highway Administration (FHWA). AASHTO Specification M288, *Geotextile Specification for Highway Applications*, discusses geotextile property requirements for strength, subsurface drainage, separation, stabilization, and permanent erosion control applications (AASHTO 2015). AASHTO Specification M288 (2015) also gives geotextile property requirements for temporary silt fence applications as well as paving fabric applications. FHWA Publication NHI-07-092, *Geosynthetic Design & Construction Guidelines*, uses the same geotextile property requirements for subsurface drainage, permanent erosion control, temporary silt fence, stabilization, separation, and paving fabric (Holtz et al. 2008). However, FHWA Publication NHI-07-092 (2008), has unique specifications for geotextiles to be used for embankment reinforcement, retaining walls, and reinforced slopes. Ultimately, the FHWA manual follows AASHTO Specification M288 (Zornberg and Thompson 2012). According to Zornberg and Thompson (2012), by identifying an appropriate survivability class based on the site conditions, the required properties of the geotextile can be determined. A description of AASHTO’s survivability classes are as follows: Class 1 is for severe or harsh survivability conditions where there is a greater potential for geotextile damage; Class 2 is for typical survivability conditions (this is the default classification to be used in absence

of site-specific information); and Class 3 is for mild survivability conditions where there is little or no potential for geotextile damage (Koerner 2005).

In the current study, the geotextile properties that were focused on were tensile strength and permittivity. Tables 1.7 through 1.14 were adapted from AASHTO Specification M288 (2015) to show the properties that were of interest to this study.

Table 1.7: Geotextile Strength Property Requirements (Adapted from AASHTO M288, 2015)

| | | Geotextile Class ^a | | | | | |
|---------------|-------------|-------------------------------|--------------------|-----------------------|--------------------|-----------------------|--------------------|
| | | Class 1 | | Class 2 | | Class 3 | |
| | | Geotextile Elongation | | Geotextile Elongation | | Geotextile Elongation | |
| | Test Method | < 50% ^b | ≥ 50% ^b | < 50% ^b | ≥ 50% ^b | < 50% ^b | ≥ 50% ^b |
| Grab Strength | ASTM D4632 | 1400 N | 900 N | 1100 N | 700 N | 800 N | 500 N |

^a All numeric values represent minimum average roll value (MARV) in the weaker principal direction.

^b As measured in accordance with ASTM D4632.

Table 1.8: Subsurface Drainage Geotextile Requirements (Adapted from AASHTO 2015)

| | | Percent in-situ Soil Passing 0.075 mm ^a | | |
|------------------------------|-------------|--|-----------------------|-----------------------|
| | | < 15% | 15% - 50% | > 50% |
| Geotextile Class | Test Method | Class 2 ^b | Class 2 ^b | Class 2 ^b |
| Permittivity ^{c, d} | ASTM D4491 | 0.5 sec ⁻¹ | 0.2 sec ⁻¹ | 0.1 sec ⁻¹ |

^a Based on grain size analysis of in-situ soil in accordance with AASHTO T88.

^b This is the default geotextile selection. The engineer may specify Class 3 for trench drain applications if the engineer has found the Class 3 geotextiles to have sufficient survivability based on field experience; or based on laboratory testing and visual inspection of a geotextile sample removed from a field test section constructed under anticipated field conditions; or subsurface drain depth is less than 2 m, drain aggregate diameter is less than 30 mm, and compaction requirement is less than 95 percent of AASHTO T99.

^c These default filtration property values are based on the predominant particle sizes of in-situ soil. In addition to the default permittivity value, the engineer may require geotextile permeability and/or performance testing based on engineering design for drainage systems in problematic soil environments.

^d Site-specific geotextile design should be performed especially if one or more of the following problematic soil environments are encountered: unstable or highly erodible soils such as noncohesive silts; gap-graded soils; alternating sand/silt laminated soils; dispersive clays; and/or rock flour.

Table 1.9: Separation Geotextile Property Requirements (Adapted from AASHTO 2015)

| | | Requirements |
|------------------|-------------|--|
| Geotextile Class | Test Method | See Required Degree of Survivability in Table 1.10 |
| Permittivity | ASTM D4491 | 0.2 sec ^{-1 a} |

^a Default value. Permittivity of the geotextile should be greater than that of the soil ($\Psi_g > \Psi_s$). The engineer may also require the permeability of the geotextile to be greater than that of the soil ($k_g > k_s$).

Table 1.10: Required Degree of Survivability as a Function of Subgrade Conditions, Construction Equipment, and Lift Thickness^{a,b} (Adapted from AASHTO 2015)

| | Low Ground Pressure Equipment < 25 kPa | Medium Ground Pressure Equipment > 25 to < 50 kPa | High Ground Pressure Equipment > 50 kPa |
|---|---|--|--|
| Subgrade has been cleared of all obstacles except grass, weeds, leaves, and fine wood debris. Surface is smooth and level so that any shallow depressions and humps do not exceed 450 mm in depth or height. All larger depressions are filled. Alternatively, a smooth working table may be placed. | Low (Class 3) | Moderate (Class 2) | High (Class 1) |
| Subgrade has been cleared of obstacles larger than small to moderate-sized tree limbs and rocks. Tree trunks and stumps should be removed or covered with partial working table. Depressions and humps should not exceed 450 mm in depth or height. Larger depressions should be filled. | Moderate (Class 2) | High (Class 1) | Very High (Class 1+ ^c) |
| Minimal site preparation is required. Trees may be felled, delimited, and left in place. Stumps should be cut to project not more than ±150 mm above subgrade. Geotextile may be draped directly over the tree trunks, stumps, large depressions and humps, holes, stream channels, and large boulders. Items should be removed only if placing the geotextile and cover material over them will distort the finished road surface. | High (Class 1) | Very High (Class 1+ ^c) | Not Recommended |

^a Recommendations are for 150 to 300 mm initial lift thickness. For other initial lift thickness:

1. 300 to 450 mm: reduce survivability requirements one level;
2. 450 to 600 mm: reduce survivability requirement two levels;
3. > 600 mm: reduce survivability requirement three levels.

^b For special construction techniques such as prerutting, increase the geotextile survivability requirement on level. Placement of excessive initial cover material thickness may cause bearing failure of the soft subgrade.

^c Class 1+ properties are higher than Class 1, but not defined at this time and, if used, must be specified by the purchaser.

Table 1.11: Stabilization Geotextile Property Requirements (Adapted from AASHTO 2015)

| | Test Method | Requirements |
|------------------|-------------|-------------------------------------|
| Geotextile Class | | Class 1 ^a |
| Permittivity | ASTM D4491 | 0.05 sec ⁻¹ ^b |

^a Default geotextile selection. The engineer may specify a Class 2 or 3 geotextile if the engineer has found the class of geotextile to have sufficient survivability based on field experience or based on laboratory testing and visual inspection of a geotextile sample removed from a field test section constructed under anticipated field conditions.

^b Default value. Permittivity of the geotextile should be greater than that of the soil ($\Psi_g > \Psi_s$). The engineer may also require the permeability of the geotextile to be greater than that of the soil ($k_g > k_s$).

Table 1.12: Permanent Erosion Control Geotextile Requirements (Adapted from AASHTO 2015)

| | <u>Test Method</u> | <u>Percent in-situ Soil Passing 0.075 mm^a</u> | | |
|--------------------------------|--------------------|--|------------------------|------------------------|
| | | <u>< 15%</u> | <u>15% - 50%</u> | <u>> 50%</u> |
| Geotextile Class: | | | | |
| Woven Monofilament Geotextiles | | Class 2 ^b | Class 2 ^b | Class 2 ^b |
| All Other Geotextiles | | Class 1 ^{b,c} | Class 1 ^{b,c} | Class 1 ^{b,c} |
| Permittivity | ASTM D4491 | 0.7 sec ⁻¹ | 0.2 sec ⁻¹ | 0.1 sec ⁻¹ |

^a Based on grain size analysis of in-situ soil in accordance with AASHTO T88.

^b As a general guideline, the default geotextile selection is appropriate for conditions of equal or less severity than either of the following:

1. Armor layer stone weights do not exceed 100 kg, stone drop height is less than 1 m, and no aggregate bedding layer is required.
2. Armor layer stone weighs more than 100 kg, stone drop height is less than 1 m, and the geotextile is protected by a 150-mm thick aggregate bedding layer designed to be compatible with the armor layer. More severe applications require an assessment of geotextile survivability based on a field trial section and may require a geotextile with strength properties.

Table 1.13: Temporary Silt Fence Property Requirements (Adapted from AASHTO 2015)

| | <u>Test Method</u> | <u>Supported Silt Fence^a</u> | <u>Unsupported Silt Fence</u> | |
|---------------------------|--------------------|---|--|---|
| | | | <u>Geotextile Elongation ≥ 50%^b</u> | <u>Geotextile Elongation < 50%^b</u> |
| Grab Strength | ASTM D4632 | | | |
| Machine Direction | | 400 N | 550 N | 550 N |
| X-Machine Direction | | 400 N | 450 N | 450 N |
| Permittivity ^c | ASTM D4491 | 0.05 sec ⁻¹ | 0.05 sec ⁻¹ | 0.05 sec ⁻¹ |

^a Silt fence support shall consist of 14-gauge steel wire with a mesh spacing of 150 mm by 150 mm or prefabricated polymeric mesh of equivalent strength.

^b As measured in accordance with ASTM D4632.

^c These default filtration property values are based on empirical evidence with a variety of sediments. For environmentally sensitive areas, review of previous experience and/or site or regionally specific geotextile tests, such as ASTM D5141, should be performed by the agency to confirm survivability of these requirements.

Table 1.14: Paving Fabric Property Requirements^a (Adapted from AASHTO 2015)

| | <u>Test Method</u> | <u>Type I^b Requirements</u> | <u>Type II^c Requirements</u> |
|---------------------|--------------------|--|---|
| Grab Strength | ASTM D4632 | - | 450 N |
| Tensile Strength | ASTM D5035 | 200 N | - |
| Ultimate Elongation | ASTM D4632 | - | ≥ 50% |

^a All numeric values represent minimum average roll value (MARV) in weaker principal direction.

^b Type I - Fabrics designed with low ultimate elongation. Fabrics may be manufactured with a combination of glass fibers or fiberglass and synthetic polymers.

^c Type II - Fabrics are designed with higher ultimate elongation. Fabrics are manufactured with synthetic polymers.

With the knowledge of geotextile strength and permittivity requirements for different functions, it is possible to determine if a geotextile is feasible for certain applications. This study performs a preliminary investigation into whether recycled textiles can meet the requirements to perform as a geotextile through tensile and permittivity testing; this study also looks to evaluate which applications could be feasible based on the results from the recycled textile testing.

References

- Adams, M., Nicks, J., Stabile, T., Wu, J., Schelatter, W. and Hartmann, J., (2011). “Geosynthetic Reinforced Soil Integrated Bridge System Interim Implementation Guide.” Publication No. FHWA-HRT-11-026, Federal Highway Administration, Washington, DC.
- Agershou, H.A. (1961). “Synthetic Material Filters in Coastal Protection.” *Journal of Waterways Harbors Divison*, ASCE, 87 (WW1), 111-124.
- American Association of State Highway and Transportation Officials (AASHTO) (2015). “Standard Specifications for Geotextile Specification for Highway Applications.” AASHTO Designation Number M288-15, Washington, DC.
- American Society for Testing Materials (ASTM). (2017), “Standard Terminology for Geosynthetics,” West Conshohocken, PA, DOI: 10.1520/D4439-17, www.astm.org.
- Barrett, R.J. (1966). “Use of Plastic Fibers in Coastal Structures.” *Proceeding from the 16th International Conference Coastal Engineers*, Tokyo, Japan, 1048-1067.
- Bremle, G., Larsson, P., Hammar, T., Helgee, A., and Troedsson, B. (1998). “PCB in a River System During Sediment Remediation.” *Water, Air, and Soil Pollution*, 107, 237-250.
- California Department of Transportation (Caltrans). (2003). “Geotextiles, Mats, Plastic Covers and EC Blankets SS-7.” *Construction Site Best Management Practices Manual*, 1-11.
- Chen, M., Shen, S.-L., Arulrajah, A., Wu, H.-N., Hou, D.-W., and Xu, Y.-S. (2015). “Laboratory Evaluation of the Effectiveness of Polypropylene Fibers on the Strength of Fiber-Reinforced and Cement-Stabilized Shanghai Soft Clay.” *Geotextiles and Geomembranes*, 43 (6), 515-523.
- Dewar, S. (1962). “The Oldest Roads in Britain.” *The Countryman*, 59 (3), 547-555.
- Environmental Protection Agency (EPA) (2018). “Advancing Sustainable Materials Management: 2015 Fact Sheet.” Office of Land and Emergency Management, Washington, DC.
- Environmental Protection Agency (EPA) (2018). “Advancing Sustainable Materials Management: 2015 Tables and Figures.” Office of Land and Emergency Management, Washington, DC.
- Federal Emergency Management Agency (FEMA) (2008). “Status Report on the Use of Geotextiles in Embankment Dam Construction and Rehabilitation.” *Geotextiles in Embankment Dams*.
- Franks, C.A., Davis, A.P., and Aydilek, A.H. (2012). “Geosynthetic Filters for Water Quality Improvement of Urban Storm Water Runoff.” *Journal of Environmental Engineering*, 138, 1018-1028.

Gorchakova, V.M., Kuchkovskaya, A.B., and Izmailov, B.A. (2013). "Influence of Organosilicon Modifiers of the Properties of Recycled Polyester Fibers and Geotextile Non-Cloth Materials." *Fibre Chemistry*, 45 (4), 214-216.

Guyer, J.P. (2013). "An Introduction to Geotextiles in Erosion Control." Course Number C01-015, Continuing Education and Development, Inc., Stony Point, NY.

Henry, K.S. (1990). "Laboratory Investigation on the Use of Geotextiles to Mitigate Frost Heave." CRREL Report 90-6, U.S. Army Corps of Engineers Cold Regions Research & Engineering Laboratory, Hanover, NH.

Holtz, R.D., Christopher, B.R., and Berg, R.R. (2008). "Geosynthetic Design & Construction Guidelines Reference Manual." Publication No. FHWA-NHI-07-092, Federal Highway Administration, Washington, DC.

Khabbazian, M., Kaliakin, V.N., and Meehan C.L. (2010). "Numerical Study of the Effect of Geosynthetic Encasement on the Behaviour of Granular Columns." *Geosynthetics International*, 17(3), 132-143.

Koerner, R. M. (2005). *Designing with Geosynthetics*, 5th Ed., Prentice Hall, Upper Saddle River, NJ.

Lekha, K.R. (2004). "Field Instrumentation and Monitoring of Soil Erosion in Coir Geotextile Stabilised Slopes - A Case Study." *Geotextiles and Geomembranes*, 22, 399-413.

Leon, A.L., Potop, G.L., Hristian, L., and Manea, L.R. (2016). "Efficient Technical Solution for Recycling Textile Materials by Manufacturing Nonwoven Geotextiles." *Proceeding from IOP Conference Series: Materials Science and Engineering*, Iasi, Romania.

Li, D., Hyslip, J.P., Sussmann, T.R., and Chrismer, S.M. (2016). *Railway Geotechnics*, Taylor & Francis Group, Boca Raton, FL.

Li, J.-H., Hsieh, J.-C., Lou, C.-W., Hsieh, C.-T., Pan, Y.-J., Hsing, W.-H., and Lin, J.-H. (2016). "Needle-Punched Thermally-Bonded Eco-Friendly Nonwoven Geotextiles: Functional Properties." *Materials Letters*, 183, 77-80.

Lin C.-W., Hsing W.-H., Lou C.-W., Chen J.-M., and Lin J.-H. (2013). "Manufacturing Technique and Property Evaluation of Eco-Friendly Kevlar/PET/Nylon Composite Geotextile." *Applied Mechanics and Materials*, 365-366, 1157-1160.

Lin, J.-H., Huang, C.-H., Tai, K.-C., Lin, C.-W., Chen, J.-M., and Lou, C.-W. (2011). "Recycling Nonwoven Fabric and Polypropylene Selvage to Create Composite Fabric." *Applied Mechanics and Materials*, 332-334, 1326-1329.

McDonough, W. and Braungart, M. (2002). *Cradle to Cradle: Remaking the Way We Make Things*, North Point Press, New York, NY.

Ruhl, S., Overmoyer, J., Barker, D., and Brown, L.C. (1999). "Using Geotextile Fabric in Livestock Operations." Publication Number AEX-304-97, The Ohio State University, Columbus, OH.

Santvoort, G.V. (1995). *Geosynthetics in Civil Engineering*, A. A. Balkema, Rotterdam, Netherlands.

Sarsby, R.W. (2007). "Use of 'Limited Life Geotextile' (LLGs) for Basal Reinforcement of Embankments Built on Soft Clay." *Geotextiles and Geomembranes*, 25, 302-310.

Shukla, S.K. and Yin, J.H. (2006). *Fundamentals of Geosynthetic Engineering*, Taylor & Francis Group, London, UK.

Talebi, M. (2016). "Analysis of the field behavior of a geosynthetic reinforced soil integrated bridge system during construction and operation", PhD Dissertation, University of Delaware, 2016.

Theisen, M.S. (1992). "The Role of Geosynthetic in Erosion and Sediment Control: An Overview." *Geotextiles and Geomembranes*, 11, 535-550.

Trajkovic, D., Stepanovic, J., Sarac, T., Stojiljkovic, D., and Dordic, D. (2015). "The Prediction of Elastic Limit of Nonwoven Geotextile made of Virgin and Recycled Polyester Fibers." *Tekstil ve Konfeksiyon*, 25 (3), 229-235.

Wu, J.T.H. and Ooi, P.S.K. (2015). "Synthesis of Geosynthetic Reinforced Soil Design Topics." Publication No. FHWA-HRT-14-094, Federal Highway Administration, Washington, DC.

Zornberg, J.G. (2017). "Function and Applications of Geosynthetics in Roadways." *Procedia Engineering*, 187, 298-306.

Zornberg, J.G. and Thompson, N. (2012). "Application Guide and Specifications for Geotextiles in Roadway Applications." Report Number FHWA/TX-10/0-5812-1, Federal Highway Administration, Washington, DC.

CHAPTER 2 – APPROACH

2.1 Materials

In order to determine which textile materials are commonly donated and readily available, collaborations with Goodwill of Delaware and Goodwill of Duluth were established. Each thrift store franchise donated a bale of used clothing that had not sold in their thrift store. Once opened, each bale of used clothing can fill approximately two to four cardboard gaylords. Figure 2.1 shows University of Delaware students sorting textile materials by composition from one of these bales.



Figure 2.1 University of Delaware students sorting one bale.

The material composition of each used textile was determined by tag labels; many articles did not have tags and were marked as having an unknown composition. Bales from each location, Delaware and Duluth, provided different distributions of textile materials. The variance in material compositions by location may reflect different styles or weather. Although some differences were observed between the sourcing locations, cotton was consistently a large material category found in both locations. Table 2.1 displays the distribution of material composition by weight and percentage for the bale from each location.

Table 2.1: Bale Material Composition Distribution

| | Location | | |
|--------------------------|------------------|-------------------|-------------------|
| | Delaware | Duluth | Total |
| Acrylic | 3.18 kg (2.1%) | 3.01 kg (0.7%) | 6.19 kg (1.1%) |
| Blends | 52.27 kg (34.1%) | 62.21 kg (14.7%) | 114.48 kg (19.9%) |
| Cotton | 51.36 kg (33.5%) | 115.42 kg (27.4%) | 166.78 kg (29.0%) |
| Nylon, Silk, Wool, Other | 1.82 kg (1.2%) | 74.89 kg (17.8%) | 76.71 kg (13.3%) |
| Polyester | 24.55 kg (16.0%) | 29.42 kg (7.0%) | 53.97 kg (9.4%) |
| Rayon | 5.91 kg (3.9%) | 1.44 kg (0.3%) | 7.35 kg (1.3%) |
| Unknown | 14.09 kg (9.2%) | 135.26 kg (32.1%) | 149.35 kg (26.0%) |
| Total | 153.18 kg (100%) | 421.65 kg (100%) | 574.83 kg (100%) |

Ignoring the textiles of unknown material, cottons form the largest total percentage followed by blends, other, and polyester. Blends are a mixture of at least two different material types. These blended textiles can be a natural fiber blend (such as linen and cotton), a synthetic fiber blend (such as polyester and elastane), or a natural-synthetic fiber blend (such as polyester and cotton). Blends may use any percentage of different fibers together. Most often this blending is done at the fiber level before any yarn is formed into the textile. Blends are very difficult to recycle due to the difficulty in separating materials from each other at the fiber level. Also, since blends are a mixture of materials, it does not seem likely that they would demonstrate a consistent set of material properties. For these reasons, blends were not included in the associated testing and analyses that were performed. Cotton and polyester were the largest single material categories present in the bales. These two materials consequently became the focus of our analysis. Cottons are biodegradable and are consequently only appropriate for temporary applications. Polyesters, on the other hand, can be quite durable provided they are not exposed to ultraviolet (UV) light. UV rays break down synthetic polymers, including those present in textiles (Li et al. 2010). Consequently, underground applications for polyester hypothetically have the potential for adequate levels of durability over time; this is a topic that needs to be explored in greater detail with future research.

Although geotextiles come as woven, knits, and nonwovens, only woven recycled textiles were tested in the current study. This is a logical place to start, as woven textiles are easy to tensile test and are likely to have greater tensile strengths than knits and nonwovens. Knits are highly elastic and deform or neck during tensile tests to such a large degree that the data may not be reliable; this was confirmed during the initial testing of textile materials before it was decided to focus the current study on woven 100% cotton denim and 100% polyester.

All textile materials that were tensile tested in this study were acquired from the Goodwill Recycling Center in New Castle, Delaware. Since a large quantity of 100% cotton denim and 100% polyester material was needed, it was decided that it would be easier to go to the Goodwill Recycling Center and hand-pick the material. To ensure the material nature could be properly assessed, only articles that had tags stating the material consistency were selected, as many modern denim articles tend to have some elastics in them. This study was completed on woven articles of clothing. On each occasion, two large gaylords were provided for the researchers to pick through. When gathering 100% cotton denim materials, the gaylords were only filled with jeans as it is quite easy for the staff at the Goodwill Recycling Center to sort these items out. From there, the

researchers made sure the articles gathered were 100% cotton denim. A total of 33 articles of 100% cotton denim were obtained, all woven. Gathering 100% polyester materials for testing proved more difficult as there is no easy way to visually separate for polyester; the staff at the Goodwill Recycling Center provided the researchers with two gaylords full of all non-denim clothing articles. The researchers then picked through the gaylords for any 100% polyester materials; from the two gaylords, only 20 100% polyester articles were acquired. Additionally, from those 20 articles, only 6 were woven. Figure 2.2 displays the researchers selecting materials for testing.



Figure 2.2 Selecting materials for testing.

2.2 Preparation of Specimens for Tensile Testing

Since there is no ASTM standard for testing recycled textiles for use as geotextiles, a hybrid standard was formed from the standard test method for break strength and elongation of textile fibers (ASTM D5034) and the standard test method for tensile properties of geotextiles by the wide-width strip method (ASTM D4595). Specimens were prepared in a temperature-controlled room with an atmosphere that was in accordance with ASTM D5034 and ASTM D4595; the relative humidity was between 60% and 70% and the temperature was between 19°C and 23°C. For preparation, the specimens were cut with a rotary fabric cutter to a rectangular shape, 175 mm long by 100 mm wide (7" x 4") which is in accordance with ASTM D5034 (Figure 2.3a). The reasoning behind using this size specimen was that it would not be possible to cut samples at the size directed in ASTM D4595 (200 mm long by 200 mm wide) for recycled textile materials, due to the stitching on the clothing articles (i.e., the denim). After cutting, specimens were then marked with targets in a grid pattern as shown in Figure 2.3b. The grid consisted of 5 rows by 5 columns for a total of 25 target points, which were spaced at approximately 1.75 mm; a contrasting color to the textile specimen that was unique enough to be different from other surrounding colors in the fabric itself was used to ensure more effective digital image analysis.

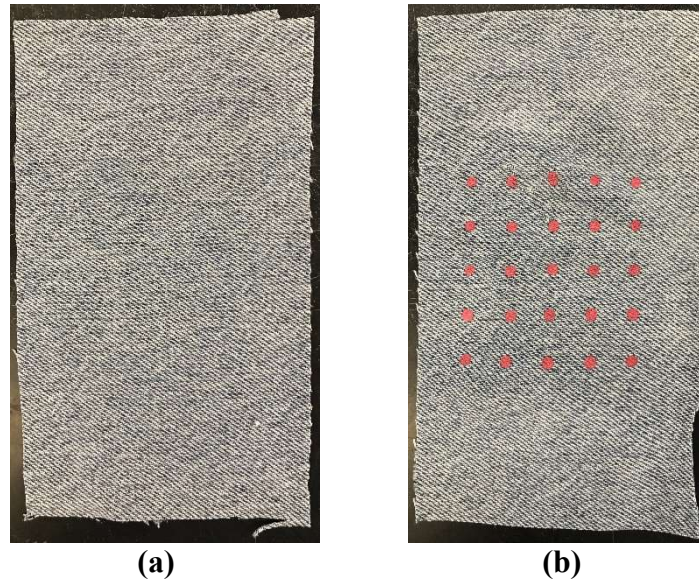


Figure 2.3 (a) A 175 mm x 100 mm cut specimen, and (b) a cut specimen with painted targets.

Due to the volume of testing that was to be performed in this study, it was determined that the most efficient way to apply the painted targets would be using a screen-printing approach. These targets are used to determine more accurate strains during the tensile testing via a digital image analysis technique that will be discussed later in this report.

2.2.1 Screen Printing Method

Due to variability in specimen material, the chosen method of applying targets in the grid pattern was screen-printing. Screen-printing is advantageous to other methods because it can be used to print upon a great variety of substances: paper, plastic, glass, metal, cotton, etc. Depending on the size of the holes in the screen used in the process, traditional inks (UV and solvent based), adhesives, lacquers, conductive silver, and dielectric inks can be printed. Furthermore, screen-printing is easily scalable; manufacturers have control on image magnitude at a cost-effective rate. Prints can be mass produced and are independent of material size and thickness. In addition, silkscreen printing can be deployed following a basic procedure that utilizes materials readily available in most markets across the globe.

For this project, a custom screen-printing stencil was created to best meet the project needs. Generally, silkscreen printing uses a primary coat of emulsion material which cures when exposed to UV light. When the UV light comes in contact with the emulsion, the photosensitizers form strong bonds with the emulsion's resin, thus forming a barrier for the ink. There are three forms of emulsions: diazo (a mixture of diazonium salt with an azo ink or bivalent nitrogen joined to two hydrocarbon groups), SBQ (Styryl Basolium Quaternary Photopolymers formed by sensitized added to either a resin base of polyvinyl alcohol or acetate) and a dual-cure substance which is a mixture of both diazo and SBQ. Following the curing process, the screen is washed with direct pressure to expose the design. The screen must then be left to dry and is ready to begin printing

using the desired ink and substrate. Below is a step by step procedure for the creation of the custom screen-printing stencil that was used for this study.

Step 1: Acquire the necessary resources to create a screen-print stencil, as shown in Figure 2.4. These materials included the following: Speedball screen-printing frame, Speedball diazo emulsion, Speedball squeegee, screen-print design on transparency paper, and a 500-watt halogen light.



Figure 2.4 Materials required to create custom screen-printing stencil.

Step 2: Apply the emulsion on the screen. The diazo resin is first mixed with the provided sensitizer and then applied in a thin and evenly distributed coat to the screen as shown in Figure 2.5a. After application, the screen must dry in a dark atmosphere with minimal light (Figure 2.5b). Drying time can vary depending on the amount of emulsion applied (the drying process in this study took approximately 4 hours). Figure 2.5c displays the screen after the emulsion has fully dried.

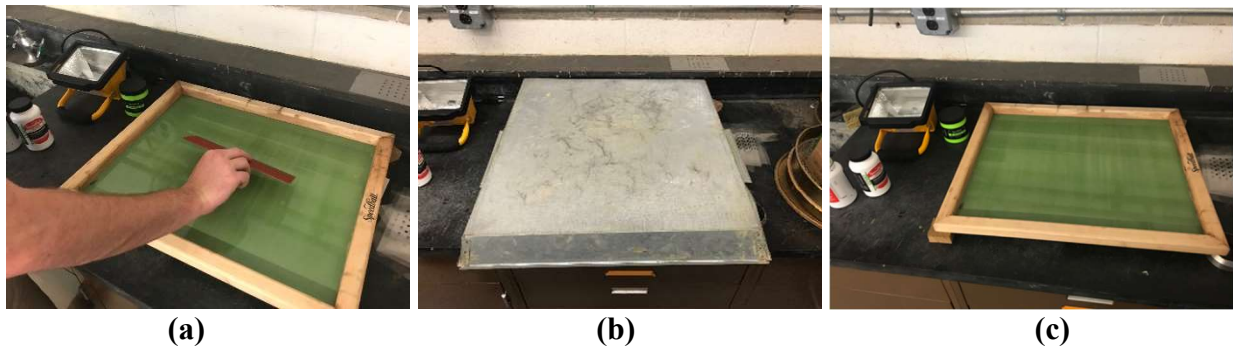


Figure 2.5 (a) Emulsion application to screen, (b) emulsion drying in dark atmosphere, and (c) screen after the emulsion has dried.

Step 3: Figure 2.6a displays the placement of the transparency paper with the design on the screen in the location desired. Light from a 500-watt halogen bulb was then applied directly to the screen as shown in Figures 2.6b and c. It should be noted that this process should be done as quickly as

possible. The light should be placed approximately 18 inches above the screen. The curing process has many variables such as emulsion type, light type, image dimensions, image color, and light wattage; all these factors will determine the amount of exposure time. For this study, 15 minutes was sufficient.

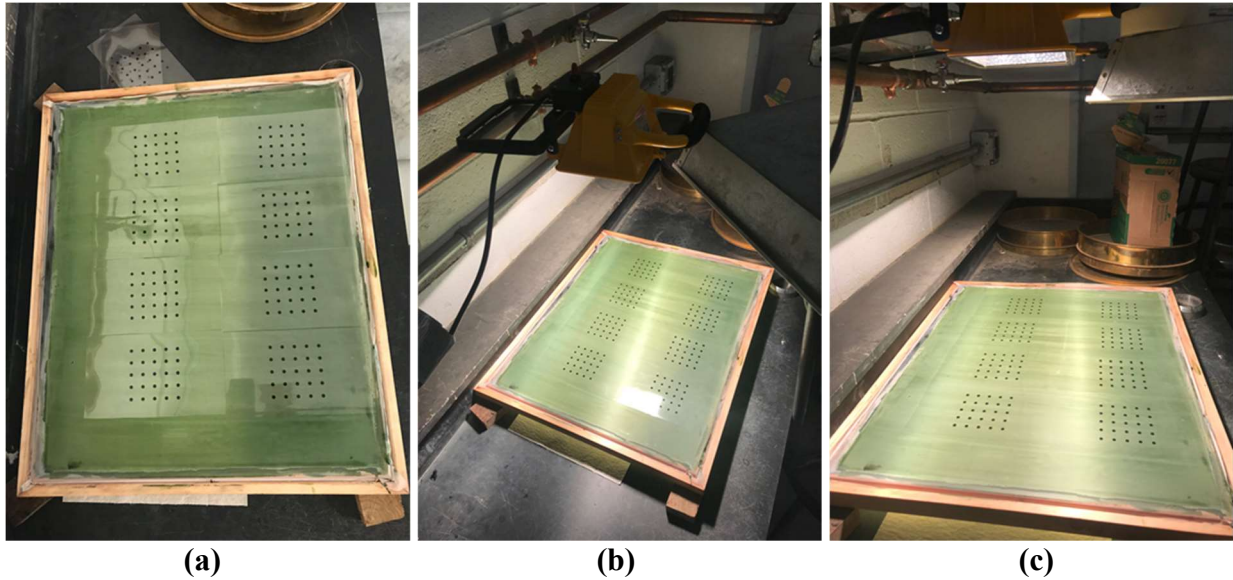


Figure 2.6 (a) Placement of transparency paper, and (b/c) application of light to screen.

Step 4: After the screen has been exposed, the transparency paper with the design must be removed and the screen should be washed with water under direct pressure as shown in Figure 2.7. After this, water should begin to flow freely through the points where the design blocked the light exposure. If the screen has been under-exposed, the emulsion on the screen will wash away completely. If the screen has been over-exposed, the design will not wash out.



Figure 2.7 Screen washing after light exposure.

After these steps were completed, the screen was ready for use. For the size of the screen used in this study, it was possible to print the targets on 8 specimens at a time. To do this, the specimens were arranged so the targets would print directly in the middle of the specimen vertically and horizontally. Once aligned, ink was applied to the screen and a squeegee was used to press the ink through the open holes of the screen onto the specimen. Once the ink dried, the specimens were ready to be tensile tested.

2.3 Preparation of Specimens for Permittivity Testing

Permittivity testing of the assessed textiles was performed following the general processes and principles outlined in ASTM D4491 Standard Test Methods for Water Permeability of Geotextiles by Permittivity. The measured permeability depends on the thickness of the material and is defined by the ASTM D4491 standard as “the rate of flow of liquid under a differential pressure through a material.” Since geotextiles may compress under different soil types, permittivity, as defined by ASTM D4491 as “the volumetric flow rate of water per unit cross sectional area per unit head under laminar flow conditions, in the normal direction through a geotextile,” is measured instead of permeability and is the standard measurement technique in the geotextile industry.

Specimens prepared for permittivity testing were cut from the same articles of clothing that were used for the tensile testing. Samples were cut to approximately 95 mm (3.75”) diameter circles in order to fully cover the two-inch diameter piping that the water would flow through. Figure 2.8 displays the initial denim specimen cut from an article of clothing, the tool to cut the specimen into a circle, and the resulting 95 mm diameter specimen.

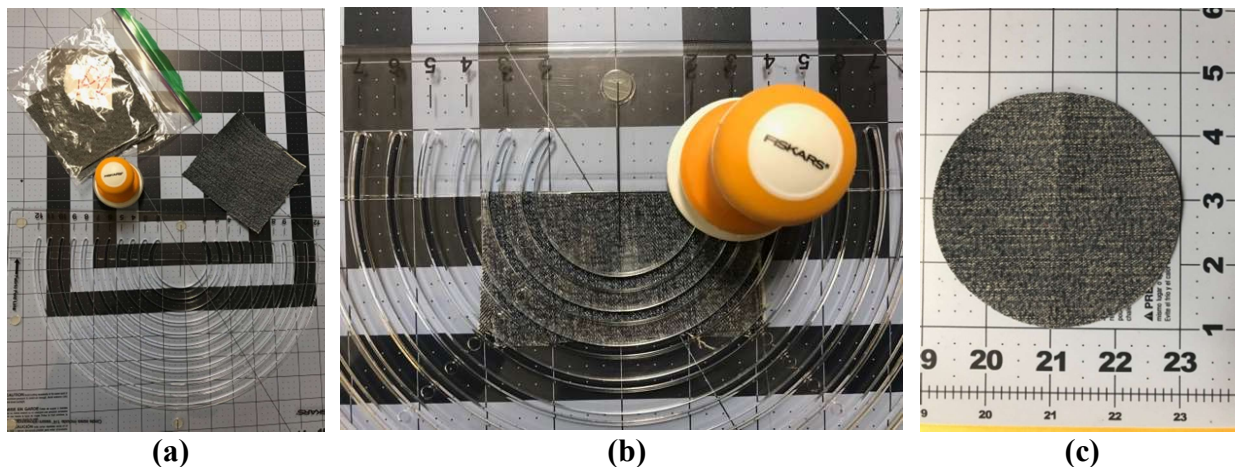


Figure 2.8 Preparation of textile specimens for permittivity testing: (a) Denim specimen and associated preparation tools, (b) cutting of specimen, and (c) final specimen for permittivity testing.

Samples underwent two hours of conditioning in de-aired water before testing (water with less than 6 ppm dissolved oxygen); tap water was de-aired in a LAB1ST Scientific 5 Gallon Vacuum Degassing Chamber Kit using a 5 CFM Pump. Four specimens were cut from four different areas of each article of clothing in order to ensure material properties were representative. 100% cotton denim samples were supplied from Goodwill of Delaware or were the same articles of clothing that underwent tensile testing. The 100% polyester samples that underwent permittivity testing

were supplied from Goodwill of Duluth and were not the same articles of clothing that underwent tensile testing.

References

Li, L., Frey, M., and Browning K.J., (2010). "Biodegradability Study on Cotton and Polyester Fabrics." *Journal of Engineered Fibers and Fabrics*, 5(4), 42-53.

CHAPTER 3 – METHODOLOGY

3.1 Tensile Testing Program

The modified tensile testing performed in this study was conducted at the University of Delaware's Fashion and Apparel Laboratory in Newark, DE. A Tinius Olsen H5KT Benchtop Tester with pneumatic grips controlled by the QMAT software provided by Tinius Olsen was utilized to conduct all of the testing in this study. For each test, extension distance and force were recorded every 0.04 mm of extension. The general setup for the tensile testing is shown in Figure 3.1.



Figure 3.1 General setup for tensile testing.

As stated previously, samples were marked with targets so a digital image analysis technique could be used to more accurately calculate strains; strains calculated using the crosshead extensions of the grips were deemed unreliable due to specimen slippage at the grips. In short, this digital image analysis technique works as follows. First, continuous video or consistent time interval photographs are taken of the sample while testing is occurring. From the recorded video stream or time interval photographs, an initial “still” image and a final still image were chosen and extracted (the initial still is the sample with no load on it and the final still is the sample just prior to failure). Then, these stills were run through a computer program to identify the exact target locations in both the initial and final images.

For this study, a photo interval approach was used because the specimens were tested at a strain rate of 10% per minute. One benefit to using this type of photo interval approach was to reduce overall data storage requirements for each test, as there were over 350 total tests completed in this study. A GoPro HERO5 Black was used with the following settings: 1080-pixel resolution, wide field of view, and an interval (time lapse) of one photograph every five seconds. The pixel resolution and field of view were chosen by trying all the options within the settings and determining that these were best for this study and setup. A photo interval of five seconds was chosen because it was determined that this was a reasonable interval to accurately capture the

failure strains within 1% of the actual. The file size of each photograph was approximately two megabytes and, on average, there were approximately 30 photographs taken per test, resulting in approximately 60 megabytes of data that needed to be stored for each test. The GoPro was set up on a mini-tripod approximately 18 inches from the fabric within the testing apparatus.

Using this digital image analysis approach, average global strains and average local strains were computed in this study using Equations 1 and 2, respectively. Average global strain was calculated across the entire width of the specimen (all 5 columns of targets) while average local strain was calculated for only the middle of the specimen (the middle column of targets); this is shown in Figure 3.2. Using the crosshead extension of the grips during testing, boundary strains can be calculated using Equation 3 where ΔL is the change in length of the test specimen, or the displacement, and L_0 is the initial length of the test specimen.

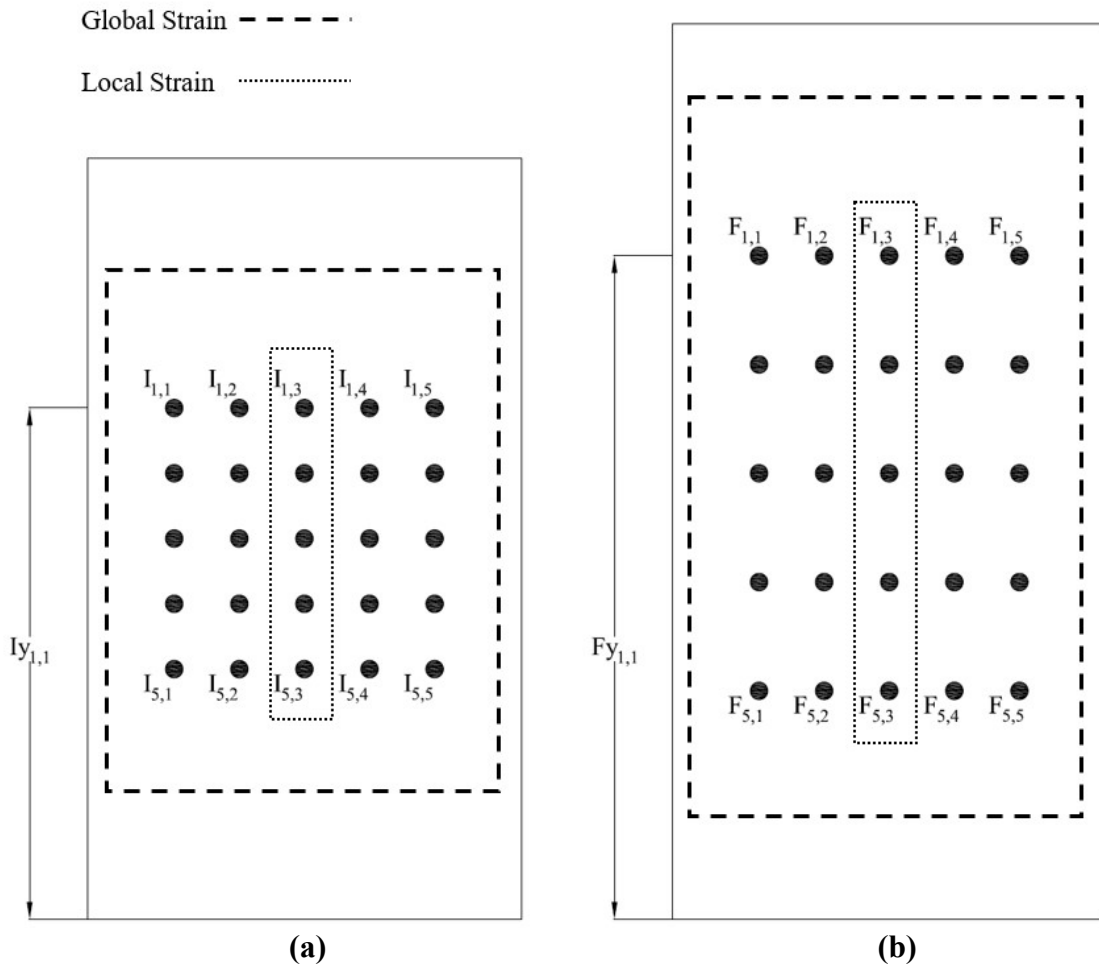


Figure 3.2. Strain calculation approach for tested specimens: a) Idealized initial position of marking points, with data point groups that were assessed identified, and b) final position of marking points, with data point groups that were assessed identified.

$$\epsilon_{global} = \frac{1}{5} \sum_{j=1}^5 \frac{(F_{y_{1,j}} - F_{y_{11,j}}) - (I_{y_{1,j}} - I_{y_{11,j}})}{(I_{y_{1,j}} - I_{y_{11,j}})} \quad (1)$$

$$\varepsilon_{local} = \frac{(Fy_{1,3}-Fy_{5,3})-(Iy_{1,3}-Iy_{5,3})}{(Iy_{1,3}-Iy_{5,3})} \quad (2)$$

$$\varepsilon_{boundary} = \frac{\Delta L}{L_o} \quad (3)$$

After samples were prepared following the steps described in Chapter 2, samples were then inserted into the testing apparatus. Again, since there is no specific standard for testing recycled textiles for use in geotextile applications, tests were conducted to investigate the effect of testing strain rate on the measured specimen strengths; this was conducted for both the 100% cotton denim and 100% polyester tested materials. From the results of this testing (which are provided in more detail in Chapter 4), it was decided that all samples would be tested at a strain rate of 10%/min.

3.2 Permittivity Testing Program

Permittivity testing was conducted using an apparatus that was custom built by the researchers for this study; the apparatus was designed to meet the calibration standards set in ASTM D4491 for the standard No. 200 sieve (which has a permittivity of 5 seconds⁻¹ +/- 1.3). This permittivity apparatus is displayed in Figure 3.3.

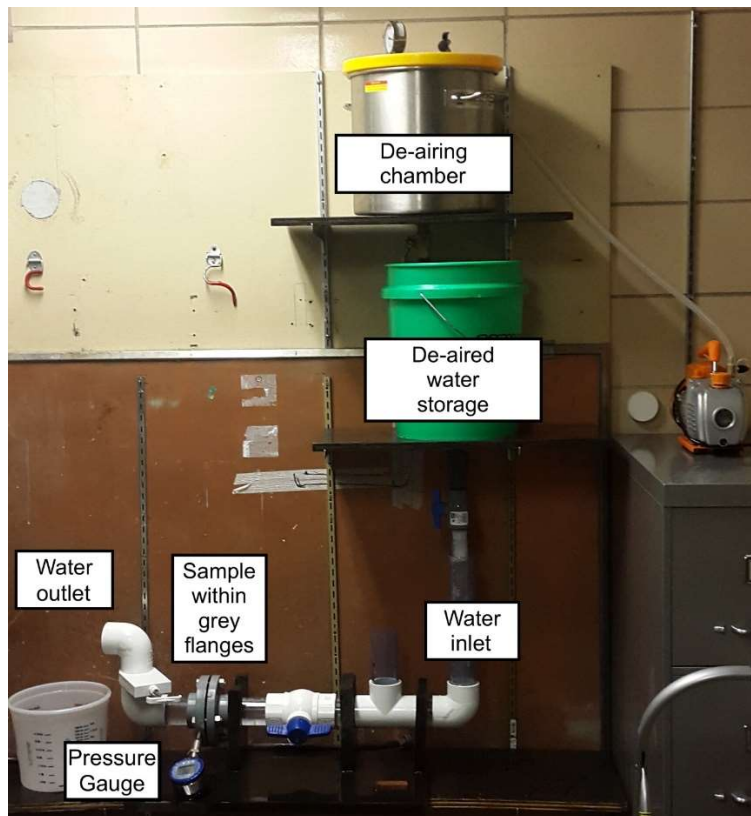


Figure 3.3 Permittivity testing setup.

Prior to testing, tap water was de-aired in a LAB1ST Scientific 5 Gallon Vacuum Degassing Chamber Kit using a 5 CFM Pump. In order to de-air water, the chamber was filled until water reached two inches from the top, in order to allow space for the air bubbles to escape. The

temperature of the tap water was first checked with an AMTAST Portable Dissolved Oxygen and Temperature Meter; the temperature was to be 21°C +/- 2 per ASTM D4491. The vacuum pump was turned on until the pressure in the chamber was between -27 to -29 inHg. The vacuum pump was then turned off and air bubbles were allowed to escape from the water into the air in the top of the chamber for five minutes or more. The pressure release valve at the top of the chamber was then opened slightly to allow the slow release of air and the induced vacuum oxygen out of the chamber. The water was then released into the green de-aired water storage chamber and then tested for dissolved oxygen in ppm using the AMTAST Portable Dissolved Oxygen and Temperature Meter. No tests were run unless the dissolved oxygen level was at or below the 6-ppm specified in ASTM D4491. The de-aired water was stored in the storage chamber in order to allow de-airing of additional water while testing. One de-airing chamber pot was enough to run one test for the standard No. 200 sieve.

Before testing commenced on samples, calibration of the permittivity apparatus was conducted. The permittivity apparatus was tested for a range of heads, from 10 to 75 mm in 5 mm increments to ensure that the apparatus was not impeding flow and that there was a region of laminar flow with the standard No. 200 sieve at 50 mm. Figure 3.4 displays that the apparatus was not impeding flow for the standard No. 200 sieve and that the 50 mm head permittivity measurements fit a linear trend and thus, achieve laminar flow. After it was proven that laminar flow was achieved, calibration was performed each day prior to testing specimens. Once it was determined that it was not necessary to calibrate every day, calibration was completed once a week.

To calibrate the permittivity apparatus, after leveling, a standard No. 200 sieve sample was tested five times to ensure that the permittivity tester was still meeting the ASTM 4491 specifications. After a textile sample was loaded between the grey flanges, de-aired water backfilled behind the specimen to the blue handled valve upstream of the specimen. Back filling was accomplished by closing the blue handled valve and dislodging the apparatus from the remaining piping, orienting the outlet under the green de-aired water storage outlet and filling the entire pipe in order to prevent any bubbles from collecting on the sieve. Figures 3.6 and 3.7 show permittivity testing with the custom-built apparatus in use. Testing with the custom-built permittivity apparatus was conducted as follows:

1. Record date, sample number, test number, dissolved oxygen (ppm), temperature, time, and permittivity measurement in the log book.
2. Level the permittivity apparatus.
 - a. Level the water outlet and the head pipe.
 - b. Read level in two directions that are 90 degrees to each other in each location.
3. Open the bottom chamber valve to let the de-aired water into the reservoir. Typically, one chamber pot is enough to run one test; having another batch of de-aired water ready is useful if more is needed, however.
4. Make sure valve at the bottom of reservoir is closed when filling with de-aired water.
5. Probe the water in the reservoir and let the measuring device sit for three to four minutes. Note the water temperature and dissolved oxygen readings.
6. Again, check to ensure the apparatus is levelled cross-directionally.
7. Fill the permittivity apparatus with water and make sure the white gate valve is closed and blue valve is open to let the water in all the way to the white gate valve.

8. Detach the apparatus from the inlet side and remove any bubbles on the test specimen.
9. Reattach apparatus.
10. In order to take a measurement: open the valve at the bottom of the reservoir to let the de-aired water into the apparatus (be sure that a head of 50 mm is maintained). Start the timer when water starts to flow into the five-liter outflow pitcher. Stop the timer and pull out the pitcher at the same time. Record the number of liters in the pitcher over specific period of time.
11. Take five measurements and average the results.

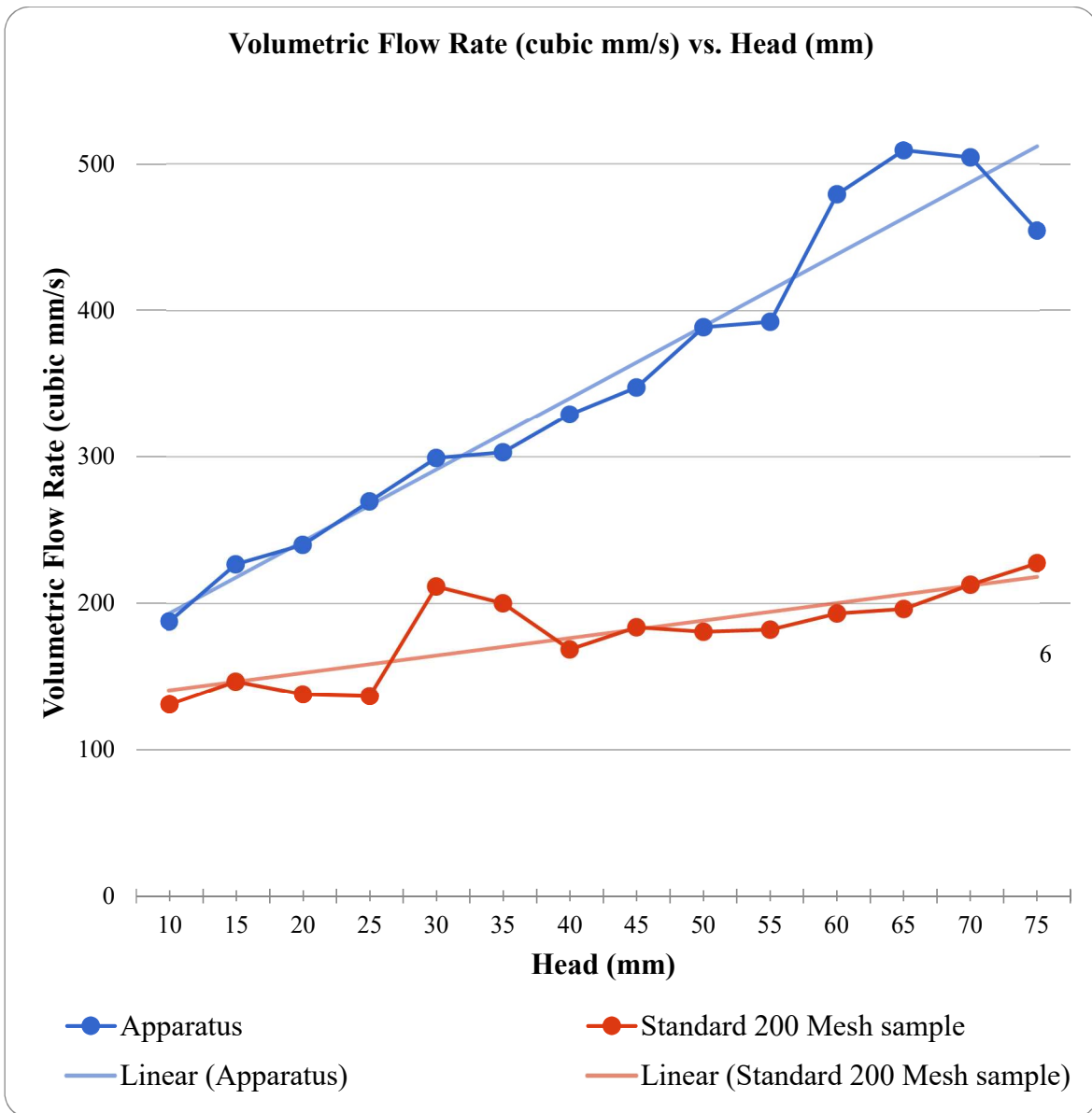


Figure 3.4 Calibration curves for the testing apparatus and for the standard No. 200 sieve.

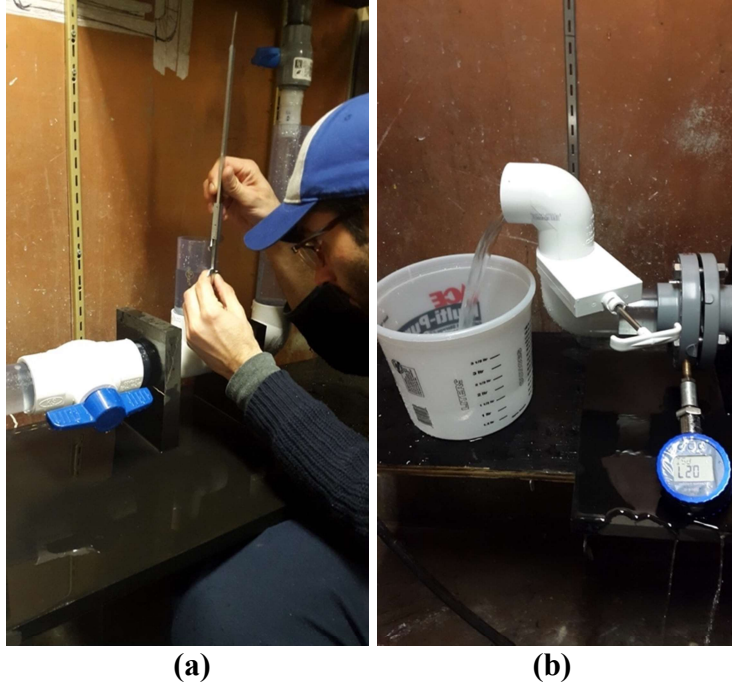


Figure 3.5. Steps to permittivity testing: (a) Measuring head with calipers, and (b) measuring flow volume.

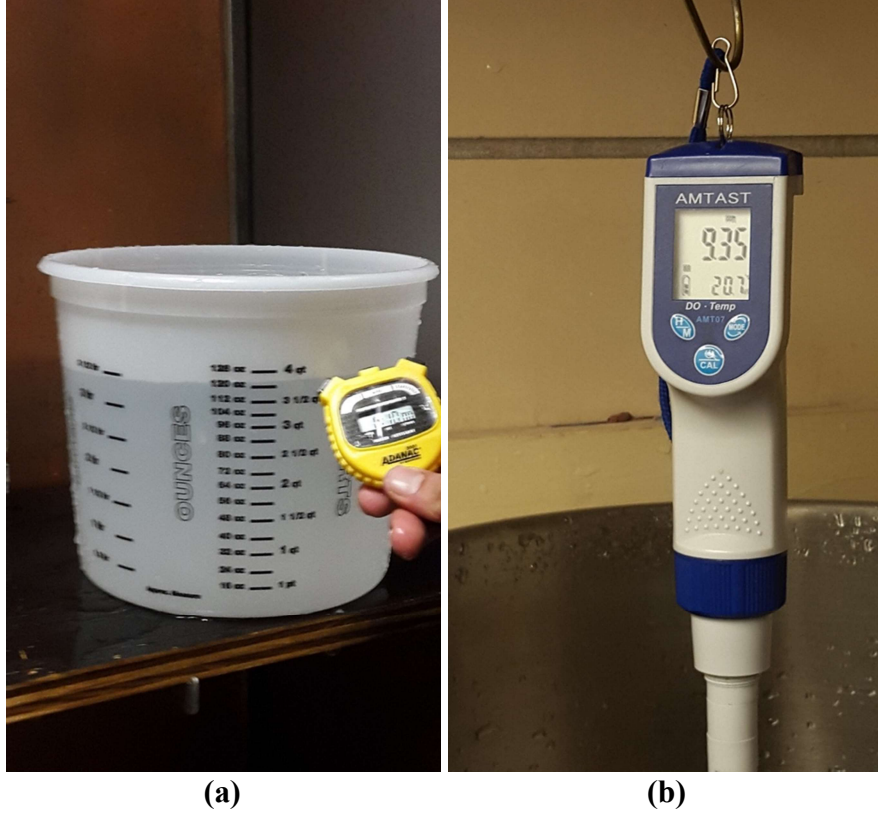


Figure 3.6 Steps to permittivity testing: (a) Keeping time on a stopwatch to determine flow rate, and (b) checking dissolved oxygen levels with AMTAST Portable Dissolved Oxygen and Temperature Meter.

Through testing, the head, time, water temperature, cross-sectional area of sample exposed to water flow, and flow volume were measured and calculated. Permittivity was then determined using Equation 4, where Q is the flow volume (mm^3), R_t is the temperature corrected water viscosity factor, H is the head (mm), t is the time (sec), and A is the cross-sectional area of the specimen exposed to water flow (mm^2). The water viscosity factor was calculated using Equation 5, where T is the water temperature ($^{\circ}\text{C}$).

$$\psi = \frac{QR_t}{hAt} \quad (4)$$

$$R_t = 1.4751 - 0.0237 * T \quad (5)$$

CHAPTER 4 - FINDINGS

4.1 Strain Rate Effect on Tensile Strength

As noted previously, since there is no standard for testing recycled textiles for use in geotextile applications, several tests at different strain rates were conducted to investigate the effect on the strength of the recycled textiles. This testing was performed for both 100% cotton denim and 100% polyester specimens. Strain rates of 400%/min, 100%/min, 10%/min, 5%/min, and 1%/min were used for this part of the study. A strain rate of 400%/min was chosen as one of the rates because it is used in the standard test method for grab breaking load and elongation of geotextiles (ASTM D4632) and the standard test method for breaking strength and elongation of textile fabrics (grab test) (ASTM D5034). A strain rate of 10%/min was chosen as one of the rates because it is used in the standard test method for tensile properties of geotextile by the wide-width strip method (ASTM D4595); this test method is also the most commonly used when testing geotextiles. The 100%/min strain rate was chosen arbitrarily as an intermediate strain rate between 400%/min and 10%/min. Strain rates of 5%/min and 1%/min were chosen because in most geotextile applications, failure occurs at much slower strain rates. It should be noted for the testing in this section, the researchers used video to capture the tests instead of pictures and five second intervals. The purpose of this was to make sure the researchers could accurately capture what was happening at intermediate stages of the testing.

4.1.1 100% Cotton Denim

Three tests were completed on the same 100% cotton denim at each of the following strain rates: 400%/min, 100%/min, 10%/min, and 5%/min. Due to issues with the testing apparatus, only one test at a strain rate of 1%/min was completed. Break force, machine break strain, global image analysis break strain, and local image analysis break strain for this testing are provided in Tables 4.1 through 4.5. Strain vs. force plots from the tensile testing from each strain rate are shown in Figures 4.1 through 4.5.

Table 4.1: 100% Cotton Denim - 400%/min Strain Rate Results

| Test I.D. | 400a | 400b | 400c | Average | Std. Dev. |
|------------------------------|------|------|------|---------|-----------|
| Break Force (N) | 2103 | 2103 | 2140 | 2115.33 | 21.36 |
| Machine Break Strain (%) | 53.4 | 53.5 | 55.0 | 53.97 | 0.90 |
| Global I.A. Break Strain (%) | 35.8 | 32.2 | 36.5 | 34.8 | 2.26 |
| Local I.A. Break Strain (%) | 40.8 | 36.8 | 40.0 | 39.2 | 2.10 |

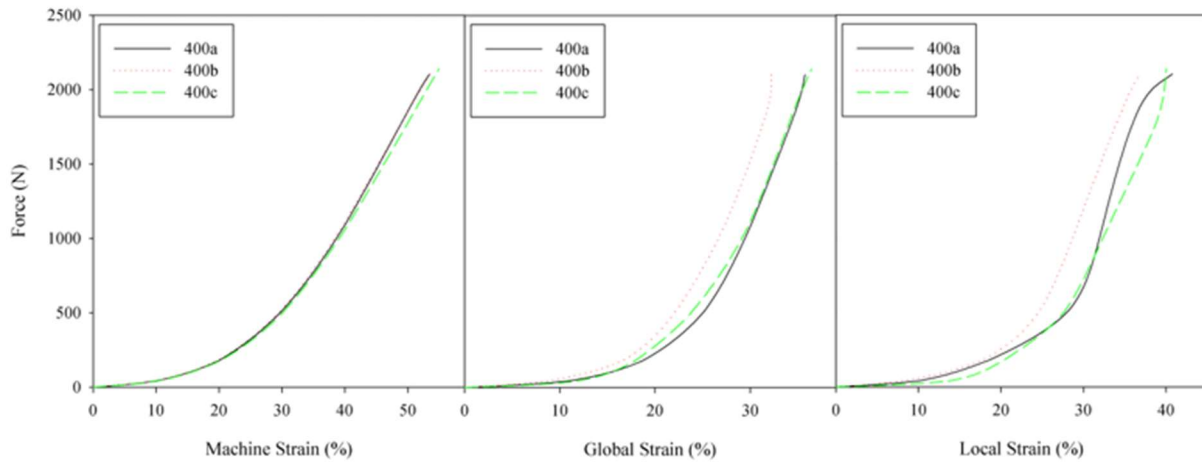


Figure 4.1. 100% cotton denim - 400%/min strain rate results.

Table 4.2: 100% Cotton Denim - 100%/min Strain Rate Results

| Test I.D. | 100a | 100b | 100c | Average | Std. Dev. |
|------------------------------|------|------|------|---------|-----------|
| Break Force (N) | 1998 | 2000 | 2083 | 2027.00 | 48.51 |
| Machine Break Strain (%) | 53.9 | 54.3 | 55.9 | 54.70 | 1.06 |
| Global I.A. Break Strain (%) | 33.8 | 35.0 | 34.3 | 34.39 | 0.621 |
| Local I.A. Break Strain (%) | 39.4 | 38.5 | 37.9 | 38.57 | 0.75 |

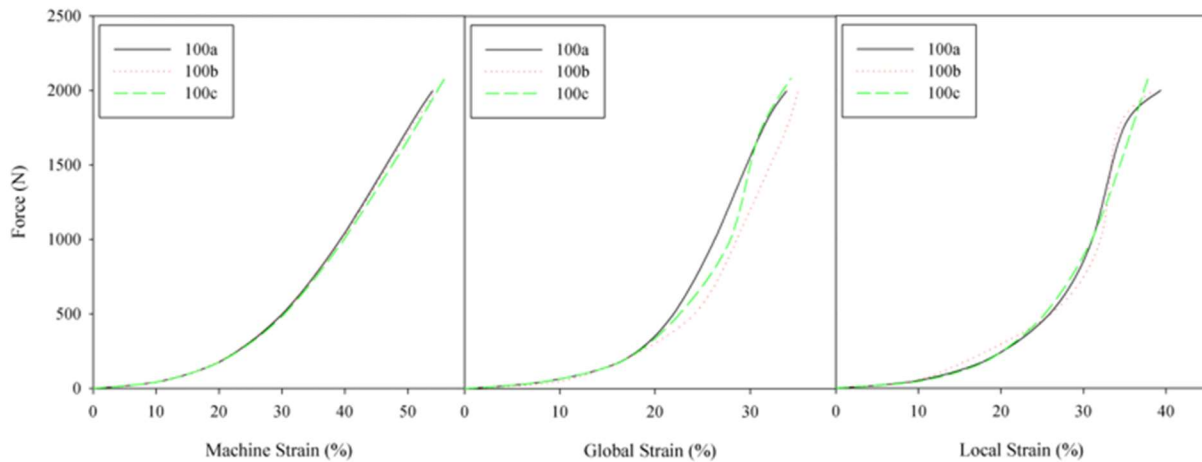


Figure 4.2. 100% cotton denim - 100%/min strain rate results.

Table 4.3: 100% Cotton Denim - 10%/min Strain Rate Results

| Test I.D. | 10a | 10b | 10c | Average | Std. Dev. |
|------------------------------|------|------|------|---------|-----------|
| Break Force (N) | 1770 | 1838 | 1798 | 1802.00 | 34.18 |
| Machine Break Strain (%) | 54.4 | 52.2 | 52.0 | 52.87 | 1.33 |
| Global I.A. Break Strain (%) | 33.1 | 34.4 | 34.1 | 33.86 | 0.70 |
| Local I.A. Break Strain (%) | 36.9 | 38.9 | 37.7 | 37.85 | 1.05 |

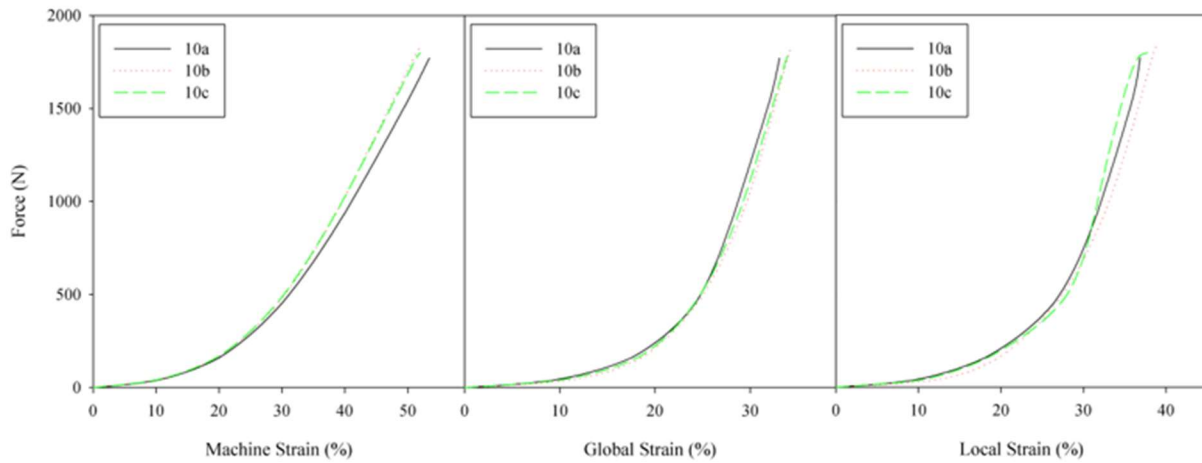


Figure 4.3. 100% cotton denim - 10%/min strain rate results.

Table 4.4: 100% Cotton Denim - 5%/min Strain Rate Results

| Test I.D. | 5a | 5b | 5c | Average | Std. Dev. |
|------------------------------|------|------|------|---------|-----------|
| Break Force (N) | 1664 | 1740 | 1674 | 1692.67 | 41.30 |
| Machine Break Strain (%) | 45.7 | 48.6 | 47.5 | 47.27 | 1.46 |
| Global I.A. Break Strain (%) | 29.6 | 33.9 | 33.6 | 32.36 | 2.42 |
| Local I.A. Break Strain (%) | 31.2 | 37.7 | 35.7 | 34.88 | 3.34 |

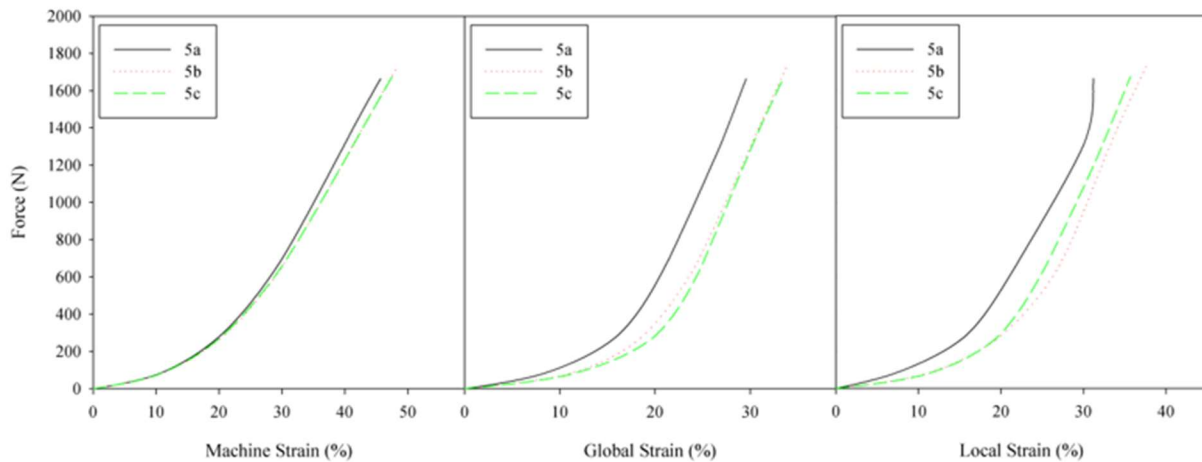


Figure 4.4. 100% cotton denim - 5%/min strain rate results.

Table 4.5: 100% Cotton Denim - 1%/min Strain Rate Results

| | |
|------------------------------|------|
| Test I.D. | 1a |
| Break Force (N) | 1467 |
| Machine Break Strain (%) | 51.0 |
| Global I.A. Break Strain (%) | 32.4 |
| Local I.A. Break Strain (%) | 36.9 |

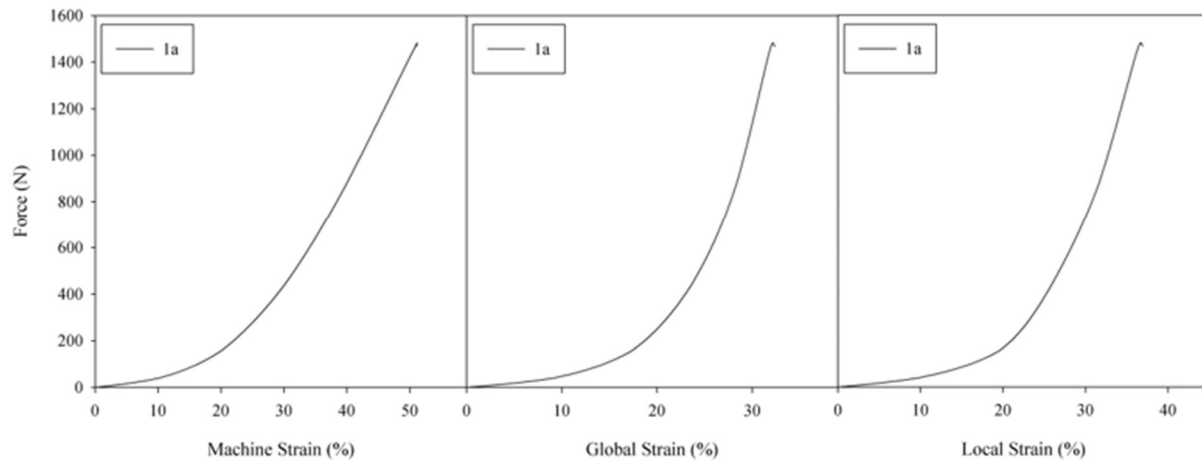


Figure 4.5. 100% cotton denim - 1%/min strain rate results.

For comparison purposes, an average break force, average machine break strain, average global image analysis break strain, and average local image analysis break strain were calculated, with the associated results being provided in Table 4.6. From this table, it is clear that as strain rate decreases (as the test is run more slowly), there is a decrease in break force; it was consequently determined that strain rate has a significant effect on break force. The average machine break strain ranges from approximately 54% to 47%. The average global image analysis break strain varies from 32.36% to 34.81% and the average local image analysis break strain varies from 34.88% to 39.21%; from this, it was determined that strain rate does not have a significant effect on break strain values and there is no clear trend. Figure 4.6 displays strain vs. force plots by taking the average of each strain rate that was investigated.

Table 4.6: 100% Cotton Denim - Average Strain Rate Results

| Strain Rate (%/min) | 400 | 100 | 10 | 5 | 1 |
|--------------------------------------|--------|--------|--------|--------|--------|
| Average Break Force (N) | 2115.3 | 2027.0 | 1802.0 | 1692.7 | 1467.0 |
| Average Machine Break Strain (%) | 53.97 | 54.70 | 52.87 | 47.27 | 51.00 |
| Average Global I.A. Break Strain (%) | 34.81 | 34.39 | 33.86 | 32.36 | 32.40 |
| Average Local I.A. Break Strain (%) | 39.21 | 38.57 | 37.85 | 34.88 | 36.90 |

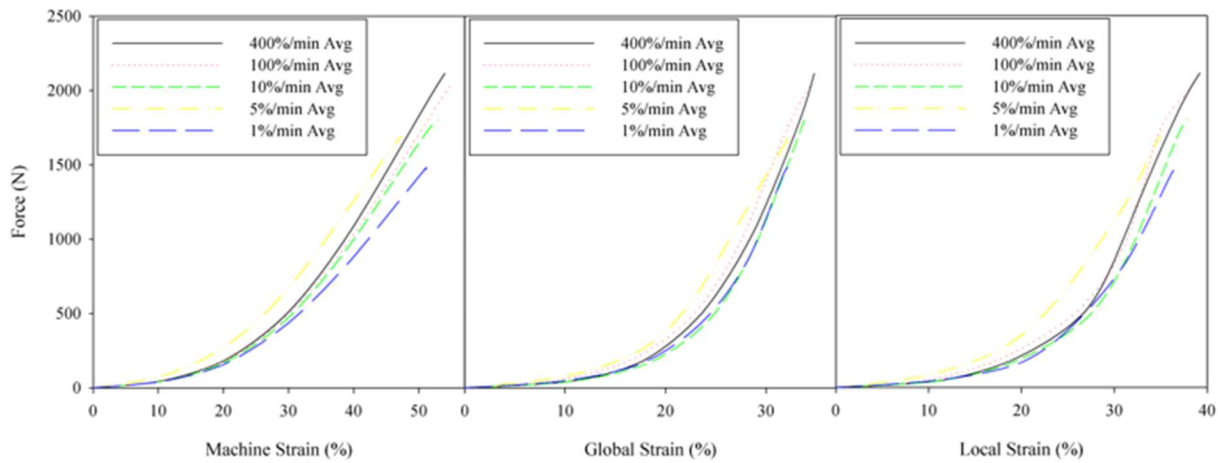


Figure 4.6. 100% cotton denim - average strain rate results.

To further investigate the effect of strain rate on break force for 100% cotton denim, strain rate was plotted against break force (Figure 4.7). A logarithmic trendline was then fit to the average of the data, which resulted in an R^2 value of 0.978; this indicates a strong relationship between strain rate and break force. This correlation allows for good approximation of break strengths at other strain rates that were not directly tested.

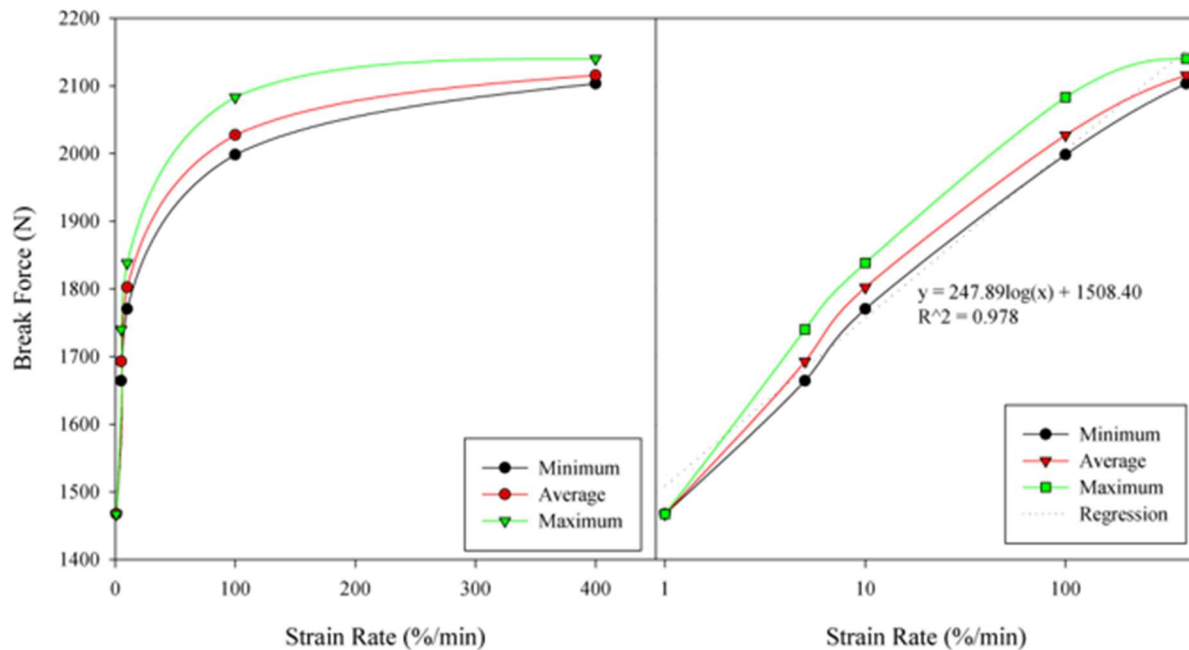


Figure 4.7. Strain rate effect on break force in 100% cotton denim.

4.1.2 100% Polyester

Three tests were completed on the same 100% polyester for each of the following strain rates: 400%/min, 100%/min, 10%/min, 5%/min, and 1%/min. Break force, machine break strain, global image analysis break strain, and local image analysis break strain for this testing are provided in Tables 4.7 through 4.11. Strain vs. force plots from the tensile testing from each strain rate are shown in Figures 4.8 through 4.12.

Table 4.7: 100% Polyester - 400%/min Strain Rate Results

| Test I.D. | 400e | 400f | 400h | Average | Std. Dev. |
|------------------------------|-------|-------|-------|---------|-----------|
| Break Force (N) | 1732 | 1717 | 1736 | 1728.33 | 10.02 |
| Machine Break Strain (%) | 37.27 | 37.74 | 38.16 | 37.72 | 0.45 |
| Global I.A. Break Strain (%) | 23.31 | 26.38 | 25.13 | 24.94 | 1.54 |
| Local I.A. Break Strain (%) | 27.62 | 32.17 | 31.29 | 30.36 | 2.41 |

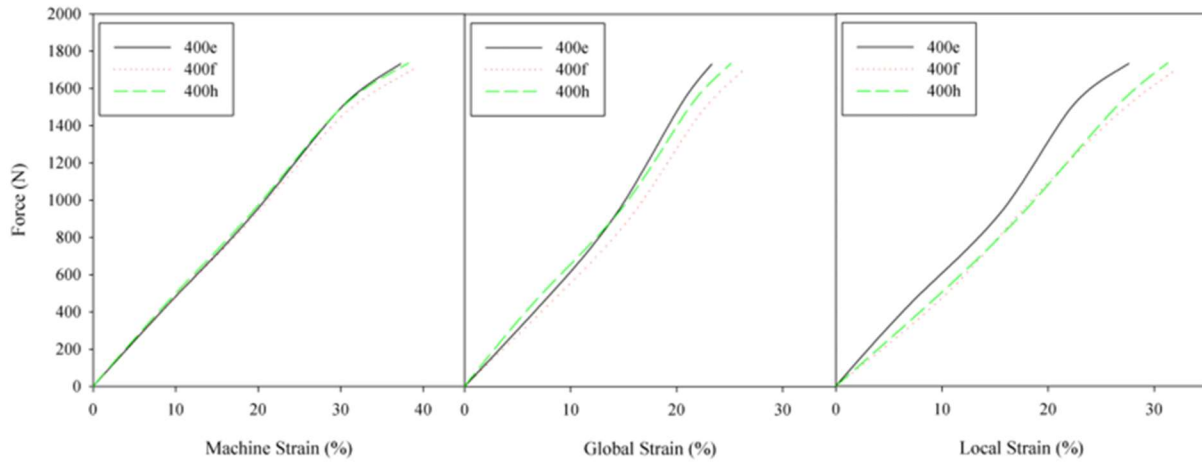


Figure 4.8. 100% polyester - 400%/min strain rate results.

Table 4.8: 100% Polyester - 100%/min Strain Rate Results

| Test I.D. | 100e | 100h | 100i | Average | Std. Dev. |
|------------------------------|-------|-------|-------|---------|-----------|
| Break Force (N) | 1832 | 1660 | 1724 | 1738.67 | 86.93 |
| Machine Break Strain (%) | 36.64 | 36.85 | 40.31 | 37.93 | 2.06 |
| Global I.A. Break Strain (%) | 26.98 | 26.68 | 30.04 | 27.90 | 1.86 |
| Local I.A. Break Strain (%) | 30.61 | 31.75 | 35.57 | 32.64 | 2.60 |

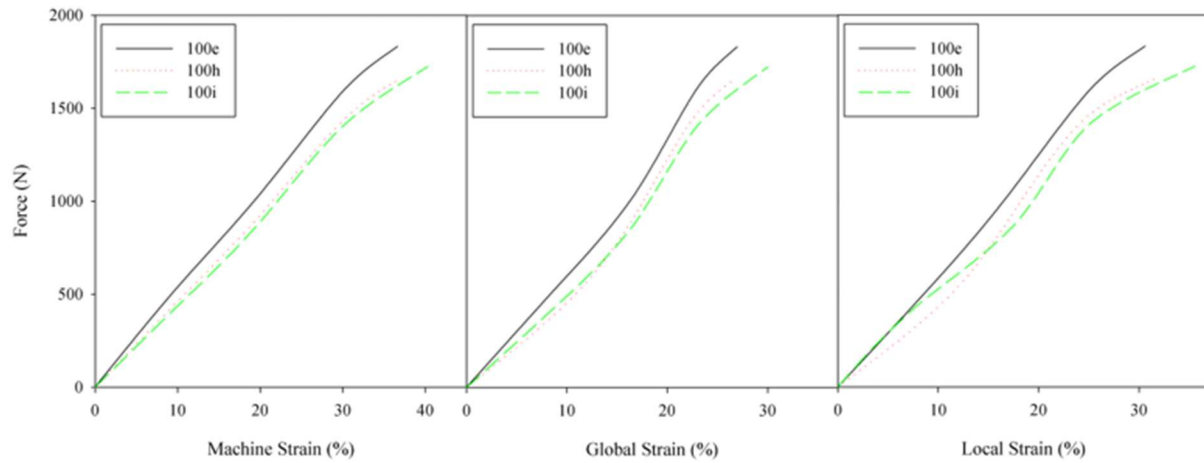


Figure 4.9. 100% polyester - 100%/min strain rate results.

Table 4.9: 100% Polyester - 10%/min Strain Rate Results

| Test I.D. | 10a | 10b | 10c | Average | Std. Dev. |
|------------------------------|-------|-------|-------|---------|-----------|
| Break Force (N) | 1668 | 1548 | 1696 | 1637.33 | 78.62 |
| Machine Break Strain (%) | 38.85 | 41.15 | 37.80 | 39.27 | 1.71 |
| Global I.A. Break Strain (%) | 27.10 | 28.72 | 25.03 | 26.95 | 1.85 |
| Local I.A. Break Strain (%) | 32.10 | 35.74 | 30.31 | 32.72 | 2.77 |

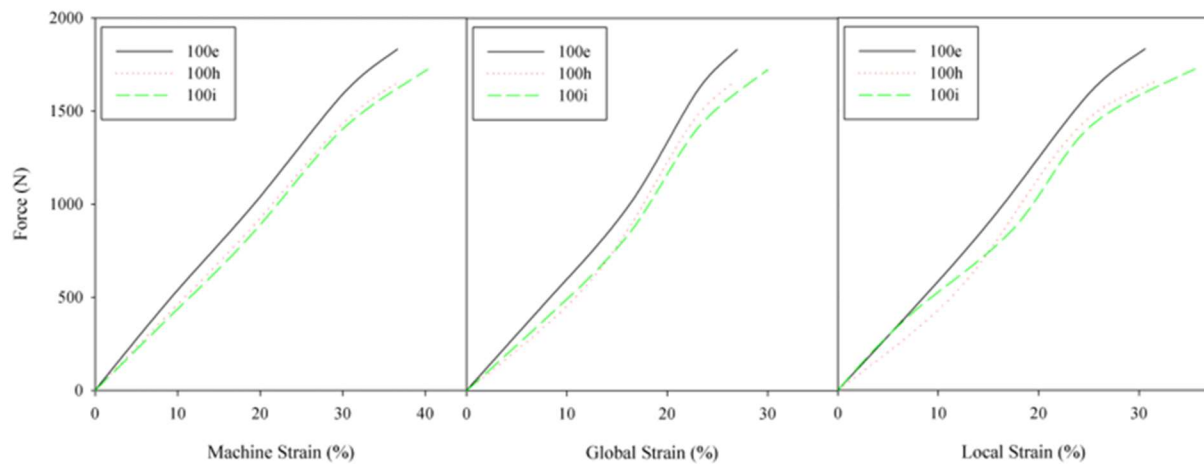


Figure 4.10. 100% polyester - 10%/min strain rate results.

Table 4.10: 100% Polyester - 5%/min Strain Rate Results

| Test I.D. | 5a | 5b | 5c | Average | Std. Dev. |
|------------------------------|-------|-------|-------|---------|-----------|
| Break Force (N) | 1646 | 1616 | 1608 | 1623.33 | 20.03 |
| Machine Break Strain (%) | 38.01 | 37.01 | 35.28 | 36.77 | 1.38 |
| Global I.A. Break Strain (%) | 26.02 | 25.93 | 23.76 | 25.24 | 1.28 |
| Local I.A. Break Strain (%) | 31.58 | 32.50 | 28.33 | 30.80 | 2.19 |

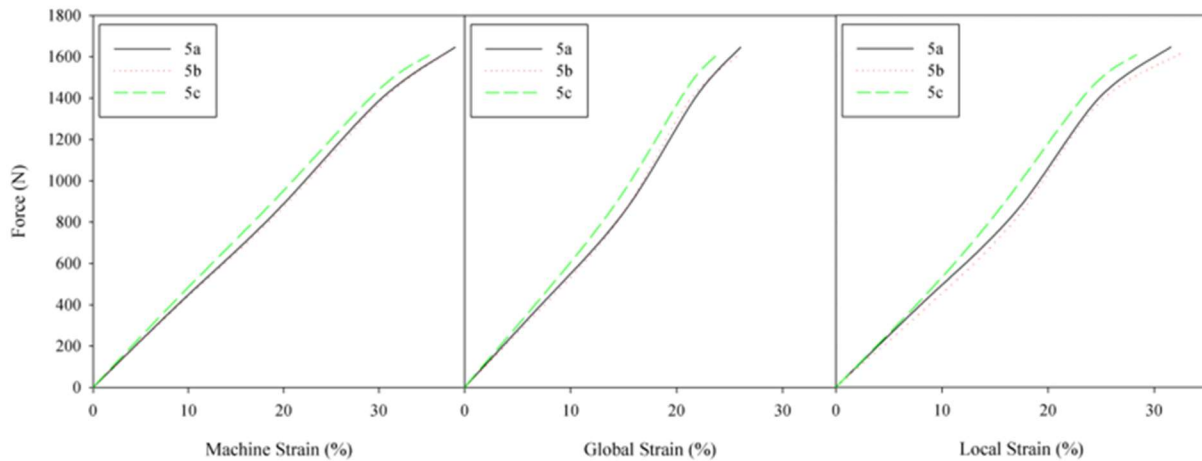


Figure 4.11. 100% polyester - 5%/min strain rate results.

Table 4.11: 100% Polyester - 1%/min Strain Rate Results

| Test I.D. | 1a | 1b | 1c | Average | Std. Dev. |
|------------------------------|-------|-------|-------|---------|-----------|
| Break Force (N) | 1352 | 1425 | 1508 | 1428.33 | 78.05 |
| Machine Break Strain (%) | 34.65 | 36.12 | 36.48 | 35.75 | 0.97 |
| Global I.A. Break Strain (%) | 21.95 | 21.65 | 23.26 | 22.29 | 0.86 |
| Local I.A. Break Strain (%) | 29.91 | 29.89 | 32.05 | 30.62 | 1.24 |

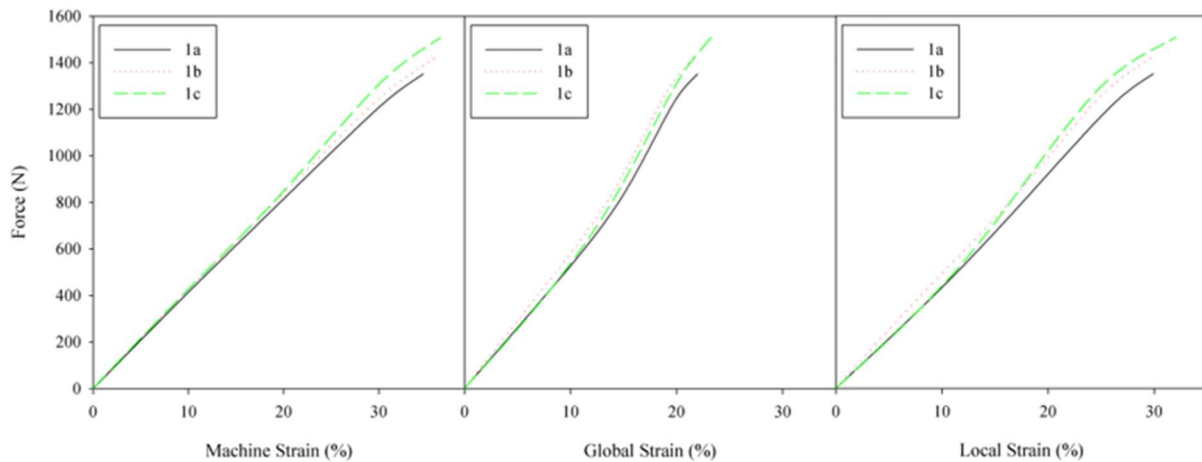


Figure 4.12. 100% polyester - 1%/min strain rate results.

For comparison purposes, an average break force, average machine break strain, average global image analysis break strain, and average local image analysis break strain were calculated, with the associated results being provided in Table 4.12. From this table, a trend can be seen that as strain rate decreases (as the test is run more slowly), there is a decrease in break force; it was consequently determined that strain rate has a significant effect on break force. The average machine break strain ranges from 36.77% to 39.27%. The average global image analysis break strain varies from 22.29% to 27.90% and the average local image analysis break strain varies from 30.36% to 32.72%; from this, it was determined that strain rate does not have a significant effect

on break strain values and there is no clear trend. Figure 4.13 displays strain vs. force plots by taking the average of each strain rate that was investigated.

Table 4.12: 100% Polyester - Average Strain Rate Results

| Strain Rate (%/min) | 400 | 100 | 10 | 5 | 1 |
|--------------------------------------|---------|---------|---------|---------|---------|
| Average Break Force (N) | 1728.33 | 1738.67 | 1637.33 | 1623.33 | 1428.33 |
| Average Machine Break Strain (%) | 37.72 | 37.93 | 39.27 | 36.77 | 35.75 |
| Average Global I.A. Break Strain (%) | 24.94 | 27.90 | 26.95 | 25.24 | 22.29 |
| Average Local I.A. Break Strain (%) | 30.36 | 32.64 | 32.72 | 30.80 | 30.62 |

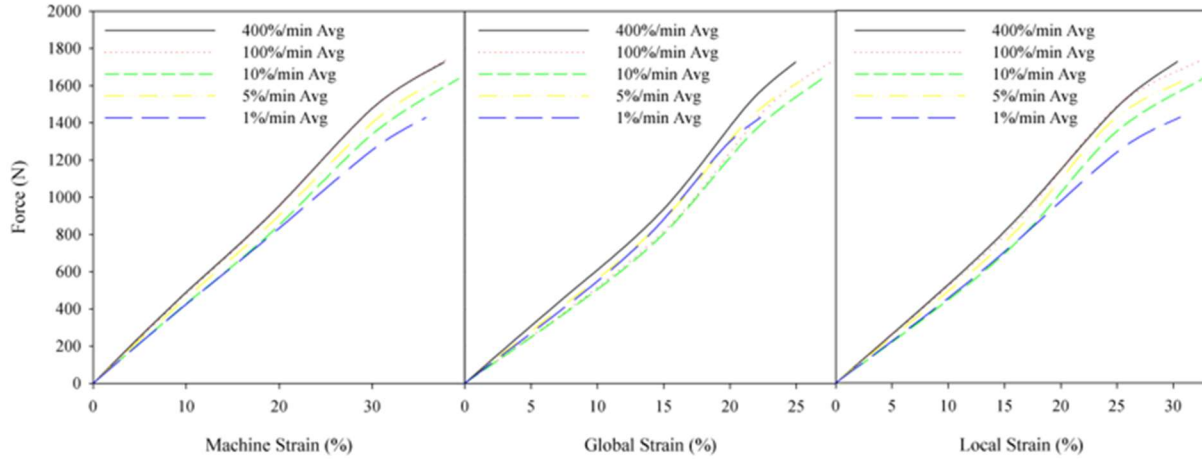


Figure 4.13. 100% polyester - average strain rate results.

To further investigate the effect of strain rate on break force in 100% polyester, strain rate was plotted against break force (Figure 4.14). A logarithmic trendline was then fit to the average of the data, which resulted in an R^2 value of 0.816; this indicates a moderate to high correlation between strain rate and break force, though not as strong as what was observed for the denim that was tested. This correlation allows for reasonable approximation of break strengths at other strain rates that were not directly tested.

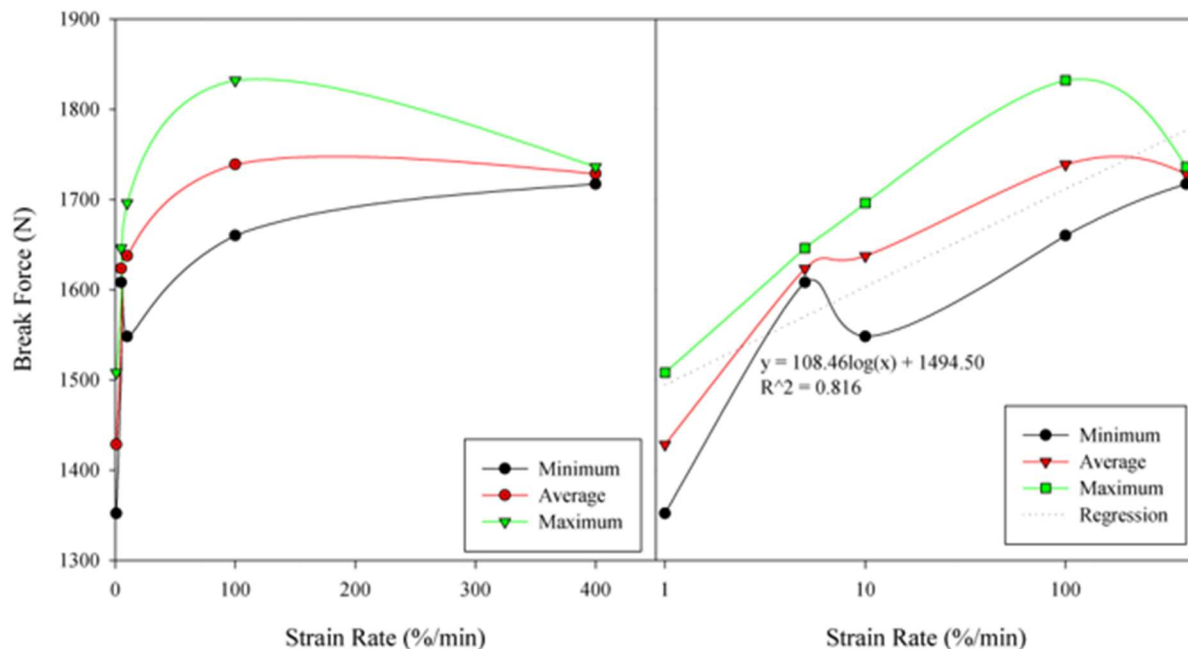


Figure 4.14. Strain rate effect on break force in 100% polyester.

From the above testing and analysis, it was decided that all tests should be run at a strain rate of 10%/min, which is in accordance with the standard test method for tensile properties of geotextile by the wide-width strip method (ASTM D4595), as this test method is the most widely used in the geotextile community when assessing geotextiles for their break forces and strain. Strain rates of 1%/min and 5%/min were dismissed as there is no standard stating that these rates should be used in testing; tests at these strain rates are also quite long which makes it difficult to test a large number of samples. The strain rate of 100%/min was also dismissed because there is no standard using this strain rate. Since it is well known that the majority of geotextiles fail due to slow, long-term strains, the strain rate of 400%/min was ruled out; however, there are some applications where a very fast strain rate is common and will cause failure. By acknowledging this, it is possible to approximate the break force of a test specimen at a strain rate of 400%/min by knowing the break force of the test specimen at a strain rate of 10%/min based on the equations that were calculated above via regression.

4.2 Tensile Testing of 100% Cotton Denim

A total of 257 samples from 33 different 100% cotton denim articles of clothing were subjected to tensile testing. Of these 257 samples, 164 were tested in the machine direction and 93 were tested in the cross direction. For each test, break force and machine break strain were obtained from the machine apparatus output. The image analysis technique was also used for each test to determine more accurate global and local strains.

4.2.1 Tensile Testing of 100% Cotton Denim - Machine Direction Results

A total of 164 samples were tested from 33 different articles of 100% cotton denim clothing in the machine direction. As discussed earlier, a digital image analysis technique was used to determine accurate break strains in the specimens while testing in an attempt to resolve the issues associated with slippage during tensile testing. Figure 4.15 displays the machine break strain vs. break force, Figure 4.16 displays the global image analysis break strain vs. break force, and Figure 4.17 displays the local image analysis strain vs. break force. Figure 4.18 displays the three different break strain mechanisms vs. break force in the same plot.

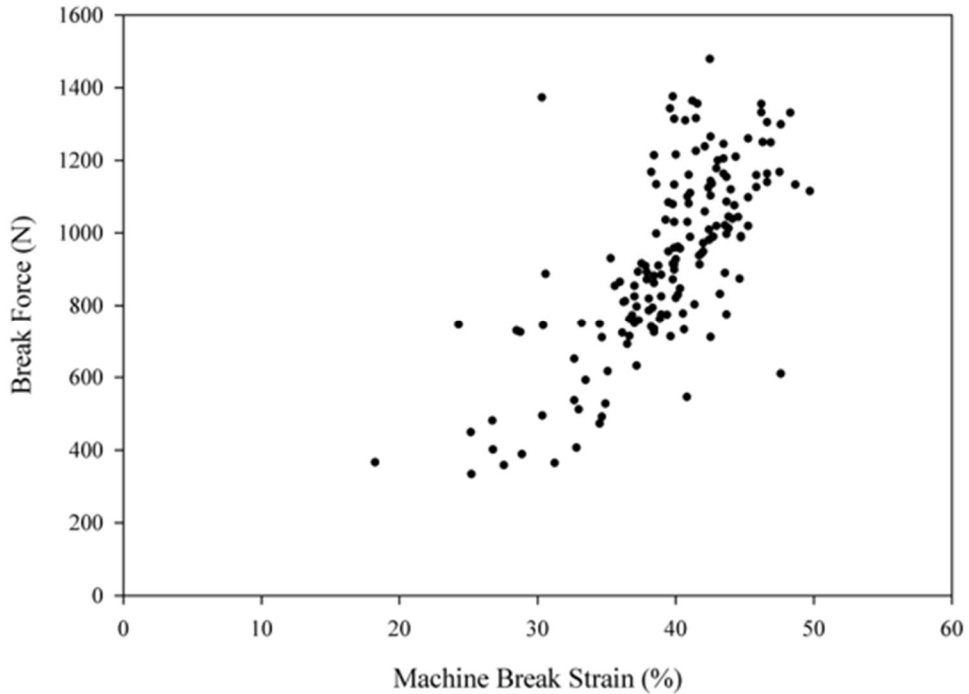


Figure 4.15 100% cotton denim machine direction - machine break strain vs. break force.

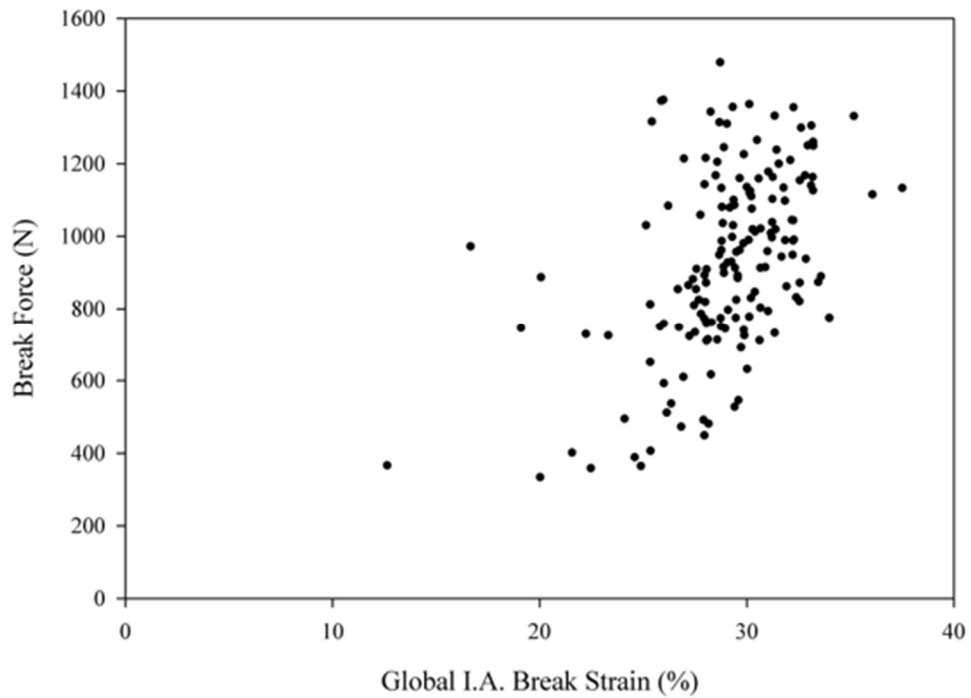


Figure 4.16 100% cotton denim machine direction - global image analysis break strain vs. break force.

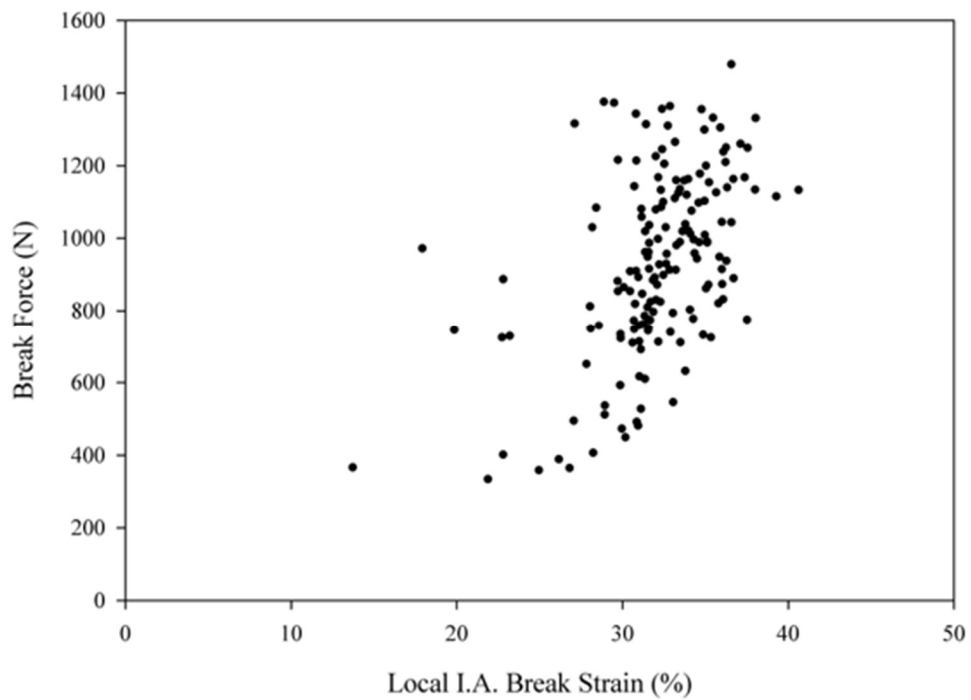


Figure 4.17 100% cotton denim machine direction - local image analysis break strain vs. break force.

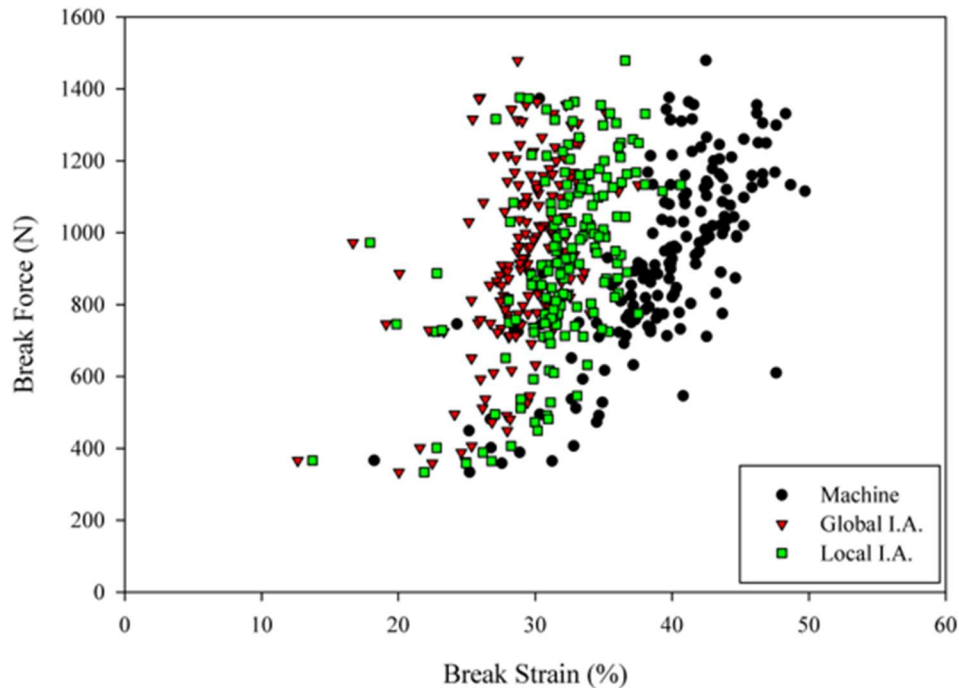


Figure 4.18 100% cotton denim machine direction - combined break strains vs. break force.

From these figures it can be observed that break values of machine strain are significantly larger than both image analysis techniques. Of the two image analysis techniques, the local image analysis technique provided larger values than the global image analysis technique. It was also observed that there is a lot of variation in break strains as well as break forces. To observe this further, a statistical analysis was completed on each variable: break force, machine break strain, local image analysis break strain, and global image analysis break strain.

Figure 4.19 displays the histogram and box plot with the 5th and 95th percentiles marked for the break force data. The mean and median break forces for the 100% cotton denim in the machine direction were 931 N (12.22 kN/m) and 934 N (12.26 kN/m), respectively. With these values being this similar and with a skewness value of -0.27, the data appears to be fairly symmetrical. The data produced a standard deviation of 251 N (3.29 kN/m) and a coefficient of variation of 26.9%. Break forces ranged from 334 N (4.38 kN/m) to 1479 N (19.41 kN/m). A 95% confidence interval was calculated to be 892 N (11.71 kN/m) to 970 N (12.73 kN/m); it was determined with 95% confidence that the population mean is within that range. No outliers were determined from this data set.

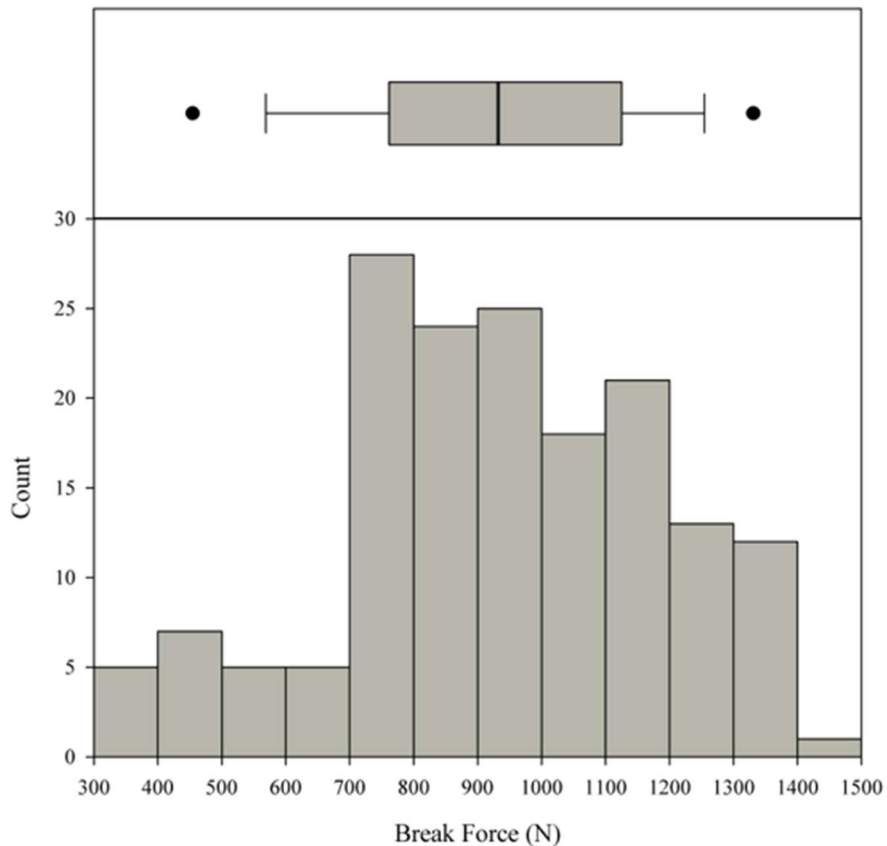


Figure 4.19 100% cotton denim machine direction - break force histogram and box plot.

Figure 4.20 displays the histogram and box plot with 5th and 95th percentiles marked for the machine break strain data. The mean and median break strains determined from the crosshead movement of the grips for the 100% cotton denim in the machine direction were 39.43% and 39.95%, respectively. Although the values of mean and median are similar, the data produced a skewness value of -1.04; this indicates that the data is skewed left. The data produced a standard deviation of 5.25% and a coefficient of variation of 13.31%. Machine break strains ranged from 18.23% to 49.71%. The 95% confidence interval was calculated to be 38.62% to 40.24%; it was determined with 95% confidence that the population mean is within that range. Some outliers in the data can be seen in the lower end of the data.

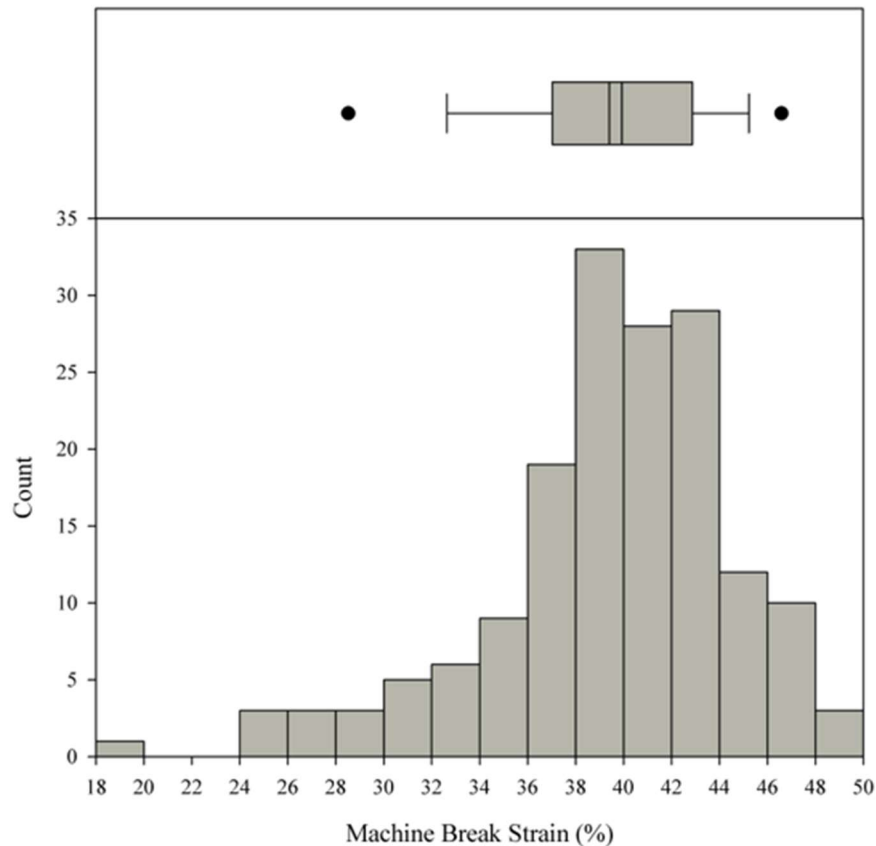


Figure 4.20 100% cotton denim machine direction - machine break strain histogram and box plot.

Figure 4.21 displays the histogram and box plot with 5th and 95th percentiles marked for the global image analysis break strain data. The mean and median break strains determined from the image analysis technique across the entire width of the specimen for the 100% cotton denim in the machine direction were 29.06% and 29.35%, respectively. Although the values of mean and median are similar, the data produced a skewness value of -1.40, which indicates that the data is skewed left. The data produced a standard deviation of 3.30% and a coefficient of variation of 11.35%. Global image analysis break strains ranged from 12.65% to 37.51%. A 95% confidence interval was calculated to be 28.56% to 29.57%; it was determined with 95% confidence that the population mean is within that range. Some outliers in the data can be seen at the extreme ends.

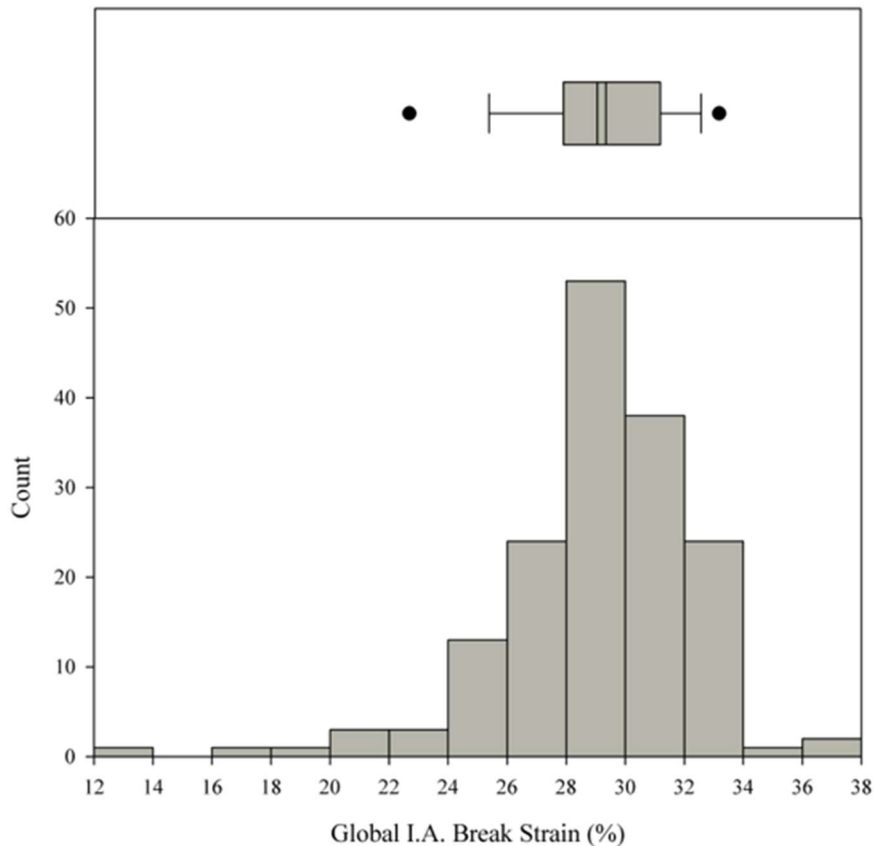


Figure 4.21 100% cotton denim machine direction - global image analysis break strain histogram and box plot.

Figure 4.22 displays the histogram and box plot with 5th and 95th percentiles marked for the local image analysis break strain data. The mean and median break strains determined from the image analysis technique for the center column of targets of the specimen for the 100% cotton denim in the machine direction were 32.06% and 32.18%, respectively. Although the values of mean and median are similar, the data produced a skewness value of -1.48, which indicates that the data is skewed left. The data produced a standard deviation of 3.78% and a coefficient of variation of 11.78%. Local image analysis break strains ranged from 13.73% to 40.63%. A 95% confidence interval was calculated to be 31.48% to 32.06%; it was determined with 95% confidence that the population mean is within that range. Some outliers in the data can be seen at the extreme ends.

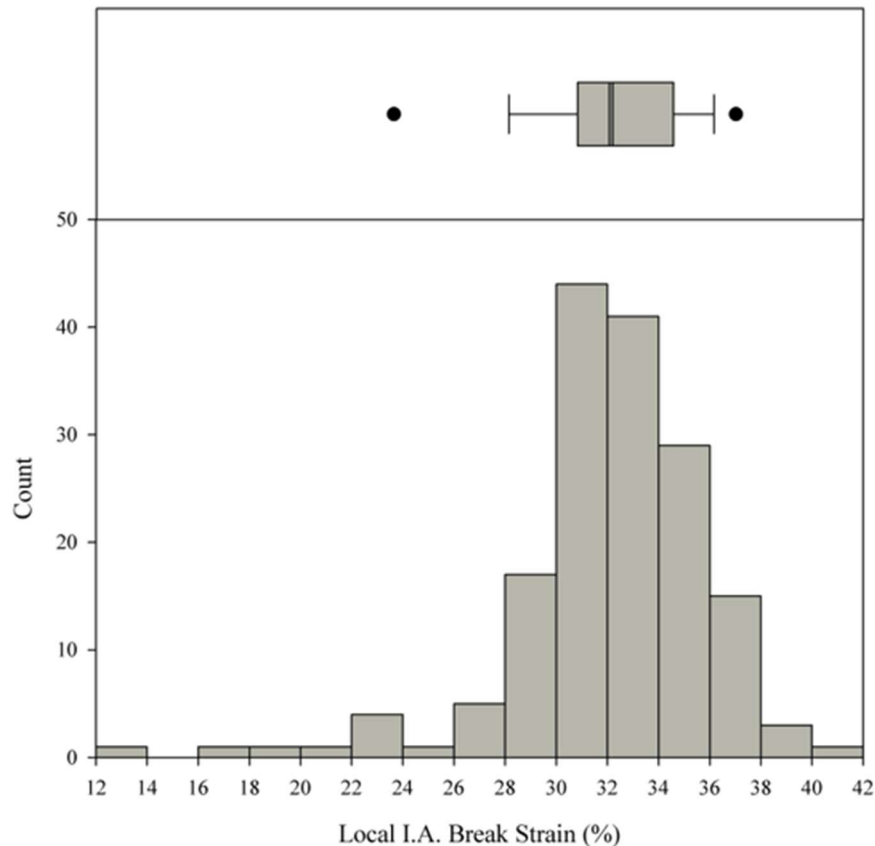


Figure 4.22 100% cotton denim machine direction - local image analysis break strain histogram and box plot.

Table 4.13 provides a summary of statistical values from the tensile testing that was completed for the 100% cotton denim in the machine direction. This table includes the mean, median, standard deviation, coefficient of variation, skewness, range, and 95% confidence interval for break force, machine break strain, global image analysis break strain, and local image analysis break strain.

Table 4.13: 100% Cotton Denim Machine Direction Testing Results Summary

| | Break Force | Machine Break Strain | Global I.A. Break Strain | Local I.A. Break Strain |
|--------------------------|----------------|----------------------|--------------------------|-------------------------|
| Mean | 931 N | 39.43% | 29.06% | 32.06% |
| Median | 934 N | 39.95% | 29.35% | 32.18% |
| Standard Deviation | 251 N | 5.25% | 3.30% | 3.78% |
| Coefficient of Variation | 26.90% | 13.31% | 11.35% | 11.78% |
| Skewness | -0.27 | -1.04 | -1.40 | -1.48 |
| Range | 334 N - 1479 N | 18.23% - 49.71% | 12.65% - 37.51% | 13.73% - 40.63% |
| 95% Confidence Interval | 892 N - 970 N | 38.62% - 40.24% | 28.56% - 29.57% | 31.48% - 32.06% |

As noted earlier, the machine break strain values are significantly larger than those obtained from either of the image analysis techniques that were utilized; this is particularly obvious when comparing the mean and median values for these data sets. Of the two image analysis techniques,

the local image analysis technique provided larger values of strain than the global image analysis technique by approximately 3% strain. Overall, this information will first be used to compare with the results from the cross direction testing and then be used to compare with specification standards to determine which applications 100% cotton denim could potentially be used for.

4.2.2 Tensile Testing of 100% Cotton Denim - Cross Direction Results

A total of 93 samples were tested from 33 different articles of 100% cotton denim clothing in the cross direction. Again, a digital image analysis technique was used to determine accurate break strains in the specimens while testing in an attempt to resolve the issues associated with slippage during tensile testing. Figure 4.23 displays the machine break strain vs. break force, Figure 4.24 displays the global image analysis break strain vs. break force, and Figure 4.25 displays the local image analysis strain vs. break force. Figure 4.26 displays the three different break strain mechanisms vs. break force in the same plot.

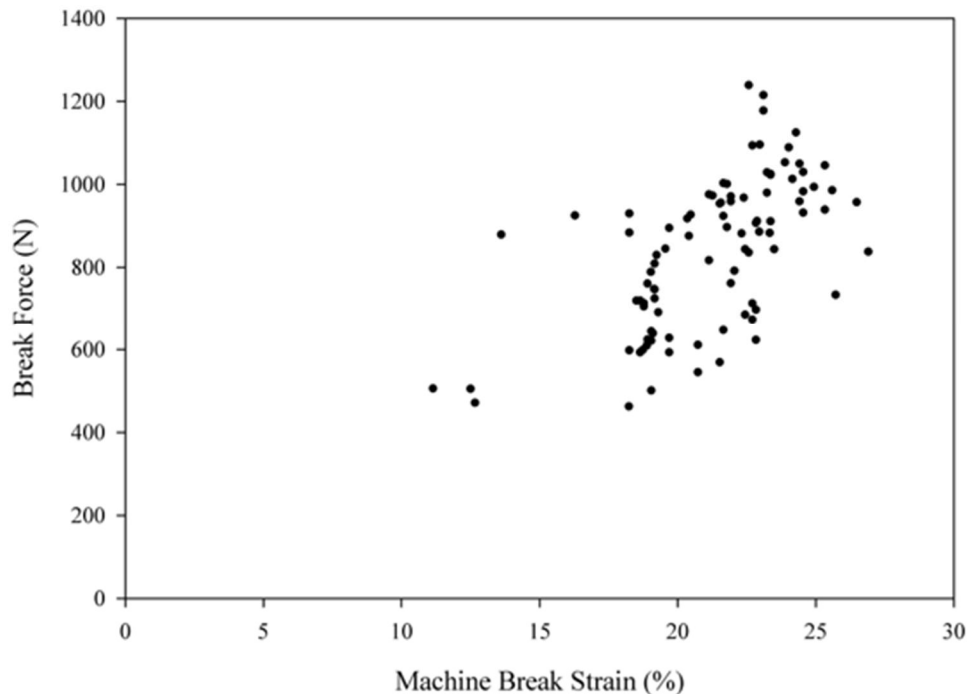


Figure 4.23 100% cotton denim cross direction - machine break strain vs. break force.

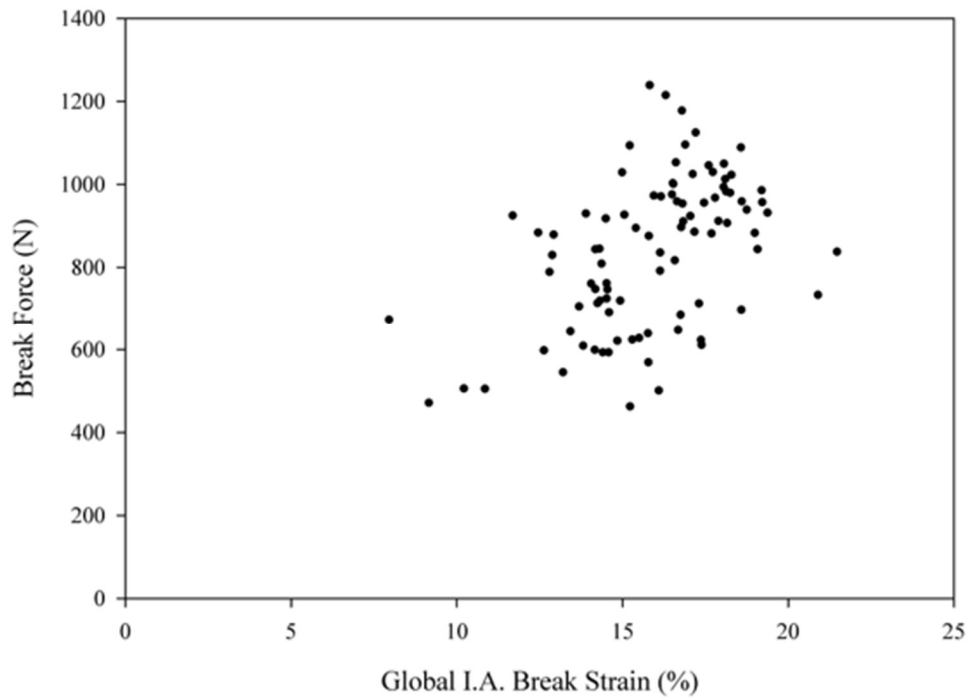


Figure 4.24 100% cotton denim cross direction - global image analysis break strain vs. break force.

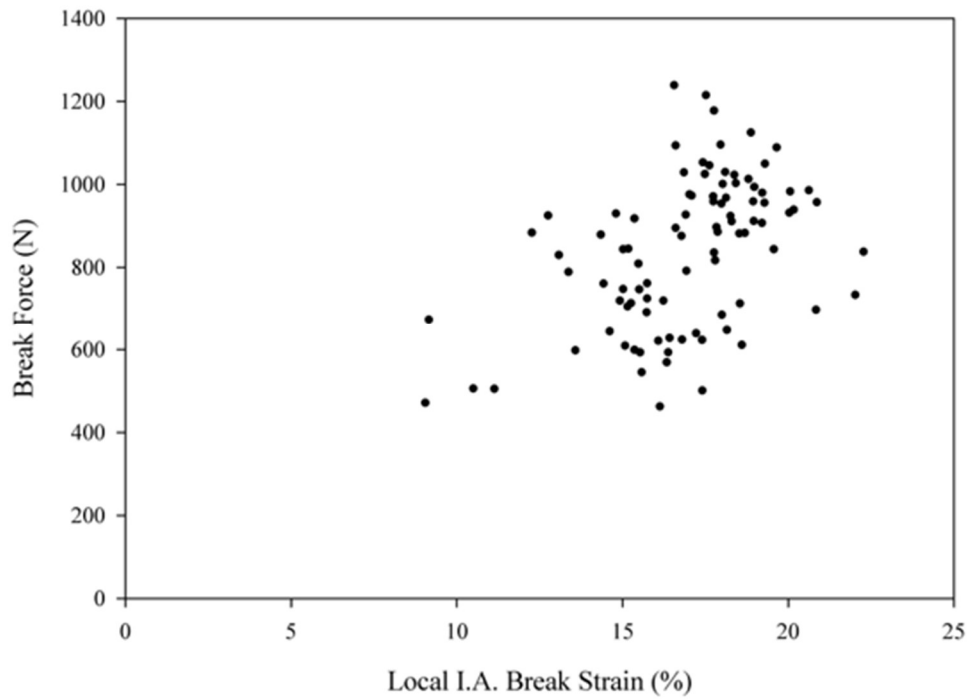


Figure 4.25 100% cotton denim cross direction - local image analysis break strain vs. break force.

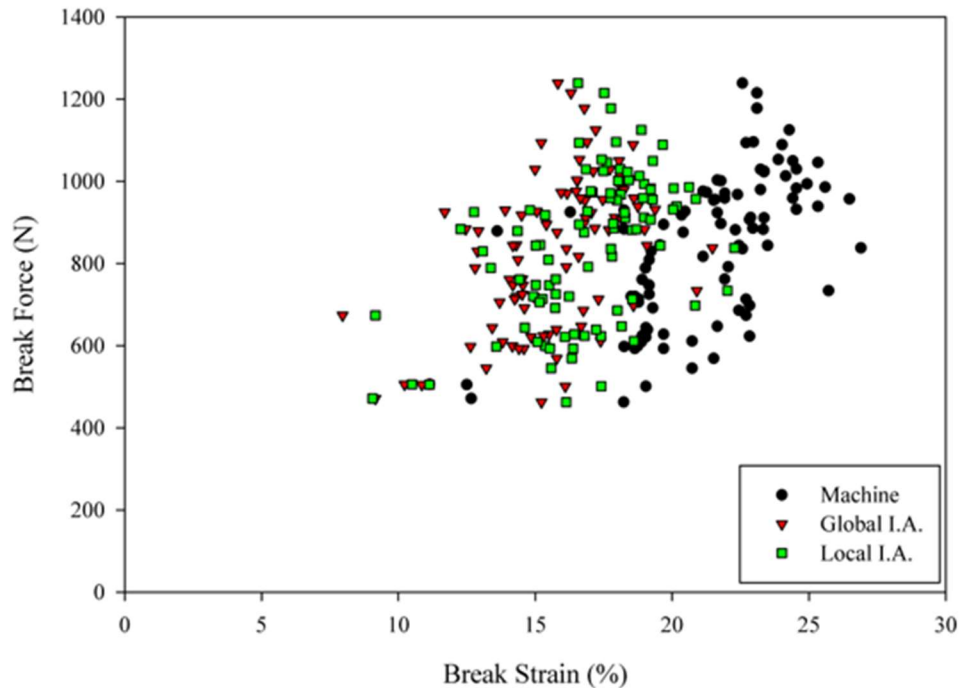


Figure 4.26 100% cotton denim cross direction - combined break strains vs. break force.

Similar to the results from the machine direction testing these figures show that break values of machine strain are significantly larger than those obtained from both image analysis techniques. Of the two image analysis techniques, the local image analysis technique provided larger values than the global image analysis technique. It was also observed that there is a lot of variation in break strains as well as break forces. To observe this phenomenon further, a statistical analysis was completed on each variable: break force, machine break strain, local image analysis break strain, and global image analysis break strain.

Figure 4.27 displays the histogram and box plot with 5th and 95th percentiles marked for the break force data. The mean and median break forces for the 100% cotton denim in the cross direction were 837 N (10.98 kN/m) and 879 N (11.54 kN/m), respectively. With these values being this similar and with a skewness value of -0.16, the data appears to be fairly symmetrical. The data produced a standard deviation of 181 N (2.38 kN/m) and a coefficient of variation of 21.59%. Break forces ranged from 462.5 N (6.07 kN/m) to 1239 N (16.26 kN/m). A 95% confidence interval was calculated to be 800 N (10.50 kN/m) to 874 N (11.47 kN/m); it was determined with 95% confidence that the population mean is within that range. No outliers were determined from this data set.

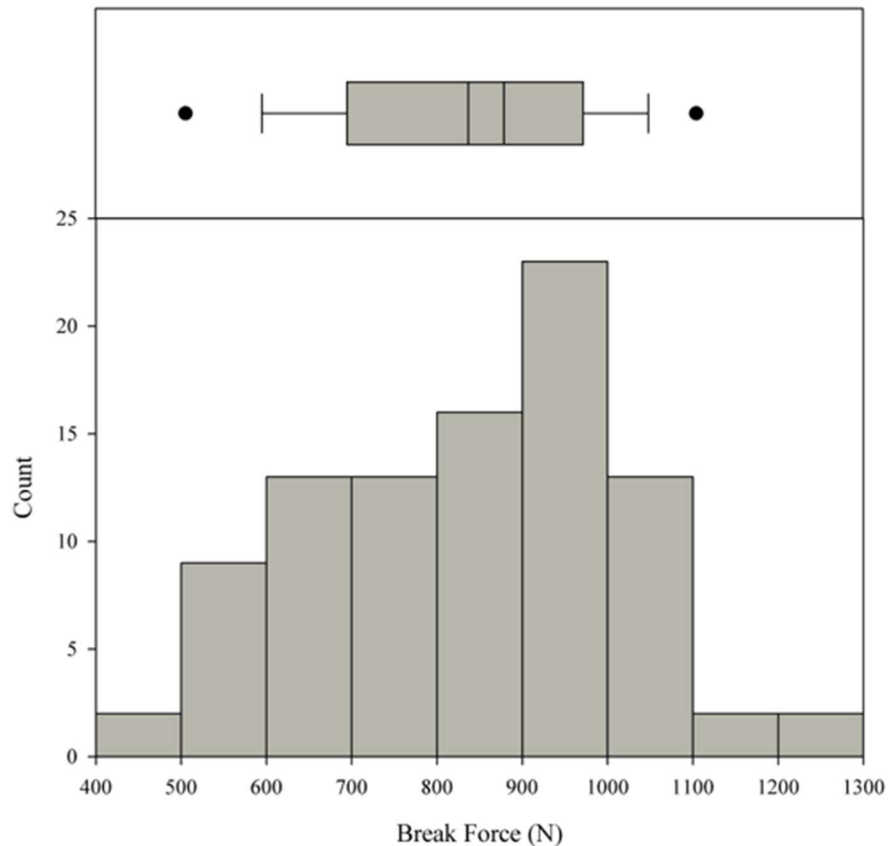


Figure 4.27 100% cotton denim cross direction - break force histogram and box plot.

Figure 4.28 displays the histogram and box plot with 5th and 95th percentiles marked for the machine break strain data. The mean and median break strains determined from the crosshead movement of the grips for the 100% cotton denim in the cross direction was 21.21% and 21.65%, respectively. Although the values of mean and median are similar, the data produced a skewness value of -0.93, which indicates that the data is moderately skewed left. The data set had a standard deviation of 2.93% and a coefficient of variation of 13.83%. Machine break strains ranged from 11.14% to 26.90%. A 95% confidence interval was calculated to be 20.61% to 21.82%; it was determined with 95% confidence that the population mean is within that range. Some outliers in the data can be seen in the lower end of the data.

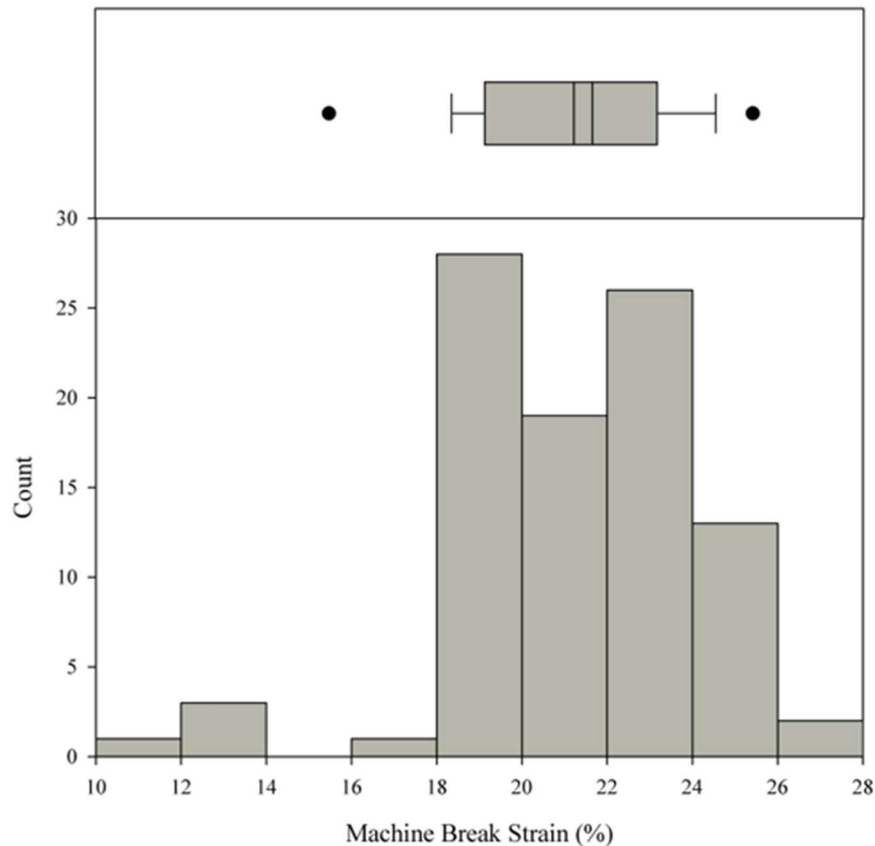


Figure 4.28 100% cotton denim cross direction - machine break strain histogram and box plot.

Figure 4.29 displays the histogram and box plot with 5th and 95th percentiles marked for the global image analysis break strain data. The mean and median break strains determined from the image analysis technique across the entire width of the specimen for the 100% cotton denim in the cross direction was 15.88% and 16.14%, respectively. Although the values of mean and median are similar, the data set produced a skewness value of -0.63, which indicates that the data is moderately skewed left. The data set had a standard deviation of 2.37% and a coefficient of variation of 14.93%. Global image analysis break strains ranged from 7.96% to 21.47%. A 95% confidence interval was calculated to be 15.39% to 16.37%; it was determined with 95% confidence that the population mean is within that range. Some outliers in the data can be seen at the extreme ends.

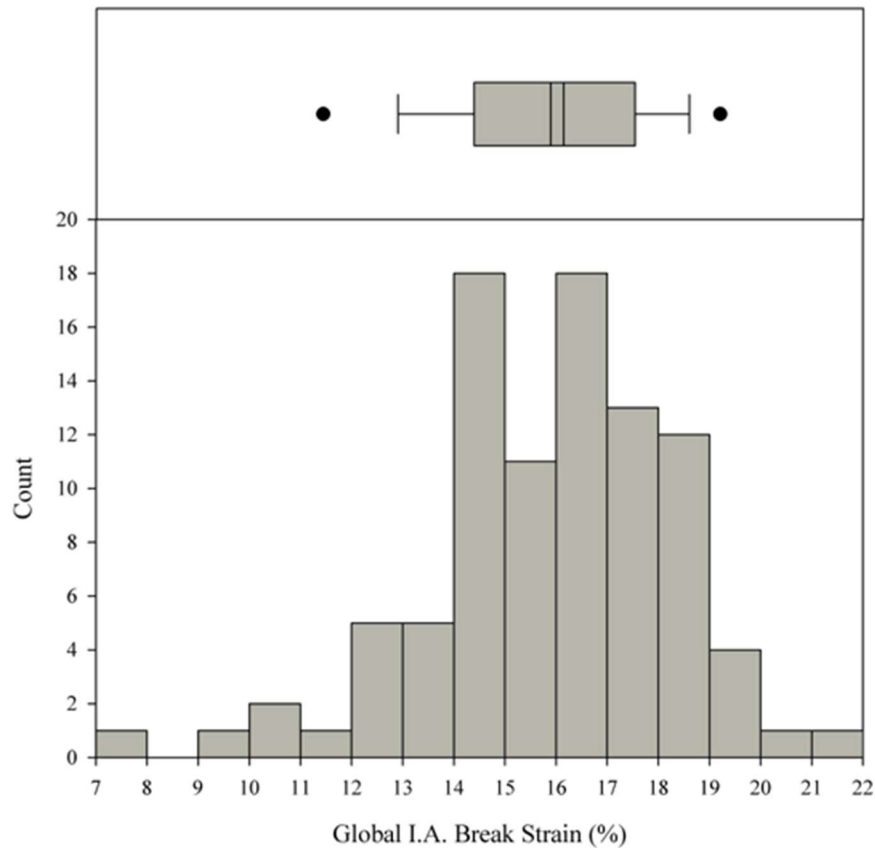


Figure 4.29 100% cotton denim cross direction - global image analysis break strain histogram and box plot.

Figure 4.30 displays the histogram and box plot with the 5th and 95th percentiles marked for the local image analysis break strain data. The mean and median break strain determined from the image analysis technique for the center column of targets of the specimen for the 100% cotton denim in the cross direction was approximately 16.91% and 17.40%, respectively. Although the values of mean and median are similar, the data set produced a skewness value of -0.81, which indicates that the data is moderately skewed left. The data set had a standard deviation of 2.47% and a coefficient of variation of 14.60%. Local image analysis break strains ranged from 9.05% to 22.27%. A 95% confidence interval was calculated to be 16.40% to 17.42%; it was determined with 95% confidence that the population mean is within that range. Some outliers in the data can be seen at the extreme ends.

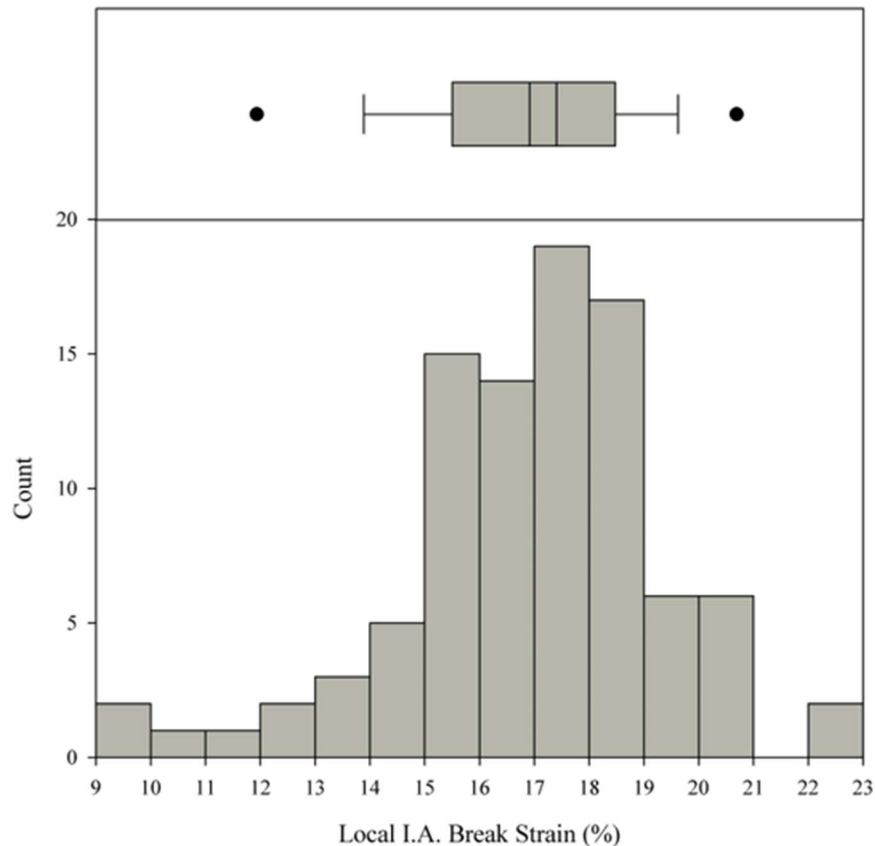


Figure 4.30 100% cotton denim cross direction - local image analysis break strain histogram and box plot.

Table 4.14 provides a summary of statistical values from the tensile testing that was completed for the 100% cotton denim in the cross direction. This table includes the mean, median, standard deviation, coefficient of variation, skewness, range, and 95% confidence interval for break force, machine break strain, global image analysis break strain, and local image analysis break strain.

Table 4.14: 100% Cotton Denim Cross Direction Testing Results Summary

| | Break Force | Machine Break Strain | Global I.A. Break Strain | Local I.A. Break Strain |
|--------------------------|------------------|----------------------|--------------------------|-------------------------|
| Mean | 837 N | 21.21% | 15.88% | 16.91% |
| Median | 879 N | 21.82% | 16.14% | 17.40% |
| Standard Deviation | 181 N | 2.93% | 2.37% | 2.47% |
| Coefficient of Variation | 21.59% | 13.83% | 14.93% | 14.60% |
| Skewness | -0.16 | -0.93 | -0.63 | -0.81 |
| Range | 462.5 N - 1239 N | 11.14% - 26.90% | 7.96% - 21.47% | 9.05% - 22.27% |
| 95% Confidence Interval | 800 N - 874 N | 20.61% - 21.82% | 15.39% - 16.37% | 16.40% - 17.42% |

Again, machine break strain values are significantly larger than those obtained from both image analysis techniques; this can be clearly observed when comparing the mean and median values.

Of the two image analysis techniques, the local image analysis technique provided larger values of strain than the global image analysis technique by approximately 1% strain.

Due to the nature of geotextile use, it is important to understand the tensile strength and break strains in both the machine and cross directions.

4.2.3 Tensile Testing of 100% Cotton Denim - Machine vs. Cross Direction Comparison

Table 4.15 compares the statistical values of break force for the machine and cross directions. The mean and median break forces in the machine direction were larger than those for the cross direction. Tensile testing for the machine direction also produced a larger standard deviation and coefficient of variation when compared to testing in the cross direction. When looking at the range of break forces produced by the two directions, the testing in the machine direction produced overall lower and higher values for break force. The 95% confidence interval was approximately 100 N larger on the lower and upper bound ends of the interval for the machine direction compared to the cross direction.

Table 4.15: 100% Cotton Denim Break Force Comparison - Machine vs. Cross Direction

| | Machine Direction | Cross Direction |
|--------------------------|-------------------|------------------|
| Mean | 931 N | 837 N |
| Median | 934 N | 879 N |
| Standard Deviation | 251 N | 181 N |
| Coefficient of Variation | 26.90% | 21.59% |
| Skewness | -0.27 | -0.16 |
| Range | 334 N - 1479 N | 462.5 N - 1239 N |
| 95% Confidence Interval | 892 N - 970 N | 800 N - 874 N |

Table 4.16 compares the statistical values of machine break strain for the machine and cross direction. The mean and median machine break strains in the machine direction were larger than those in the cross direction, by approximately double. Tensile testing from the machine direction also produced a larger standard deviation but a similar coefficient of variation when compared to the cross directional testing. The overall range of machine break strains was larger for the machine direction with a range of approximately 30% compared to the cross direction with a range of approximately 15%. The 95% confidence interval bounds for the machine direction were approximately double than the 95% confidence interval bounds for the cross direction (38.62% - 40.24% compared to 20.61% - 21.82%).

Table 4.16: 100% Cotton Denim Machine Break Strain Comparison - Machine vs. Cross Direction

| | Machine Direction | Cross Direction |
|--------------------------|-------------------|-----------------|
| Mean | 39.43% | 21.21% |
| Median | 39.95% | 21.82% |
| Standard Deviation | 5.25% | 2.93% |
| Coefficient of Variation | 13.31% | 13.83% |
| Skewness | -1.04 | -0.93 |
| Range | 18.23% - 49.71% | 11.14% - 26.90% |
| 95% Confidence Interval | 38.62% - 40.24% | 20.61% - 21.82% |

Table 4.17 compares the statistical values of global image analysis break strain for the machine and cross directions. The mean and median machine break strains in the machine direction were larger than those in the cross direction, by approximately double. Tensile testing from the machine direction also produced a larger standard deviation but a similar coefficient of variation when compared to the cross directional testing. The overall range of global image analysis break strains was larger for the machine direction with a range of approximately 25% compared to the cross direction with a range of approximately 14%. The 95% confidence interval bounds for the machine direction were much larger than the 95% confidence interval bounds for the cross direction (28.56% - 29.57% compared to 15.39% - 16.37%).

Table 4.17: 100% Cotton Denim Global I.A. Break Strain Comparison - Machine vs. Cross Direction

| | Machine Direction | Cross Direction |
|--------------------------|-------------------|-----------------|
| Mean | 29.06% | 15.88% |
| Median | 29.35% | 16.14% |
| Standard Deviation | 3.30% | 2.37% |
| Coefficient of Variation | 11.35% | 14.93% |
| Skewness | -1.4 | -0.63 |
| Range | 12.65% - 37.51% | 7.96% - 21.47% |
| 95% Confidence Interval | 28.56% - 29.57% | 15.39% - 16.37% |

Table 4.18 compares the statistical values of local image analysis break strain for the machine and cross directions. The mean and median machine break strains in the machine direction were larger than those in the cross direction, by approximately double. Tensile testing from the machine direction also produced a larger standard deviation but a similar coefficient of variation when compared to testing in the cross direction. The overall range of local image analysis break strains was larger for the machine direction with a range of approximately 25% compared to the cross direction with a range of approximately 13%. The 95% confidence interval bounds for the machine direction were much larger than the 95% confidence interval bounds for the cross direction (31.48% - 32.06% compared to 16.40% - 17.42%).

Table 4.18: 100% Cotton Denim Local I.A. Break Strain Comparison - Machine vs. Cross Direction

| | Machine Direction | Cross Direction |
|--------------------------|-------------------|-----------------|
| Mean | 32.06% | 16.91% |
| Median | 32.18% | 17.40% |
| Standard Deviation | 3.78% | 2.47% |
| Coefficient of Variation | 11.78% | 14.60% |
| Skewness | -1.48 | -0.81 |
| Range | 13.73% - 40.63% | 9.05% - 22.27% |
| 95% Confidence Interval | 31.48% - 32.06% | 16.40% - 17.42% |

Overall, larger break forces and break strains were observed from tensile testing in the machine direction when compared to tensile testing in the cross direction. However, it should be noted that for break force, minimum average roll value (MARV) is used in AASHTO Specification M288 (2015).

4.3 Permittivity Testing of 100% Cotton Denim

A total of seven 100% cotton denim articles were tested to measure permittivity. As stated in an earlier section, four specimens were cut from each article of clothing and each specimen was tested five times and the results were averaged; this produces a total of 28 specimens tested and 140 total permittivity tests for the 100% cotton denim. However, only three specimens were cut from one of the seven articles of recycled clothing for a total of 27 specimens, totaling 135 permittivity tests. The mean and median permittivity of the specimens for the 100% cotton denim was 0.016 sec^{-1} and 0.012 sec^{-1} , respectively. The data produced a skewness value of 1.69, which indicates that the data is skewed right. The data set had a standard deviation of 0.010 sec^{-1} and a coefficient of variation of 63.41%. Permittivity values ranged from 0.001 sec^{-1} to 0.049 sec^{-1} . A 95% confidence interval was calculated to be 0.014 sec^{-1} to 0.018 sec^{-1} ; it was determined with 95% confidence that the population mean is within that range. Figure 4.31 displays the histogram and boxplot for the permittivity results of the 100% cotton denim articles.

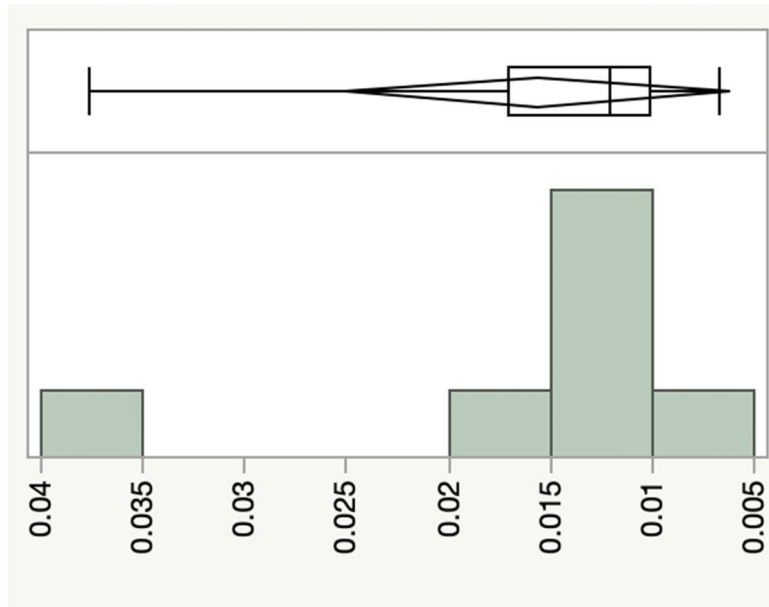


Figure 4.31 100% cotton denim permittivity test results.

4.4 Tensile Testing of 100% Polyester

A total of 100 samples from 11 different 100% Polyester articles of clothing were tensile tested. Of those 100 samples, 58 were tested in the machine direction and 42 were tested in the cross direction. However, after testing, it was determined that some of the materials that were tested were nonwoven when previously thought to be woven (articles P4, P6, P30, and P60). After those results were filtered out, 58 total samples from 7 different textile articles were used for analysis; 30 were tested in the machine direction and 28 were tested in the cross direction. For each test, break force and machine break strain were given from the machine apparatus output. The image analysis technique was also used for each test to determine more accurate global and local strains. Figure 4.32 displays the machine break strain vs. break force, Figure 4.33 displays the global image analysis break strain vs. break force, and Figure 4.34 displays the local image analysis strain vs. break force. Figure 4.35 displays the three different break strain mechanisms vs. break force in the same plot.

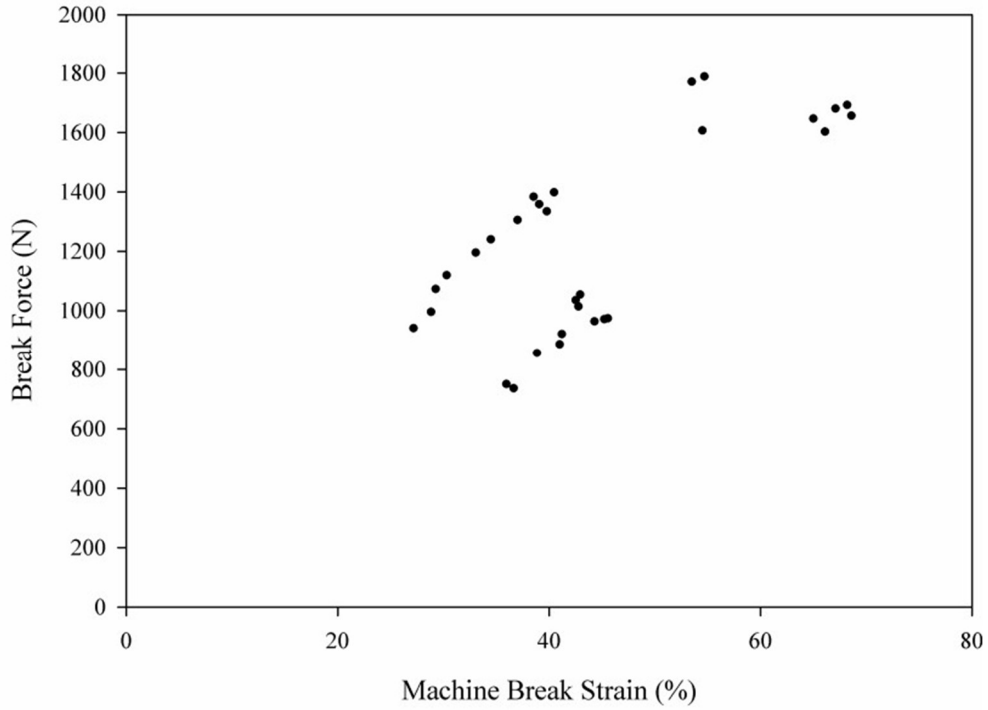


Figure 4.32 100% polyester machine direction - machine break strain vs. break force.

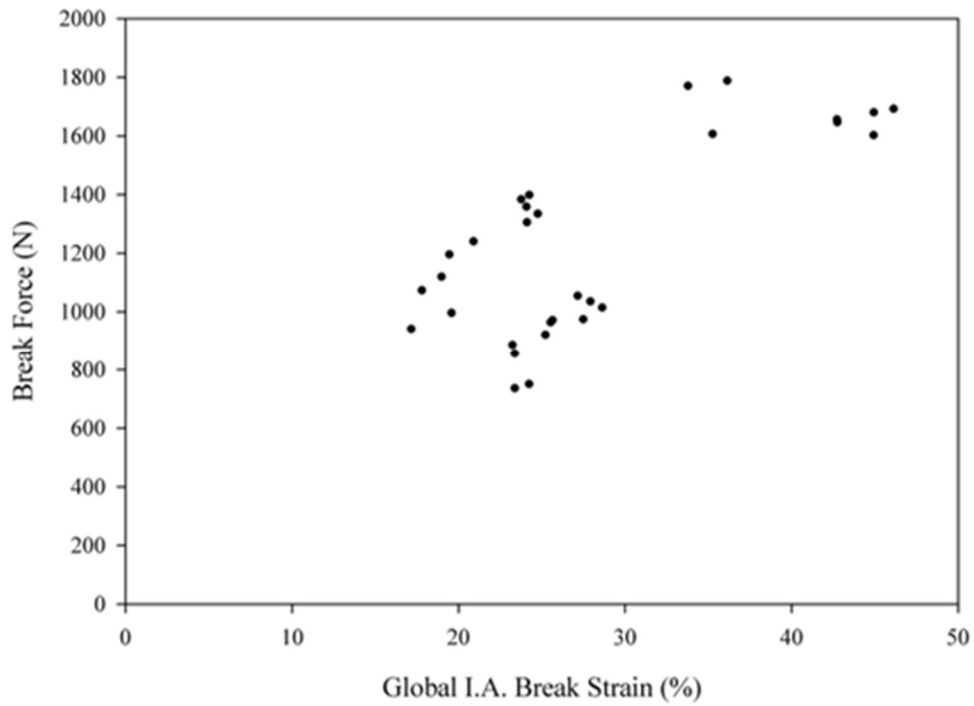


Figure 4.33 100% polyester machine direction - global image analysis break strain vs. break force.

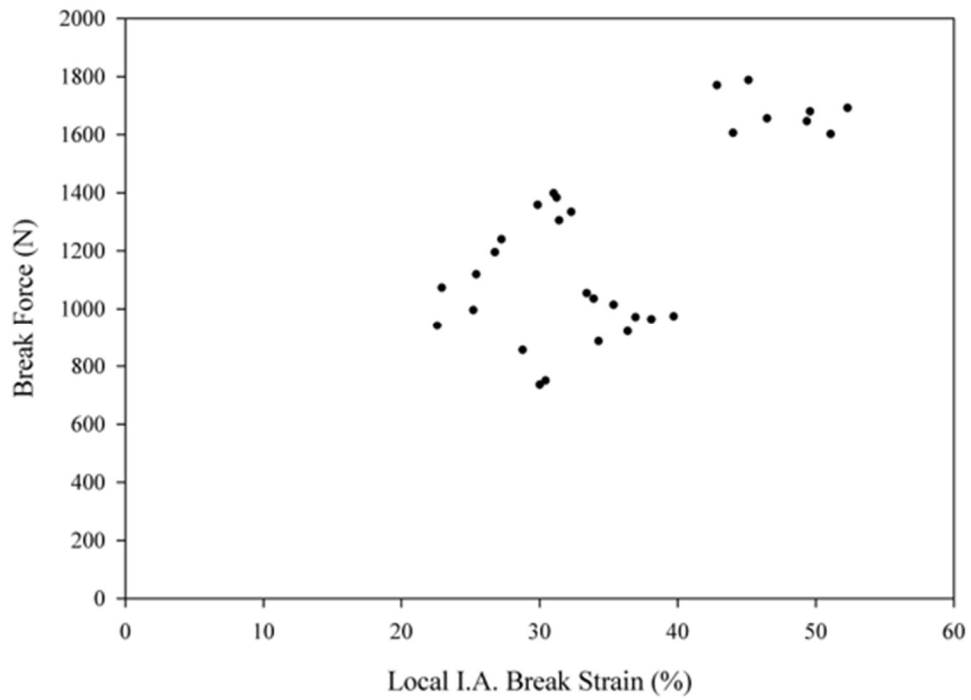


Figure 4.34 100% polyester machine direction - local image analysis break strain vs. break force.

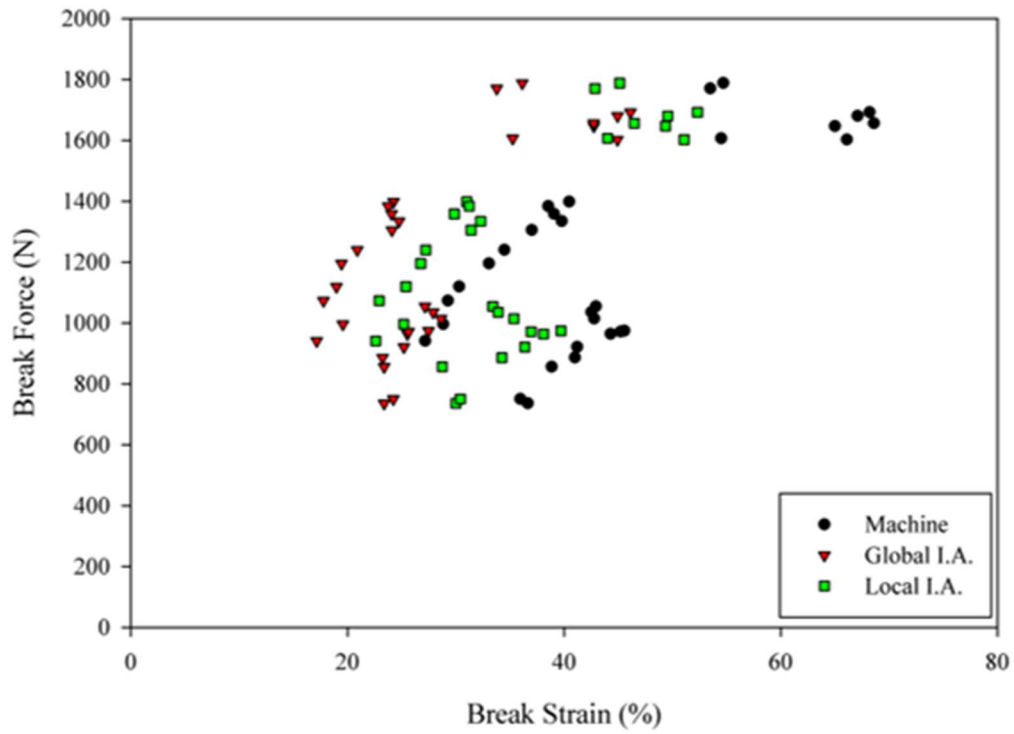


Figure 4.35 100% polyester machine direction - combined break strains vs. break force.

From these figures it can be observed that break values of machine strain are significantly larger than those that were determined from either of the image analysis techniques. Of the two image analysis techniques, the local image analysis technique provided larger values of strain than the global image analysis technique. It was also observed that there is a lot of variation in break strains as well as break forces. To examine this phenomenon further, a statistical analysis was completed on each variable: break force, machine break strain, local image analysis break strain, and global image analysis break strain.

4.4.1 Tensile Testing of 100% Polyester - Machine Direction Results

Figure 4.36 shows the histogram and box plot with 5th and 95th percentiles marked for the break force data. The mean and median break forces for the 100% polyester in the machine direction were 1231 (16.15 kN/m) and 1157 N (15.18 kN/m), respectively. With these values being this similar and with a skewness value of 0.32, it was determined that the data is fairly symmetrical. The data had a standard deviation of 325 N (4.27 kN/m) and a coefficient of variation of 26.4%. Break forces ranged from 736 N (9.66 kN/m) to 1788 N (23.46 kN/m). The 95% confidence interval was calculated to be from 1110 N (14.57 kN/m) to 1353 N (17.76 kN/m); it was determined with 95% confidence that the population mean is within this range. No outliers were determined from this data set.

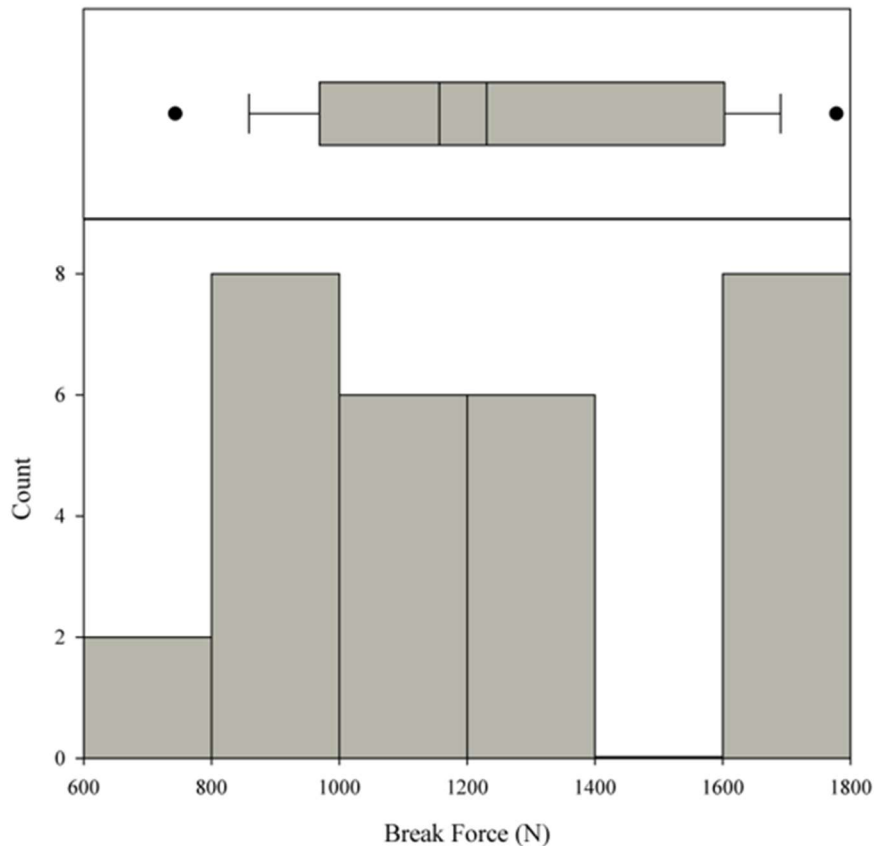


Figure 4.36 100% polyester machine direction - break force histogram and box plot.

Figure 4.37 displays the histogram and box plot with 5th and 95th percentiles marked for the machine break strain data. The mean and median break strains determined from the crosshead movement of the grips for the 100% polyester in the machine direction were 44.42% and 41.11%, respectively. Although the values of mean and median are similar, the data produced a skewness value of 0.81, which indicates that the data is moderately skewed right. The data produced a standard deviation of 12.31% and a coefficient of variation of 27.71%. Machine break strains ranged from 27.17% to 68.6%. A 95% confidence interval was calculated to be 39.83% to 49.02%; it was determined with 95% confidence that the population mean is within this range. Some outliers in the data can be seen in the higher end of the data set.

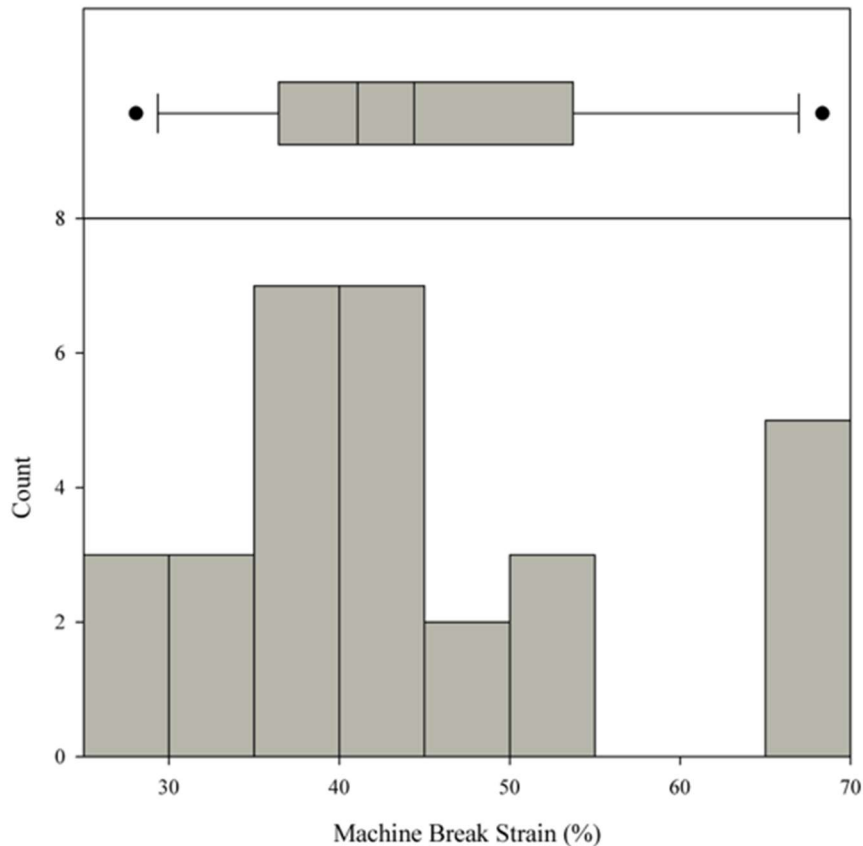


Figure 4.37 100% polyester machine direction - machine break strain histogram and box plot.

Figure 4.38 displays the histogram and box plot with 5th and 95th percentiles marked for the global image analysis break strain data. The mean and median break strains determined from the image analysis technique across the entire width of the specimen for the 100% polyester in the machine direction were 28.11% and 24.99%, respectively. Although the values of mean and median are similar, the data produced a skewness value of 0.98, which indicates that the data is moderately skewed right. The data produced a standard deviation of 8.63% and a coefficient of variation of 30.70%. Global image analysis break strains ranged from 17.16% to 46.12%. A 95% confidence interval was calculated to be 24.88% to 31.33%; it was determined with 95% confidence that the population mean is within this range. Some outliers in the data can be seen at the higher end of the data set.

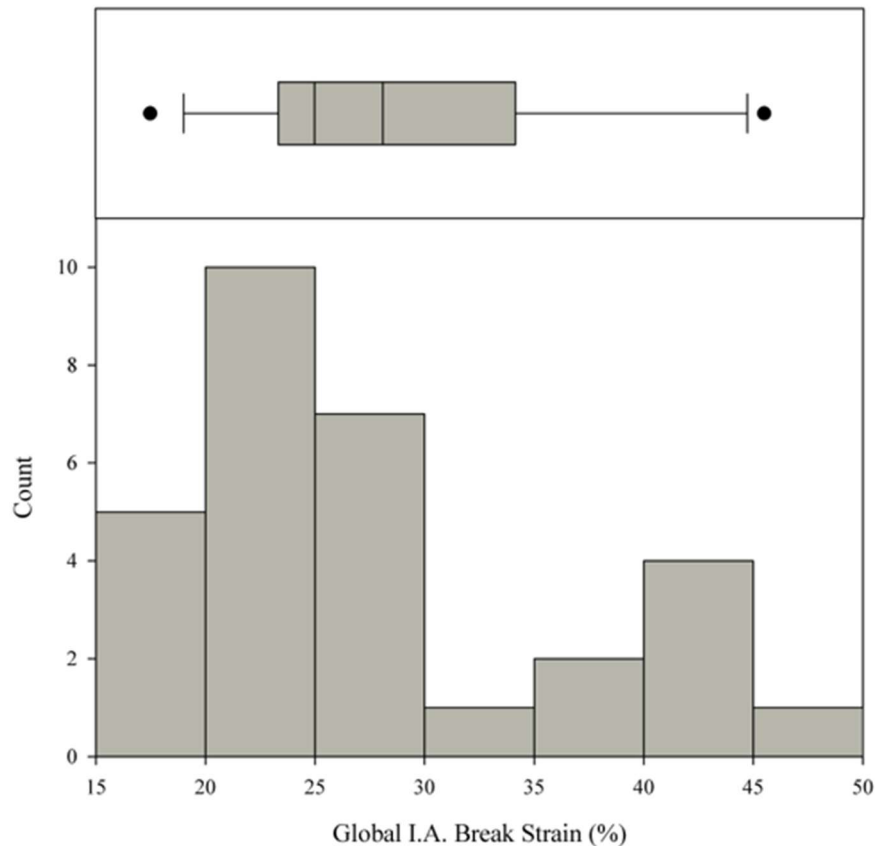


Figure 4.38 100% polyester machine direction - global image analysis break strain histogram and box plot.

Figure 4.39 displays the histogram and box plot with 5th and 95th percentiles marked for the local image analysis break strain data. The mean and median break strains determined from the image analysis technique for the center column of targets of the specimen for the 100% polyester in the machine direction were 35.47% and 33.67%, respectively. Although the values of mean and median are similar, the data produced a skewness value of 0.51, which indicates that the data is moderately skewed right. The data produced a standard deviation of 8.64% and a coefficient of variation of 24.37%. Local image analysis break strains ranged from 22.59% to 52.31%. A 95% confidence interval was calculated to be 32.24% to 38.69%; it was determined with 95% confidence that the population mean is within this range. Some outliers in the data can be seen at the higher end of the data set.

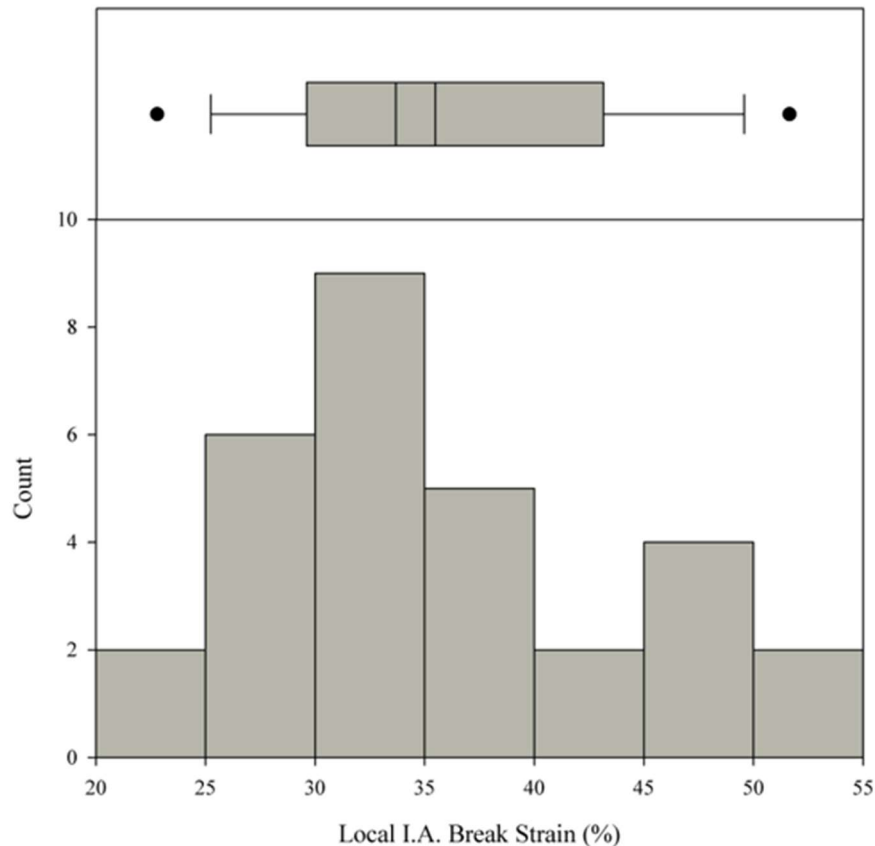


Figure 4.39 100% polyester machine direction - local image analysis break strain histogram and box plot.

Table 4.19 provides a summary of statistical values from the tensile testing that was completed for the 100% polyester in the machine direction. This table includes the mean, median, standard deviation, coefficient of variation, skewness, range, and 95% confidence interval for break force, machine break strain, global image analysis break strain, and local image analysis break strain.

Table 4.19: 100% Polyester Machine Direction Testing Results Summary

| | Break Force | Machine Break Strain | Global I.A. Break Strain | Local I.A. Break Strain |
|--------------------------|-----------------|----------------------|--------------------------|-------------------------|
| Mean | 1231 N | 44.42% | 28.11% | 35.47% |
| Median | 1157 N | 41.11% | 24.99% | 33.67% |
| Standard Deviation | 325 N | 12.31% | 8.63% | 8.64% |
| Coefficient of Variation | 26.38% | 27.71% | 30.70% | 24.37% |
| Skewness | 0.33 | 0.81 | 0.99 | 0.51 |
| Range | 736 N - 1788 N | 27.17% - 68.60% | 17.16% - 46.12% | 22.59% - 52.31% |
| 95% Confidence Interval | 1110 N - 1353 N | 39.83% - 49.02% | 24.88% - 31.33% | 32.24% - 38.69% |

As noted earlier, machine break strain values are significantly larger than both those determined using either of the image analysis techniques; this can easily be observed when comparing the means and medians. Of the two image analysis techniques, the local image analysis technique

provided larger values of strain than the global image analysis technique by approximately 8% strain. Overall, this information will first be used to compare with the results from the cross direction testing and then be used to compare with specification standards to assess which applications 100% polyester could potentially be used for.

4.4.2 Tensile Testing of 100% Polyester - Cross Direction Results

A total of 28 samples were tested from 7 different articles of 100% polyester denim clothing in the cross direction. A digital image analysis technique was used to determine accurate break strains in the specimens while testing in an attempt to resolve the issues associated with slippage during tensile testing. Figure 4.40 displays the machine break strain vs. break force, Figure 4.41 displays the global image analysis break strain vs. break force, and Figure 4.42 displays the local image analysis strain vs. break force. Figure 4.43 displays the three different break strain mechanisms vs. break force in the same plot.

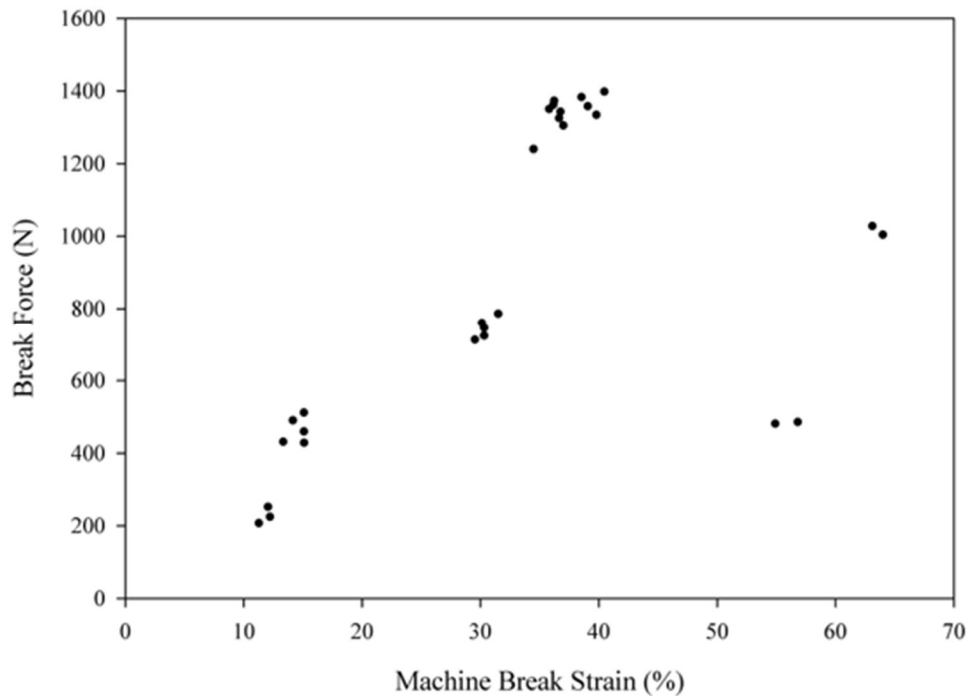


Figure 4.40 100% polyester cross direction - machine break strain vs. break force.

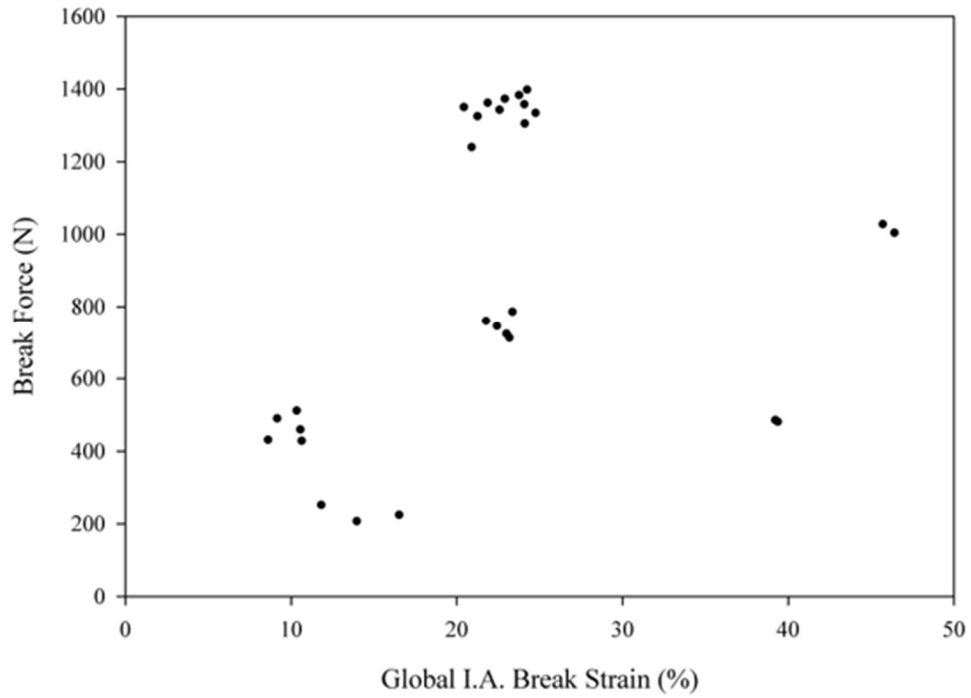


Figure 4.41 100% polyester cross direction - global image analysis break strain vs. break force.

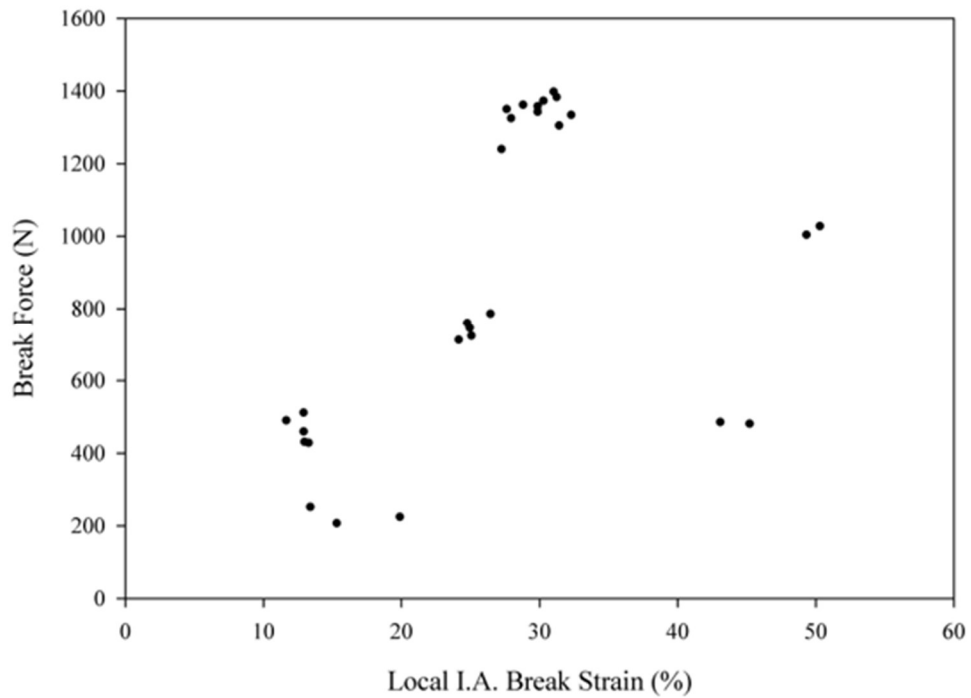


Figure 4.42 100% polyester cross direction - local image analysis break strain vs. break force.

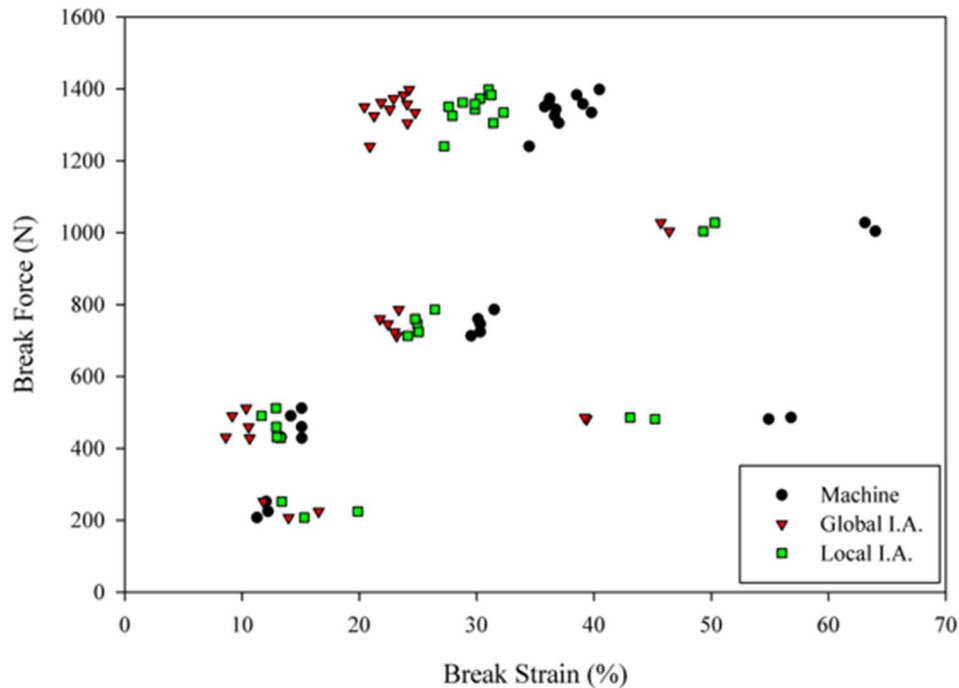


Figure 4.43 100% polyester cross direction - combined break strains vs. break force.

Similar to the results from the machine direction testing, these figures show that the break values of machine strain are significantly larger than those determined from either of the image analysis techniques. Of the two image analysis techniques, the local image analysis technique produced larger values than the global image analysis technique. It was also observed that there is a lot of variation in break strains as well as break forces. To investigate this further, a statistical analysis was completed on each variable: break force, machine break strain, local image analysis break strain, and global image analysis break strain.

Figure 4.44 displays the histogram and box plot with 5th and 95th percentiles marked for the break force data. The mean and median break forces for the 100% polyester in the cross direction were approximately 875 N (11.48 kN/m) and 773 N (10.14 kN/m), respectively. With these values being this similar and with a skewness value of -0.07, it can be determined that the data is fairly symmetrical. The data had a standard deviation of 429 N (5.63 kN/m) and a coefficient of variation of 49.00%. Break forces ranged from 207 N (2.72 kN/m) to 1398 N (18.35 kN/m). The 95% confidence interval was calculated to be 709 N (9.30 kN/m) to 1041 N (13.66 kN/m); it was determined with 95% confidence that the population mean is within this range. No outliers were observed for this data set.

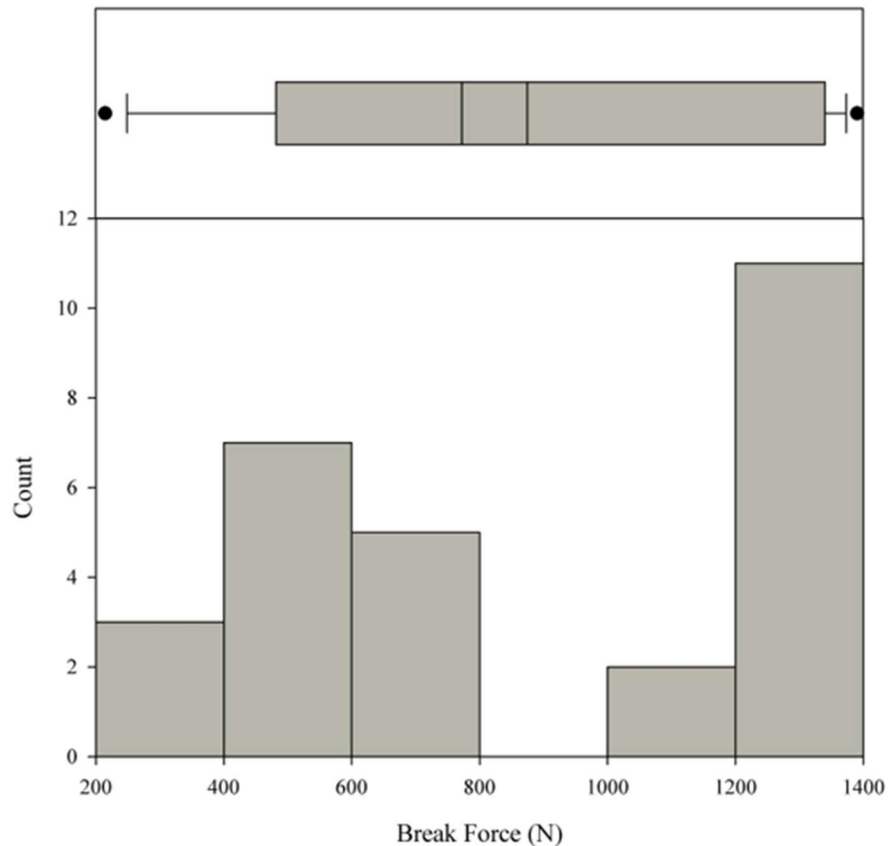


Figure 4.44 100% polyester cross direction - break force histogram and box plot.

Figure 4.45 displays the histogram and box plot with the 5th and 95th percentiles marked for the machine break strain data. The mean and median break strains determined from the crosshead movement of the grips for the 100% polyester in the cross direction were 32.49% and 35.15%, respectively. Although the values of mean and median are similar, the data produced a skewness value of 0.36, which indicates that the data is moderately skewed right. The data had a standard deviation of 15.19% and a coefficient of variation of 46.76%. Machine break strains ranged from 11.27% to 64.00%. The 95% confidence interval was calculated to be 26.60% to 38.38%; it was determined with 95% confidence that the population mean is within this range. No outliers were determined from this data set.

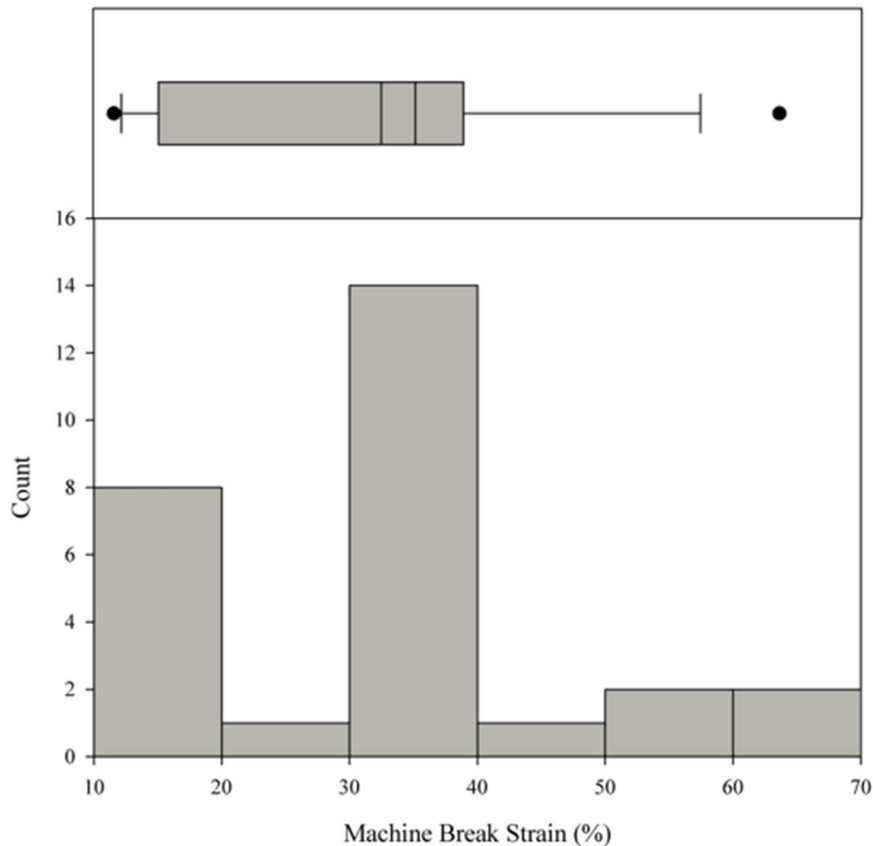


Figure 4.45 100% polyester cross direction - machine break strain histogram and box plot.

Figure 4.46 displays the histogram and box plot with the 5th and 95th percentiles marked for the global image analysis break strain data. The mean and median break strains determined from the image analysis technique across the entire width of the specimen for the 100% polyester in the cross direction were 22.39% and 22.51%, respectively. Although the values of mean and median are similar, the data produced a skewness value of 0.96, which indicates that the data is moderately skewed right. The data had a standard deviation of 10.04% and a coefficient of variation of 44.86%. Global image analysis break strains ranged from 8.61% to 46.41%. The 95% confidence interval was calculated to be 18.50% to 26.29%; it was determined with 95% confidence that the population mean is within this range. Some outliers in the data can be seen at the higher end of the data set.

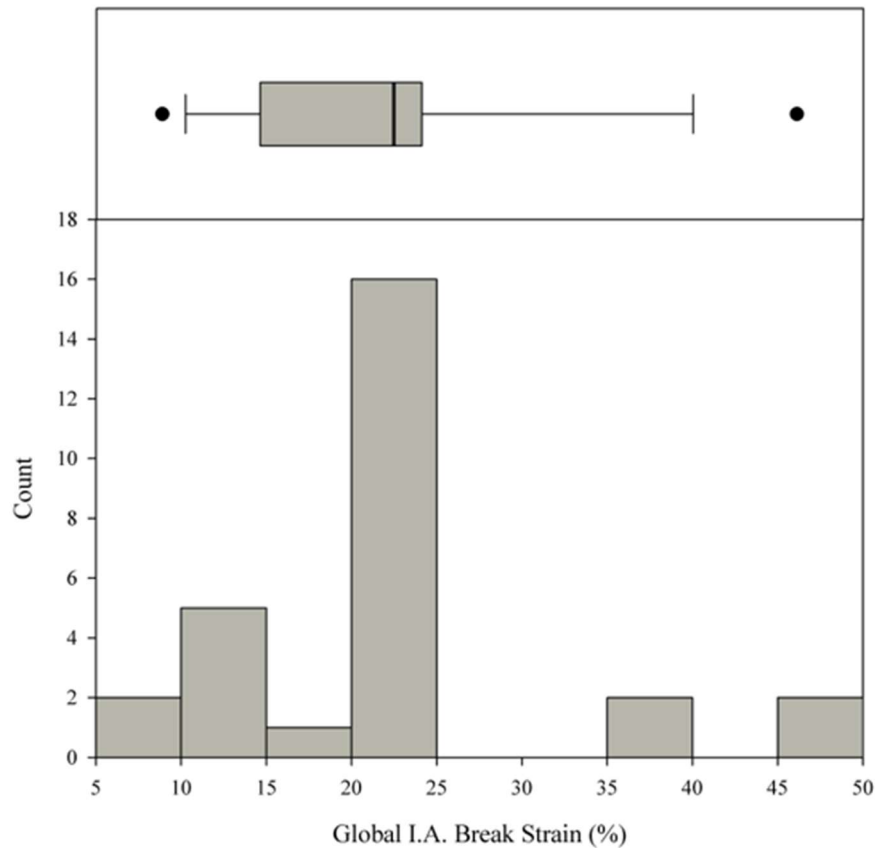


Figure 4.46 100% polyester cross direction - global image analysis break strain histogram and box plot.

Figure 4.47 displays the histogram and box plot with the 5th and 95th percentiles marked for the local image analysis break strain data. The mean and median break strains determined from the image analysis technique for the center column of targets of the specimen for the 100% polyester in the cross direction were 26.90% and 27.43%, respectively. Although the values of mean and median are similar, the data produced a skewness value of 0.52, which indicates that the data is moderately skewed right. The data had a standard deviation of 10.81% and a coefficient of variation of 40.20%. Local image analysis break strains ranged from 11.65% to 50.3%. The 95% confidence interval was calculated to be 22.70% to 31.09%; it was determined with 95% confidence that the population mean is within this range. No outliers were determined from this data set.

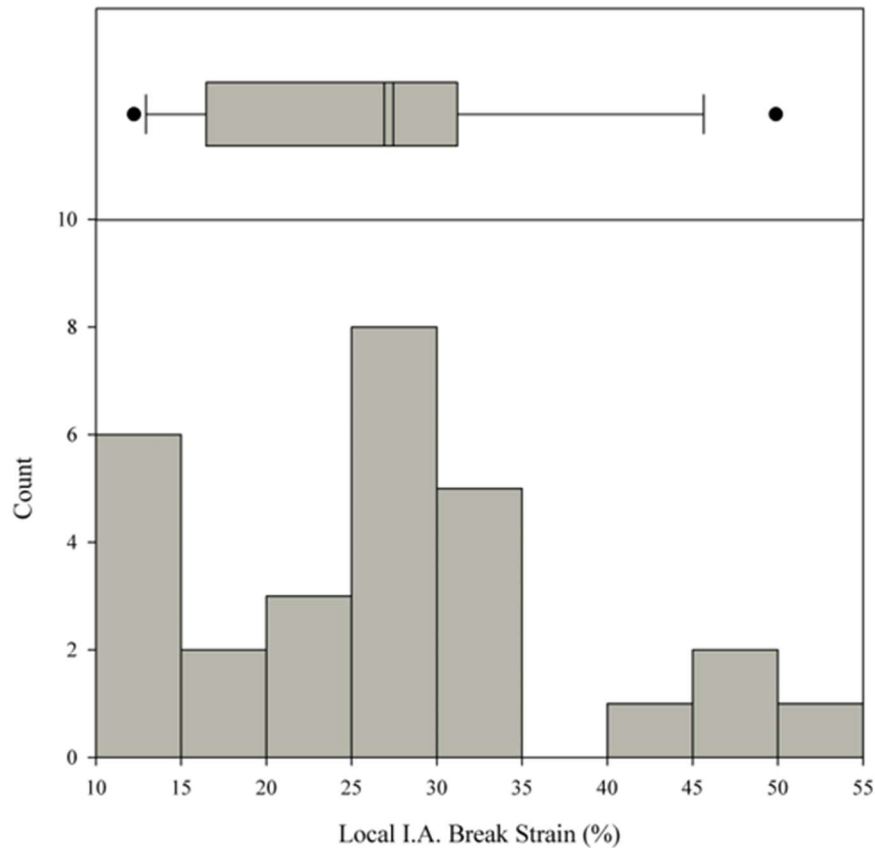


Figure 4.47 100% polyester cross direction - local image analysis break strain histogram and box plot.

Table 4.20 provides a summary of statistical values from the tensile testing that was completed for the 100% polyester in the cross direction. This table includes the mean, median, standard deviation, coefficient of variation, skewness, range, and 95% confidence interval for break force, machine break strain, global image analysis break strain, and local image analysis break strain.

Table 4.20: 100% Polyester Cross Direction Testing Results Summary

| | Break Force | Machine Break Strain | Global I.A. Break Strain | Local I.A. Break Strain |
|--------------------------|----------------|----------------------|--------------------------|-------------------------|
| Mean | 875 N | 32.49% | 22.39% | 26.90% |
| Median | 773 N | 35.15% | 22.51% | 27.43% |
| Standard Deviation | 429 N | 15.19% | 10.04% | 10.81% |
| Coefficient of Variation | 49.00% | 46.76% | 44.86% | 40.20% |
| Skewness | -0.07 | 0.36 | 0.96 | 0.52 |
| Range | 207 N - 1398 N | 11.27% - 64.00% | 8.61% - 46.41% | 11.65% - 50.30% |
| 95% Confidence Interval | 709 N - 1041 N | 26.60% - 38.38% | 18.50% - 26.29% | 22.70% - 31.09% |

Again, machine break strain values are significantly larger than both image analysis techniques; this can be clearly observed when comparing the means and medians. Of the two image analysis

techniques, the local image analysis technique provided larger values of strain than the global image analysis technique by approximately 5% strain.

Due to the nature of geotextile use, it is important to understand the tensile strength and break strains in both the machine and cross direction.

4.4.3 Tensile Testing of 100% Polyester - Machine vs. Cross Direction Comparison

Table 4.21 compares the statistical values of break force for the machine and cross directions. The mean and median break forces in the machine direction were larger than the corresponding forces measured in the cross direction. Tensile test results from the machine direction had a smaller standard deviation and coefficient of variation than test results for the cross direction. When comparing the range of break forces produced by the two directions, the testing in the machine direction had overall higher values for break force, while the cross direction had overall lower values. The 95% confidence interval is approximately 300 N larger on the lower and upper bound ends of the interval for the machine direction relative to the cross direction.

Table 4.21: 100% Polyester Break Force Comparison - Machine vs. Cross Direction

| | Machine Direction | Cross Direction |
|--------------------------|-------------------|-----------------|
| Mean | 1231 N | 875 N |
| Median | 1157 N | 773 N |
| Standard Deviation | 325 N | 429 N |
| Coefficient of Variation | 26.38% | 49.00% |
| Skewness | 0.33 | -0.07 |
| Range | 736 N - 1788 N | 207 N - 1398 N |
| 95% Confidence Interval | 1110 N - 1353 N | 709 N - 1041 N |

Table 4.22 compares the statistical values of machine break strain for the machine and cross direction. The mean and median machine break strains in the machine direction were larger than the corresponding values in the cross direction. Tensile testing from the machine direction produced a smaller standard deviation and coefficient of variation relative to the cross directional testing. The overall range of machine break strains was smaller for the machine direction with a range of approximately 41% compared to the cross direction with a range of approximately 53%. The 95% confidence interval bounds for the machine direction are larger than the 95% confidence interval bounds for the cross direction (39.83% - 49.02% compared to 26.60% - 38.38%).

Table 4.22: 100% Polyester Machine Break Strain Comparison - Machine vs. Cross Direction

| | Machine Direction | Cross Direction |
|--------------------------|-------------------|-----------------|
| Mean | 44.42% | 32.49% |
| Median | 41.11% | 35.15% |
| Standard Deviation | 12.31% | 15.19% |
| Coefficient of Variation | 27.71% | 46.76% |
| Skewness | 0.81 | 0.36 |
| Range | 27.17% - 68.60% | 11.27% - 64.00% |
| 95% Confidence Interval | 39.83% - 49.02% | 26.60% - 38.38% |

Table 4.23 compares the statistical values of global image analysis break strain for the machine and cross directions. The mean and median machine break strains in the machine direction were larger than those in the cross direction. Tensile testing from the machine direction produced a smaller standard deviation and coefficient of variation than those for the cross directional testing. The overall range of global image analysis break strains was smaller for the machine direction than the cross direction; both directions have a maximum global image analysis break strain value of approximately 46%; however, the low value for the testing in the cross direction was approximately 10% less than the low value for the machine direction. The 95% confidence interval bounds for the machine direction were larger than the 95% confidence interval bounds for the cross direction (24.88% - 31.33% compared to 18.50% - 26.29%).

Table 4.23: 100% Polyester Global I.A. Break Strain Comparison - Machine vs. Cross Direction

| | Machine Direction | Cross Direction |
|--------------------------|-------------------|-----------------|
| Mean | 28.11% | 22.39% |
| Median | 24.99% | 22.51% |
| Standard Deviation | 8.63% | 10.04% |
| Coefficient of Variation | 30.70% | 44.86% |
| Skewness | 0.99 | 0.96 |
| Range | 17.16% - 46.12% | 8.61% - 46.41% |
| 95% Confidence Interval | 24.88% - 31.33% | 18.50% - 26.29% |

Table 4.24 compares the statistical values of local image analysis break strain for the machine and cross directions. The mean and median machine break strains in the machine direction were larger than those in the cross direction. Tensile testing from the machine direction produced a smaller standard deviation but a similar coefficient of variation when compared to the testing in the cross direction. The overall range of local image analysis break strains is smaller for the machine direction with a range of approximately 30% compared to the cross direction with a range of approximately 40%. The 95% confidence interval bounds for the machine direction are larger than the 95% confidence interval bounds for the cross direction (32.24% - 38.69% compared to 22.70% - 31.09%).

Table 4.24: 100% Polyester Local I.A. Break Strain Comparison - Machine vs. Cross Direction

| | Machine Direction | Cross Direction |
|--------------------------|-------------------|-----------------|
| Mean | 35.47% | 26.90% |
| Median | 33.67% | 27.43% |
| Standard Deviation | 8.64% | 10.81% |
| Coefficient of Variation | 24.37% | 40.20% |
| Skewness | 0.51 | 0.52 |
| Range | 22.59% - 52.31% | 11.65% - 50.30% |
| 95% Confidence Interval | 32.24% - 38.69% | 22.70% - 31.09% |

Overall, larger break forces and break strains were observed from tensile testing in the machine direction when compared to tensile testing in the cross direction. However, it should be noted that for break force, minimum average roll value (MARV) is used in AASHTO Specification M288 (2015).

4.5 Permittivity Testing of 100% Polyester

Similar to the permittivity testing conducted for 100% cotton, seven 100% polyester articles were tested to measure permittivity. As stated in an earlier section, four specimens were cut from each article and each specimen was tested five times and the results were averaged; this produced a total of 28 specimens tested and 140 total permittivity tests completed on the 100% polyester test specimens. The mean and median permittivity of the tested specimens for the 100% polyester were 1.28 sec^{-1} and 0.68 sec^{-1} , respectively. The data produced a skewness value of 1.81, which indicates that the data is skewed right. The data set had a standard deviation of 1.368 sec^{-1} and a coefficient of variation of approximately 107%. Permittivity values ranged from approximately 0.12 sec^{-1} to 5.16 sec^{-1} . A 95% confidence interval was calculated to be 1.05 sec^{-1} to 1.51 sec^{-1} ; it was determined with 95% confidence that the population mean is within that range. Figure 4.48 displays the histogram and boxplot for the permittivity results of the 100% polyester articles.

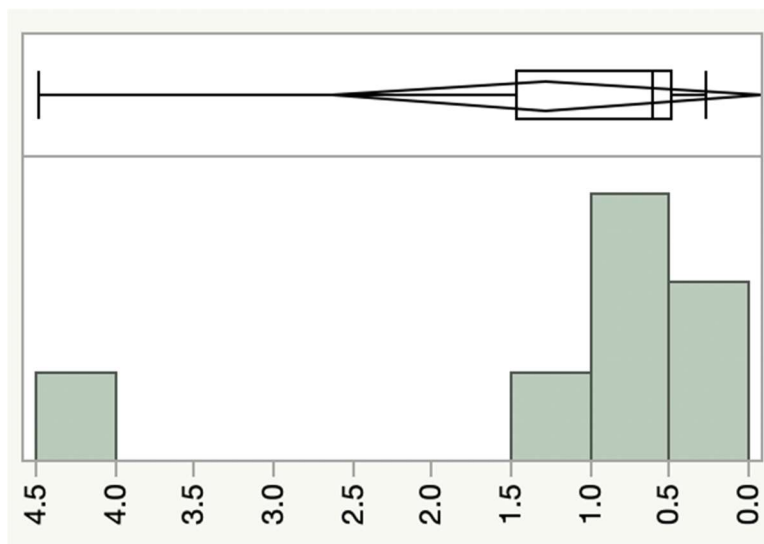


Figure 4.48 100% polyester permittivity results.

CHAPTER 5 – CONCLUSIONS

1. The screen-printing method described in this report used in conjunction with the digital image analysis technique proved successful. The two techniques together provided a rapid way to prepare, test, and obtain tensile testing results. Overall, the equipment and processes used in this study were sufficient for accurately obtaining break forces and break strains for tensile testing of 100% cotton and 100% polyester materials.
2. Permittivity test results provide useful information about the behavior of the tested fabrics as water flows through them. Additional permittivity testing is warranted to develop a broader understanding of the statistical variation of measured permittivities for the different types of tested fabric. This can be completed by running a large number of tests on several different specimens of the same material.
3. Overall, although the strength requirements were met for most specifications, the permittivity for 100% cotton denim was significantly lower than the requirements provided by AASHTO Specification M288. Without further modification of the recycled 100% cotton denim to increase permeability, 100% cotton denim would be a poor choice for most geotextile applications; 100% cotton denim only meets the requirements for paving fabric. Below is a summary comparing the tensile and permittivity testing results of 100% cotton denim with the standard geotextile requirements as provided by AASHTO Specification M288 (items that are in bold and italicized are where strength, elongation, and permittivity requirements are met):

- **Geotextile Strength Property Requirements**
 - **100% cotton denim in the machine direction meets the requirements for Class 2 with less than 50% elongation and greater than 1100 N grab strength.**
 - **100% cotton denim in the cross direction meets requirements for Class 3 with less than 50% elongation and greater than 800 N grab strength.**
- Subsurface Drainage Geotextile Requirements
 - 100% cotton denim in the machine direction meets the strength requirements but not the permittivity requirements.
 - 100% cotton denim in the cross direction does not meet the strength or permittivity requirements.
- Separation Geotextile Property Requirements
 - 100% cotton denim in the machine direction meets the strength requirements but not the permittivity requirements when medium ground pressure equipment (> 25 to ≤ 50 kPa) is used and the subgrade has been cleared of all obstacles except grass, weeds, leaves, and fine wood debris. Surface is smooth and level so that any shallow depressions and humps do not exceed 450 mm in depth or height. All larger depressions are filled. Alternatively, a smooth working table may be placed.
 - 100% cotton denim in the machine direction also meets the strength requirements but not the permittivity requirements when low ground pressure equipment (≤ 25 kPa) is used and the subgrade has been cleared of obstacles

larger than small to moderate-sized tree limbs and rocks. Tree trunks and stumps should be removed or covered with partial working table. Depressions and humps should not exceed 450 mm in depth or height. Larger depressions should be filled.

- 100% cotton denim in the cross direction meets the strength requirements but not the permittivity requirements when low ground pressure equipment (≤ 25 kPa) is used and the subgrade has been cleared of all obstacles except grass, weeds, leaves, and fine wood debris. Surface is smooth and level so that any shallow depressions and humps do not exceed 450 mm in depth or height. All larger depressions are filled. Alternatively, a smooth working table may be placed.
 - **Stabilization Geotextile Property Requirements**
 - 100% cotton denim in both the machine or cross direction do not meet the strength or permeability requirements.
 - **Permanent Erosion Control Geotextile Requirements**
 - 100% cotton denim in the machine direction meets the strength requirements but not the permittivity requirements
 - 100% cotton denim in the cross direction does not meet the strength or permittivity requirements
 - **Temporary Silt Fence Property Requirements**
 - 100% cotton denim in both the machine and cross direction meet the strength requirements for supported silt fence and unsupported silt fence when geotextile elongation is less than 50% however neither meet the permittivity requirements.
 - **Paving Fabric Property Requirements**
 - **100% cotton denim in the machine and cross direction both meet the strength requirements for Type I and there are no permittivity requirements (fabrics designed with low ultimate elongation).**
4. Recycled 100% polyester meets several geotextile strength and permittivity requirements as provided by AASHTO Specification M288; it was concluded that there is significant potential for recycled 100% polyester to be used as a geotextile in transportation infrastructure applications. Specifically, recycled 100% polyester met strength and permittivity requirements for subsurface drainage, separation, permanent erosion control, temporary silt fence, and paving fabric applications. Below is a summary comparing the tensile and permittivity testing results of 100% polyester with the standard geotextile requirements as provided by AASHTO Specification M288 (items that are in bold are where strength, elongation, and permittivity requirements are met):
- **Geotextile Strength Property Requirements**
 - **100% polyester in the machine direction meets the requirements for Class 2 with less than 50% elongation and greater than 1100 N grab strength.**
 - **100% polyester in the cross direction meets requirements for Class 3 with less than 50% elongation and greater than 800 N grab strength.**
 - **Subsurface Drainage Geotextile Requirements**
 - **100% polyester in the machine direction meets the strength and permittivity requirements for all percent in-situ soil passing categories.**

- 100% polyester in the cross direction does not meet the strength requirements but meets the permittivity requirements for all percent in-situ soil passing categories.
- **Separation Geotextile Property Requirements**
 - **100% polyester in the machine direction meets the strength and permittivity requirements when medium ground pressure equipment (> 25 to ≤ 50 kPa) is used and the subgrade has been cleared of all obstacles except grass, weeds, leaves, and fine wood debris. Surface is smooth and level so that any shallow depressions and humps do not exceed 450 mm in depth or height. All larger depressions are filled. Alternatively, a smooth working table may be placed.**
 - **100% polyester in the machine direction also meets the strength and permittivity requirements when low ground pressure equipment (≤ 25 kPa) is used and the subgrade has been cleared of obstacles larger than small to moderate-sized tree limbs and rocks. Tree trunks and stumps should be removed or covered with partial working table. Depressions and humps should not exceed 450 mm in depth or height. Larger depressions should be filled.**
 - **100% polyester in the cross direction meets the strength and permittivity requirements when low ground pressure equipment (≤ 25 kPa) is used and the subgrade has been cleared of all obstacles except grass, weeds, leaves, and fine wood debris. Surface is smooth and level so that any shallow depressions and humps do not exceed 450 mm in depth or height. All larger depressions are filled. Alternatively, a smooth working table may be placed.**
- **Stabilization Geotextile Property Requirements**
 - 100% polyester in both the machine and cross direction do not meet the strength requirements but do meet the permeability requirements.
- **Permanent Erosion Control Geotextile Requirements**
 - **100% polyester in the machine direction meets the strength and permittivity requirements for all percent in-situ soil passing categories.**
 - 100% polyester in the cross direction does not meet the strength requirements but meets the permittivity requirements for all percent in-situ soil passing categories.
- **Temporary Silt Fence Property Requirements**
 - **100% polyester in both the machine and cross direction meet the strength and permittivity requirements for supported silt fence and unsupported silt fence when geotextile elongation is less than 50%.**
- **Paving Fabric Property Requirements**
 - **100% polyester in the machine and cross direction both meet the strength requirements for Type I and there are no permittivity requirements (fabrics designed with low ultimate elongation).**

CHAPTER 6 – RECOMMENDATIONS

This section provides recommendations for future research regarding the topic of this study.

1. The researchers recommend using video capturing techniques if fewer tests are being conducted to obtain more accurate results. The benefit of this method is that it is possible to plot strain vs. load as time progresses throughout the test and it is then possible to evaluate what is happening at intermediate steps of the test. This is similar to what was completed in section 4.1 of this report, strain rate effect on tensile strength. Again, this was not performed for the entirety of this study as it would have been too time consuming for the number of tests that were conducted and for the overall length of time this study had to be completed in.
2. Conduct a similar tensile testing procedure as what was conducted in sections 4.1 (strain rate effect on tensile strength), 4.2 (tensile testing of 100% cotton denim), and 4.4 (tensile testing of 100% polyester) with roller grips instead of pneumatic grips. This can prove valuable in verifying break strengths because historically, when using pneumatic or hydraulic grips, the gripping mechanism can cause specimens to fail at the grips. The result of the specimen breaking the gripping mechanism can result in inaccurate break strength and strains. It should be noted, however, that the boundary strains produced during tensile testing with roller grips are not representative as there is a tightening phenomenon that occurs around the grips as the test progresses. Due to this tightening phenomenon, it is necessary to use some type of other method to obtain accurate strain measurements; most labs will use a laser extensometer to accurately measure strain, but this study found that the digital image analysis used throughout this study is accurate as well.
3. Conduct a similar tensile testing procedure as what was conducted in sections 4.1 (strain rate effect on tensile strength), 4.2 (tensile testing of 100% cotton denim), and 4.4 (tensile testing of 100% polyester) with nonwoven and knit materials as well as other textile materials including acrylic, blends, nylon, silk, wool, and rayon.
4. Develop an approach to quantify the quality of the recycled textiles. The researchers identified that the break strength and strain could potentially be affected by the overall wear and condition of the textile, however, this was not a focus of this research study. For this research study, only articles of clothing that looked to be in usable condition were tested (no visible rips or excessive wear). A visual quality rating system was developed by the researchers but, ultimately, was not used during this study as it was determined to be too time consuming and was affected by one's judgement. This rating system is provided in Table 6.1 below.

Table 6.1: Quality Condition Rating System

| Rating | Condition | Wearable? | Flaws | Fade | Worn |
|--------|-----------|-----------|-------------------------|---------------|--------|
| 4 | Like New | Yes | None | None | No |
| 3 | Good | Yes | None | Mild* | Yes |
| 2 | Average | Yes | ≤ 2 (≤ 1 cm) | Significant** | Yes*** |
| 1 | Unusable | No | > 2 (> 1 cm) | Significant** | Yes*** |

* Mild: lightening of color between exterior and interior textiles in the garment

** Significant: unrecognizable color difference between interior and exterior textiles of garment

*** Yes: pilling is observed

5. Investigate how simple mechanical degradation, such as punching holes in the 100% cotton denim may be sufficient to increase permittivity to meet acceptable standards.
6. Investigate how recycled 100% polyester textiles, like any synthetic polymer, degrade when exposed to ultraviolet rays present any time the sun is shining directly on the material. For this reason, it would be important to understand the degradation rate for the material if used in an above ground application.
7. Investigate techniques to shred and uniformly join fibers from recycled textiles into sheets for use as geotextiles and subject them to a similar tensile and permittivity testing; some techniques were investigated throughout the duration of this study and are discussed in the following paragraphs.

Discarded 100% cotton denim textiles were not recommended for direct reuse as geotextiles in transportation infrastructure applications. Although the recycled 100% cotton denim textiles are not of high enough quality for direct reuse, remanufacturing or shredding these textiles back to fiber and manufacturing new textiles from these used materials is a possibility. Two proof of concept shredding tests were carried out with collaborators Dr. Anil Netravali of Cornell University (Fiberizer) and Mat Inc. in Floodwood, MN.

Dr. Anil Netravali is one of the inventors of the Fiberizer, now on its third iteration of design, which can shred 8-inch wide pieces of used textiles, of any length, of all types of materials. The Fiberizer did not effectively shred the used textiles into fiber for making new geotextiles. The Fiberizer did shed the polyesters and polyester-cotton blends to small pieces, approximately 1 in² or larger as seen in Figure 6.1. The Fiberizer shredded the cottons to threads and approximately 0.5 in² pieces with the fabric still intact as shown in Figure 6.2a and b. The researchers used a handheld orbital sander to abrade recycled 100% cotton denim and were able to achieve a much higher level of fibers and lower number of threads and no fabric pieces as shown in Figure 6.2c.

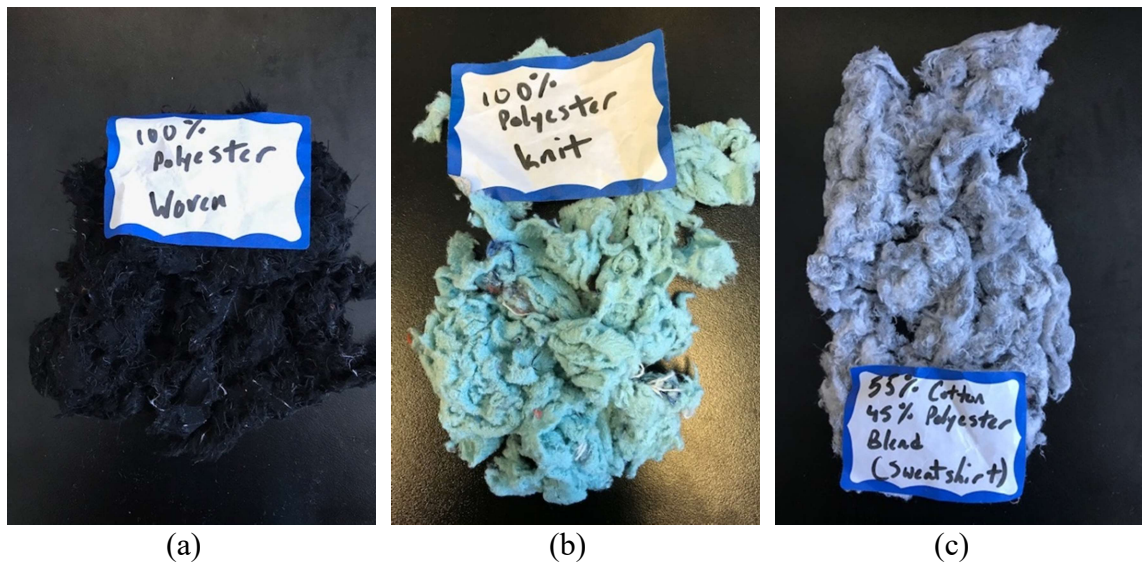


Figure 6.1 Fiberizer shredded 100% polyester (a) woven, (b) knit, and (c) 55%/45% cotton/polyester blended knit.

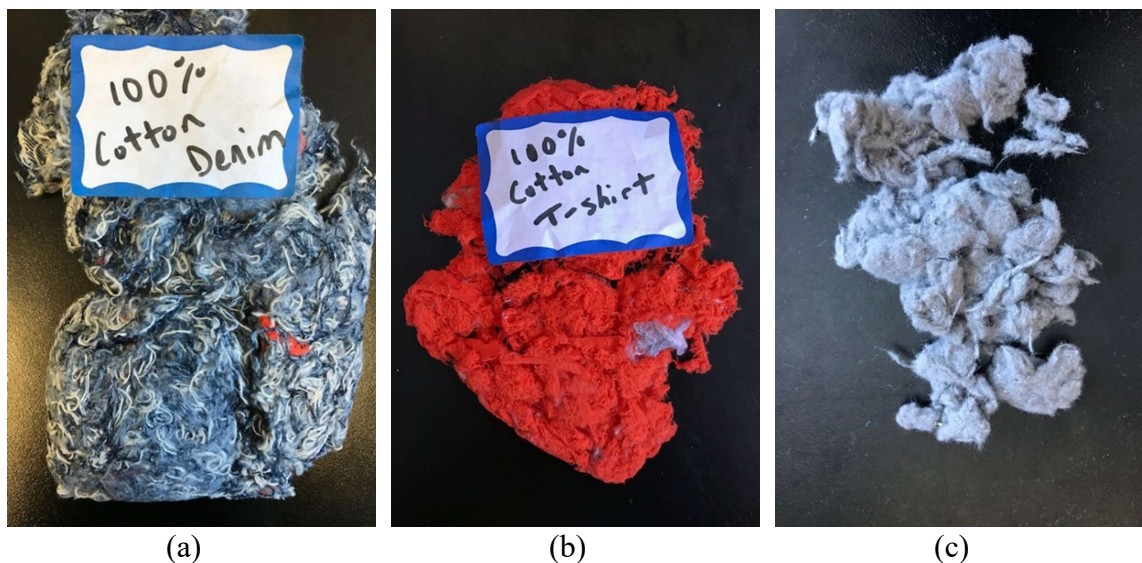


Figure 6.2 100% Cotton (a) Fiberizer shredded woven, (b) Fiberizer shredded knit, and (c) researcher's equipment shredded woven.

Fibers were also shredded at Mat Inc., a nonwoven manufacturer for erosion control blankets and similarly biodegradable textile products, in Floodwood, Minnesota. Mat Inc. had two carding cloth cylindrical drums that were used to separate or shred fibers. Carding cloth is a toothed wire that is wound around cylindrical drums to form a toothed surface. These drums effectively shredded 100% woven cotton denim into fiber and threads in less than a minute (Figure 6.3b). In spring of 2018, a used clothing shredder design incorporating carding clothed cylindrical drums to shred recycled clothing was developed for this project (Figure 6.4). Professional mechanical and electrical engineers evaluated the design for safety and operability in December 2018. Design changes per the professional

engineers' suggestions are currently being made and manufacturing of the fiber shredder is planned for later spring/summer of 2019.

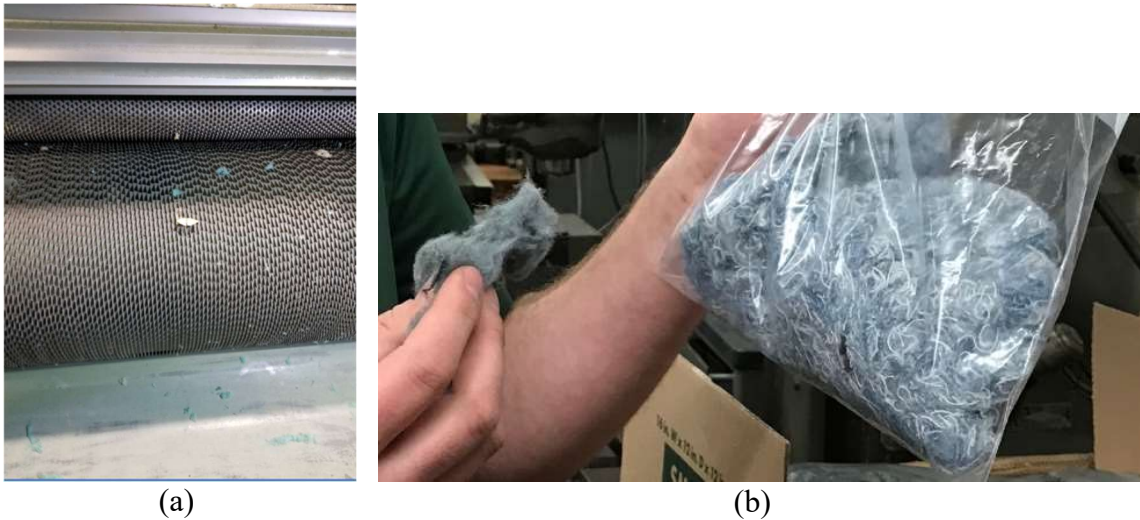


Figure 6.3 (a) Carding wire wound cylinder drums for shredding recycled textiles and (b) 100% cotton denim shredded from the drums.

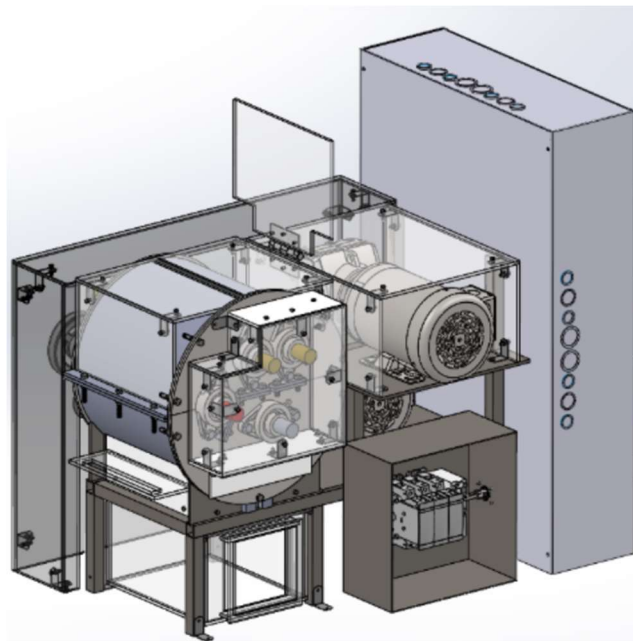


Figure 6.4 Researchers' fiber shredder design.

In addition to the above, unsuccessful proof of concept testing was performed in an attempt to create thermally bonded nonwoven textiles from shredded recycled textile materials. Shredded recycled textiles that were 100% cotton and 100% polyester were mixed together and placed under a weighted plate that was heated in an oven at 200 to 246°C and checked every 5-15 minutes for an hour or more. The cotton degraded, singed and turned brown, as seen in Figure 6.5, before the polyester melted. No successful nonwoven thermally bonded materials were created. However, adding polymers with a lower melting point than

polyester (below that of the degradation point for cotton) could potentially allow for a cohesive nonwoven textile.



Figure 6.5 Charred shredded cotton and polyester recycled textiles after attempted thermal bonding.

In summary more testing of the properties of shredded fibers and nonwoven textiles made from these fibers is essential for reuse of discarded 100% cotton denim textiles. In addition, shredding combined with nonwoven manufacturing needs further exploration for reuse and recycling of any type of discarded clothing material for geotextiles in transportation infrastructure applications. Preliminary results with shredding and thermally bonded nonwoven textiles mostly showcase the need for further investigation.